Characterisation of C-terminal RyR1 variants linked to neuromuscular disorders

A thesis presented in partial fulfilment of the requirements for the degree of

Master of Science in Genetics

at Massey University, Manawatū, New Zealand

Remai Parker

2015

Abstract

Intracellular calcium influences a large array of cellular processes in skeletal muscle cells and as a result the movement of free calcium is tightly-regulated by a diverse set of calcium channels and accessory proteins. The main store of calcium in skeletal muscle cells is the sarcoplasmic reticulum, from which the ryanodine receptor one calcium channel (RyR1) controls calcium release. Changes in calcium homeostasis often result in the manifestation of neuromuscular disorders, most notably central core disease (CCD) and malignant hyperthermia (MH). While CCD is usually apparent from the presence of certain physical characteristics, MH is typically asymptomatic unless exposed to a trigger, at which point the disease rapidly manifests as a crisis event which is potentially fatal. Currently, the diagnosis of these disorders requires the testing of a muscle biopsy, which is an expensive and invasive procedure, and thus a genetic test would be an ideal diagnostic alternative.

For the most part, CCD and MH cases are linked to the inappropriate release of calcium by defective RyR1 channels – located in the calcium storage organelle membrane – but both are complex disorders with variable penetrance and genetic heterogeneity. A hypoactive RyR1 is thought to cause CCD while a hyperactive RyR1 is thought to cause MH, and yet individuals have been observed to be carriers of both diseases. Most of these instances have been linked to variants in the C-terminal region of RyR1, corresponding to the transmembrane portion of the channel.

This research described in this thesis focused on the functional analysis of five C-terminal domain RyR1 variants identified in patients with neuromuscular disorders. The ability of the variant RyR1 channels to release calcium in response to a stimulus in a heterologous system was measured and compared with that of the wild type channel. Moreover, one of these variants was also examined in several B-lymphoblastoid cell lines taken from carriers of the variant. Of the five variants tested in the heterologous system, four different phenotypes were observed, reinforcing the theory that these disorders are caused by a variety of factors that combine to produce a complex phenotype.

Acknowledgements

I would like to extend my gratitude to my supervisor, Associate Professor Kathryn Stowell, for her support and encouragement over the last two years which has been considerable. Her unfailing confidence in me has been a motivation to challenge myself and to persevere. Moreover, I would like to thank her for the immortalised B-lymphocyte cell lines she so kindly provided for this project.

I would like to thank Mrs. Lili Rhodes and Dr. Anja Schiemann for teaching me the majority of the methods used in this project and for their friendships over the past two years. In addition, special thanks to Lili for the cloning work she contributed as without her amazing ability to clone difficult DNA fragments this project would have yielded minimal results.

I would especially like to thank my friends Dr. Rebecca Smith and Chay Fhun Low for providing me with endless entertainment during the long hours spent in the lab. I am particularly grateful for Rebecca who has been a mentor, a good friend and a wealth of information for the duration of my post-graduate studies.

Special thanks should go to Dr. Keisaku Sato for providing his protocols and the wild type and MHS positive control full-length *RYR1* plasmids in this project and Dr. Natisha Magan for the use of two full-length *RYR1* variants and a set of mutagenic primers used in this project.

I would also like to thank the Manawatu Microscopy and Imaging Centre for the imaging of my western blot and the use of the confocal microscope. Special thanks to Niki Murray, Jordan Taylor and Dr. Matthew Savoian for their training and assistance.

Finally I would like to extend my gratitude for the financial support provided by the following scholarships: Livestock Improvement Corporation Patrick Shannon Scholarship; Henry Kelsey Research Scholarship; Massey University Masterate Scholarship; and Massey University Molecular Genetics Research Scholarship.

Abbreviations

-(d/dT)	Decrease (of fluorescence) over time
α-tubulin	Alpha-tubulin
µg	Microgram
µL	Microlitre
34C	Ryanodine receptor antibody
4-C*m*C	4-chloro-*m*-cresol
A260	Absorbance at 260 nm
A280	Absorbance at 280 nm
APS	Ammonium persulfate
ATP	Adenosine triphosphate
BSA	Bovine serum albumin
BSS	Buffered salt solution
CACNA1S	Gene encoding α1 subunit of DHPR
CASQ1	Calsequestrin in skeletal muscle
Casq1	Gene encoding skeletal muscle form of calsequestrin
Cat. No.	Catalogue number
CCD	Central core disease
cDNA	Complementary DNA
CHCT	Caffeine-halothane contracture test
C-terminal	Carboxyl-terminal

DAPI	4’,6-diamidino-2-phenylindole
DHPR	Dihydropyridine receptor
DMEM	Dulbecco’s modified Eagle medium
DMSO	Dimethyl sulfoxide
DNA	Deoxyribonucleic acid
Dyspedic	Lacking the ryanodine receptor 1 gene
E. coli	*Escherichia coli*
EC	Excitation-contraction
EC_{50}	Half maximal effective concentration
ECCE	Excitation-coupled calcium entry
EDTA	Ethylenediaminetetraacetic acid
EHS	Exertional heat stroke
EMHG	European malignant hyperthermia group
ER	Endoplasmic reticulum
FBS	Foetal bovine serum
FITC	Fluorescein isothiocyanate
FKBP12	FK506-binding protein of skeletal muscle
gDNA	Genomic DNA
HEK-293	Human embryonic kidney 293 cell line
HEK-293T	HEK-293 cell line containing the *Simian virus 40* large T antigen
HRM	High resolution melting
IP3R	Inositol triphosphate receptor

IVCT	*In vitro* contracture test
kb	Kilobase
kDa	Kilodalton
KDS	King-Denborough syndrome
LB broth	Luria Bertani broth
L-type	Long lasting activation
mg	Milligram
MH	Malignant hyperthermia
MHN	Malignant hyperthermia negative
MHS	Malignant hyperthermia susceptible
MHS(c)	MHS in response only to caffeine in IVCT
MHS(h)	MHS response only to halothane in IVCT
mL	Millilitre
MmD	Multiminicore disease
nm	Nanometres
N-terminal	Amino-terminal
Opti-MEM	Opti-minimum essential medium
PBS	Phosphate-buffered saline
PCR	Polymerase chain reaction
PDI	Protein disulfide isomerase
PolyPhen-2	Polymorphism phenotyping version two
P-value	Statistic denoting statistical significance

PVDF	Polyvinylidene fluoride
RYR1	Gene encoding skeletal muscle form of RyR1 protein
RyR1	Type one ryanodine receptor found in skeletal muscle
RyR2	Type two ryanodine receptor found in cardiac muscle
RyR3	Type three ryanodine receptor found in the brain
SDM	Site-directed mutagenesis
SDS	Sodium dodecyl sulfate
SDS-PAGE	SDS polyacrylamide gel electrophoresis
SEM	Standard error of the mean
SERCA	Sarco/endoplasmic reticulum calcium ATPase
SOCE	Store-operated calcium entry
SR	Sarcoplasmic reticulum
Stim1	Stromal interaction molecule one
TAE	Tris-acetate-EDTA
TBST	Tris-buffered saline containing Tween 20
TE	Tris-EDTA
TEMED	Tetramethylethylenediamine
TRITC	Tetramethylrhodamine isothiocyanate
TRPC	Transient receptor potential channel
T-tubule	Transverse tubule
UV	Ultraviolet

Table of Contents

List of Figures

List of Tables

CHAPTER ONE: Introduction

CALCIUM HOMEOSTASIS

Calcium is a potent second messenger ion that serves as a signal for the cell to carry out critical metabolic and physiological processes that are functionally tissue-specific and governed by strict regulatory mechanisms. In skeletal muscle cells, a major role of calcium is to regulate the contraction and relaxation of the muscle in a process known as excitation-contraction (EC) coupling. The cell first receives a signal to contract when a somatic motor neuron fires, releasing neurotransmitters which cause depolarisation of the sarcolemma. This depolarisation spreads down the transverse tubule (t-tubule) where the voltage-sensing dihydropyridine receptor (DHPR) is located, causing it to undergo a conformational change (Melzer et al. 1995). This signals the type 1 ryanodine receptor (RyR1), to which it is physically-coupled, to undergo a conformational change and switch to its open state, releasing calcium into the cytoplasm from the calcium store of muscle cells, the sarcoplasmic reticulum (SR). When free calcium floods into the myoplasm it binds the troponin complex, causing contraction of the muscle fibre at the expense of energy in the form of adenosine triphosphate (ATP). This increase in ATP consumption requires an equal increase in ATP production through cellular respiration in order to meet the energy needs of the muscle.

Relaxation of skeletal muscle requires the troponin complex to be deprived of calcium, reversing the force created by the myofibrils. Removing the excess calcium from the cytoplasm is achieved by binding specialised proteins such as calmodulin; pumping calcium out of the cell itself; and pumping it back into the SR. The latter is carried out by the sarco/endoplasmic reticulum calcium ATPase (SERCA) which is activated by increased calcium levels in the cytoplasm. This channel in the SR membrane pumps calcium back into the SR against the concentration gradient both during and after muscle contraction in an ATP-dependent manner (Martonosi 1995).

There are three independent pathways that function to rapidly replenish the cell's store of calcium from extracellular sources. Store-operated calcium entry (SOCE) is activated by stromal interaction molecule 1 (Stim1) – a transmembrane protein located in the SR membrane that detects calcium levels with an N-terminal domain located in the SR lumen (Liou et al. 2005). Stim1 relays the signal of calcium store depletion by interacting with and activating a calcium channel, Orai1, located in the plasma membrane (Stiber et al. 2008). The importance of this was shown in a study by Stiber et al. (2008) where mouse myotubes lacking Stim1 demonstrated a loss of SOCE and were easily fatigued compared to wild type myotubes. Another calcium influx pathway activated by SR store depletion was discovered recently by Eltit et al. (2013) which was reported to be independent of Stim1 and Orai1 function. Instead, it is thought to be regulated by non-specific cation channels in the plasma membrane which are hypothesised as belonging to the transient receptor potential cation (TRPC) family of channels – namely TRPC3 and TRPC6 (Eltit et al. 2013). The third pathway to replenish intracellular calcium from extracellular sources is excitation-coupled calcium entry (ECCE) which is independent of the SR and is instead activated by the prolonged depolarisation of the plasma membrane (Cherednichenko et al. 2004). This pathway was also shown to be independent of both Orai1 and Stim1 activity in mouse myotubes (Lyfenko & Dirksen 2008); instead, it appears to require the interaction between DHPR and RyR1 (Bannister et al. 2009). The existence of these functionally independent pathways that provide the cell with extracellular calcium emphasises the essential role calcium influx plays in skeletal muscle calcium homeostasis.

1.2 RYANODINE RECEPTOR 1

1.2.1 STRUCTURE AND FUNCTION

While most mammalian cells use the endoplasmic reticulum (ER) as the major calcium storage organelle, some muscle cell types use a specialised organelle known as the sarcoplasmic reticulum. The SR contains the transmembrane calcium channel, the ryanodine receptor, named after the plant alkaloid to which it binds – ryanodine. The ryanodine receptor family consists of three mammalian isoforms – RyR1, RyR2 and RyR3 – which are found primarily in skeletal muscle, cardiac muscle and the brain,

respectively, and share a large amount of sequence identity. Both RyR1 and RyR3 are expressed in skeletal muscle cells (Tarroni et al. 1997) but the type 3 ryanodine receptor has been shown to have no noticeable effect on calcium homeostasis in this tissue (Dietze et al. 1998) unlike RyR1, which is essential. The type 1 ryanodine receptor is a homotetramer with the majority of the protein located in the cytoplasm and the remaining C-terminal region in the membrane and the SR lumen. RyR1 is a large protein; the ryanodine receptor 1 gene (*RYR1*) is approximately 160 kb in length and the RyR1 tetramer is around 2.2 MDa and contains three distinct regions: The N-terminal, central and C-terminal regions. The N-terminal and central regions – located in the cytoplasm – make up 80% of the total mass of the protein and are thought to interact with each other to control the opening and closing of the channel, meanwhile the C-terminal region forms the pore through which calcium is released from the SR (Figure 1.1A). This pore is an extension of the central column that extends through the entire RyR1 tetramer (Samsó et al. 2005). This C-terminal region is essential for the normal function of the protein as a whole. Studies with cells expressing only the C-terminal region of the *RYR1* gene have shown that the cytoplasmic region is not required for the protein to tetramerise and translocate to the SR (Bhat & Ma 2002, Stewart et al. 2003). C-terminal constructs were also used to demonstrate that the binding sites of 4-chloro-*m*-cresol (4-C*m*C) and ryanodine – both specific RyR1 agonists – are located in the C-terminal region (Fessenden et al. 2003). In addition, this region has been shown to respond to calcium levels in the SR by calcium binding to a low-affinity site on the luminal side of the membrane to result in channel opening (Bhat et al. 1997, Balshaw et al. 1999).

1.2.2 C-TERMINAL REGION OF RyR1

The first model of the RyR1 C-terminal region structure was suggested by Zorzato et al. (1990) which predicted four helices crossing the membrane. This model was updated when structure-function studies carried out on rabbit RyR1 produced a model for the arrangement of the C-terminal region which contained two probable helices and six definite helices crossing the membrane as well as a selectivity filter (Du et al. 2002). Recently, the topology of the C-terminal region of rabbit RyR1 in its closed state was determined to near atomic resolution using cryoelectron microscopy by Yan et al.

(2015). This region contains residues corresponding to 4546 – 5038 in human RyR1, and was shown to consist of six helices (S1 – S6) which cross the membrane, confirming results from previous studies (Figure 1.1B). The identity of the amino acid sequence referred to in this chapter is from human RyR1 with the GenBank accession number NP_000531.2.

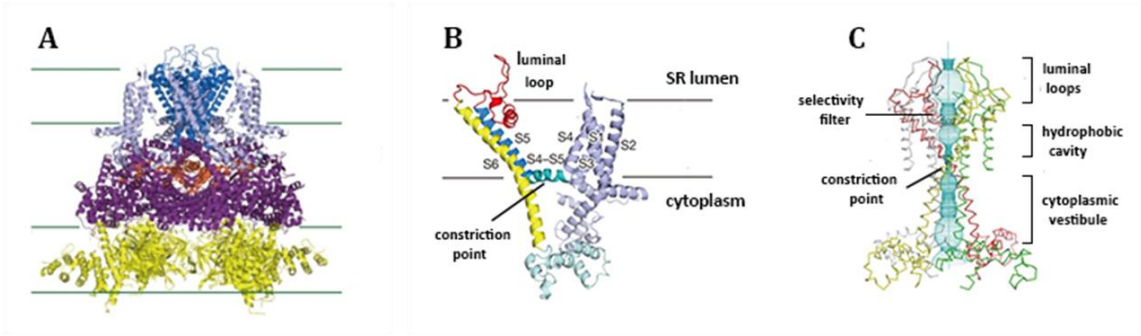

FIGURE 1.1 Proposed model of RyR1 structure

A. Lateral view of the RyR1 tetramer with its three distinct sections: the C-terminal domains in two shades of blue; the central domains in purple and red; and the N-terminal domains in yellow. The central column through which calcium is transported is shown by the darker blue and red regions. **B.** Topology of the C-terminal region of a RyR1 monomer in the SR membrane which is located between the black lines. Six transmembrane helices are labelled S1 through S6. **C.** Organisation and structure of the central column with the width of pore shown in cyan.

Adapted by permission from Macmillan Publishers Ltd: *Nature*, (Yan et al. 2015), *517*(7532): 50–55, © 2015.

Yan et al. found the luminal loops (luminal edge of the SR membrane) between helices S5 and S6 to contain a large proportion of electronegative amino acids which suggests a role in the attraction of the positively-charged calcium ions. The structure of these loops was reported to be difficult to elucidate which is indicative of flexibility and movement within this region. The selectivity filter which consists of residues 4894 – 4902 in human RyR1 is positioned within the pore in the linker region between helices S5 and S6 (Yan et al. 2015). This has been shown to be critical for the function of RyR1, as variants within this region have altered ryanodine binding and calcium conductance

in a heterologous cell system expressing rabbit RyR1 (Gao et al. 2000). Yan et al. described a hydrophobic cavity below the selectivity filter followed by a large number of electronegative residues thought to enable the rapid movement of calcium ions through the channel (Figure 1.1C). Each monomer contributes two helices – the S6 helix and the linker helix between S4 and S5 – to form a constriction point at the cytoplasmic edge of the membrane which is reported by Yan et al. (2015) to be impermeable to calcium.

The opening of the channel is associated with major conformational changes throughout the cytoplasmic region and a four degree shift in relation to the transmembrane domain (Orlova et al. 1996). The interface between the transmembrane and cytoplasmic regions is extensive and, in its closed state, the entire C-terminal pore of RyR1 is open with the exception of the cytoplasmic constriction point (Yan et al. 2015). This suggests the signal to open the channel is relayed from the N-terminal and central regions through widespread conformational changes which results in the opening of this constriction point and therefore the calcium channel itself.

1.2.3 PROTEINS ASSOCIATED WITH RyR1

The dihydropyridine receptor, shown in Figure 1.2, is the physical link between the extracellular signal relayed from the motor neuron and the release of calcium from the sarcoplasmic reticulum within the cell (Rios & Brum 1987). As the DHPR causes RyR1 to release calcium from the SR, RyR1 in turn activates the conductance of calcium through the L-type (long-lasting activation) DHPR channel from the extracellular space (Nakai et al. 1996). The DHPR protein consists of five subunits, one of which – the α1 subunit – serves as a calcium channel through both binding sites for calcium antagonists and its function as a voltage sensor (Beam et al. 1989). The gene encoding this subunit, *CACNA1S*, is the only gene other than *RYR1* with substitutions unequivocally linked to malignant hyperthermia, although the frequency of linkage is very low (Monnier et al. 1997).

The role of skeletal muscle calsequestrin (CASQ1) in the sarcoplasmic reticulum is to sequester calcium and make it available at the terminal cisternae – the enlarged

regions of the SR surrounding the t-tubules – where calsequestrin (CASQ1) is enriched (see Figure 1.2). Each molecule of CASQ1 is able to bind up to sixty calcium ions, and the highly-charged C-terminal tail of CASQ1 forms the major calcium binding site (Sanchez et al. 2012). While this is likely its main function, it has been shown that calsequestrin can act as a sensor of SR store depletion in cardiac muscle, affecting the gating of the RyR2 channel (Györke & Terentyev 2008, Zima et al. 2010). This was confirmed in mouse skeletal muscle, where continuous membrane depolarisation caused the SR to release 93% of its calcium stores in *Casq1*-null (lacking the gene encoding CASQ1) muscle cells, compared to the 65% released in wild type cells, which was shown to be independent of the DHPR (Sztretye et al. 2011). Calsequestrin has been suggested to be an essential factor in the closing of the RyR1 channel, as *Casq1*-null mice show a phenotype similar to malignant hyperthermia in response to exposure to halothane and heat stress, suggesting the RyR1 channel is unstable in the absence of CASQ1 (Protasi et al. 2009). To date, no genetic variants in *Casq1* have been shown to be linked to MH susceptibility.

Triadin and junctin are transmembrane proteins located in the SR membrane (Figure 1.2); both have a short N-terminal domain in the cytoplasm and a large, highly charged C-terminal domain in the SR lumen. The main role of both proteins is to collect calcium-bound CASQ1 for the transport of calcium through RyR1; however, recent evidence suggests a greater and more specific role for each protein individually. Ablation of triadin in mice severely reduces EC coupling efficiency, whereas the ablation of junctin has little effect (Boncompagni et al. 2012), demonstrating the distinct roles these two proteins have in the SR. Triadin binds RyR1 in the luminal loops between helices S5 and S6 (Lee et al. 2004, Goonasekera et al. 2007) and increases the activity of the channel by enhancing the degree to which it opens (Wei et al. 2009). In contrast, junctin – which binds luminal residues between helices S1 and S2 and helices S5 and S6 – has been shown to inhibit the opening of the channel by binding calsequestrin, suggesting a role in the closing of the channel (Wei et al. 2009).

JP-45 is a transmembrane protein located in the SR membrane (Figure 1.2) thought to down-regulate EC coupling (Gouadon et al. 2006). Its N-terminal domain located in the cytoplasm interacts with the DHPR while its C-terminal domain located in the SR lumen

interacts with CASQ1 (Anderson et al. 2003). Two substitutions in JP-45 – p.P108L and p.G150A (GenBank accession NP_653217.1) – were identified in a study by Althobiti et al. (2009) and proposed to be modifiers of EC coupling machinery. Both variants cause decreased sensitivity in DHPR to voltage depolarisation in the muscle fibres of transgenic mice (Yasuda et al. 2013) which could be related to the function of JP-45 as a regulator of functional expression of DHPR into the t-tubule (Anderson et al. 2006). This suggests that JP-45 – and the p.P108L and p.G150A variants in particular – may contribute to the complexity of neuromuscular disorders and have the potential to phenotypically modulate RyR1 activity.

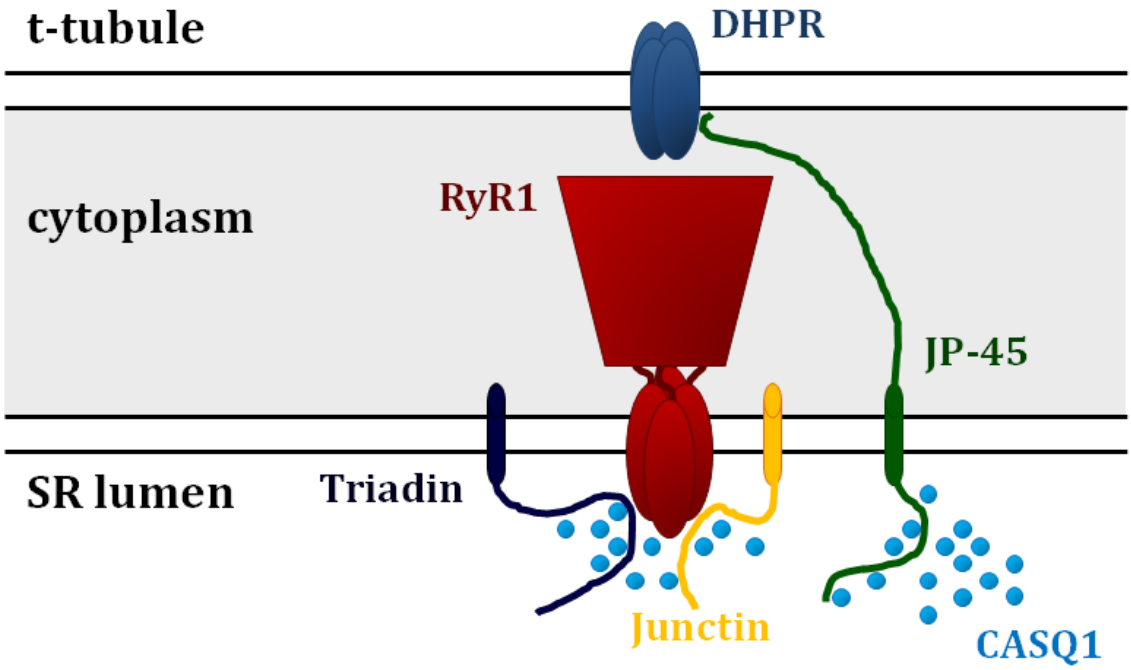

FIGURE 1.2 Protein-protein interactions involved in EC coupling

The major proteins found at terminal cisternae are shown: DHPR (medium blue) located in the plasma membrane (black lines); RyR1 (red), Triadin (dark blue), Junctin (yellow) and JP-45 (green) located in the SR membrane (black lines); and CASQ1 (light blue circles) located in the SR lumen.

The FK506-binding protein of skeletal muscle, FKBP12, is a small cytoplasmic protein that binds RyR1 at a ratio of four FKBP12 molecules per channel (Jayaraman et al. 1992). Its role is thought to be in the stabilisation of the closed state of the RyR1 tetramer and facilitation of the opening and closing of the channel (Williams et al. 2001). FKBP12 deficiency *in vitro* has resulted in increased RyR1 sensitivity to agonists and partial conductance states which are reversed upon reintroduction of FKBP12 (MacKrill, 1999).

Calmodulin (CaM) and S100A1 are small calcium-binding proteins located in the cytoplasm of skeletal muscle cells that undergo conformational changes upon calcium-binding. They share a binding site on RyR1 and so interact with the channel in a competitive and calcium-dependent manner. In resting conditions there is a low concentration of cytoplasmic calcium and S100A1 enhances calcium release from the SR when the muscle is stimulated, while after sustained stimulation there are high cytoplasmic calcium levels and CaM displaces S100A1 from RyR1 and promotes inactivation of the channel (Prosser et al. 2011). The two proteins are thought to compete to precisely regulate channel gating as the disruption of this can lead to reduced muscle performance.

1.2.4 PHENOTYPIC EFFECTS OF *RYR1* VARIANTS

1.2.4.1 DISEASES LINKED TO RyR1 DEFECTS

Changes in RyR1 function have been linked to several neuromuscular diseases that have phenotypes with a large number of similarities. Malignant hyperthermia (MH) is a dominant pharmacogenetic disorder which normally presents with no symptoms unless the patient is exposed to one of several triggers, at which point RyR1 opens uncontrollably, potentially causing an MH crisis. An MH episode manifests in a large number of symptoms including the rapid elevation of core body temperature, hyperkalaemia, rigid muscles, acidosis, elevated end-tidal carbon dioxide levels and tachycardia. It has been estimated that around 70% of all cases of malignant hyperthermia are caused by altered RyR1 function (Rosenberg 2013).

Exertional heat stroke (EHS) is a rare disorder caused by strenuous activity and/or heat stress and presents with similar symptoms to MH, namely a huge increase in intracellular calcium causing a hypermetabolic state that can lead to widespread organ failure and death (Bouchama & Knochel 2002). While anyone can experience EHS in extreme conditions, it is thought that people may be genetically predisposed to an EHS attack, much like malignant hyperthermia. Several individuals with a history of EHS have been diagnosed with MH by IVCT (Köchling et al. 1998, Wappler et al. 2001), some of which were found to have *RYR1* mutations causative of MH (Davis et al. 2002, Capacchione et al. 2010, Sato et al. 2013). In addition, people with MH may experience a higher than normal temperature increase during exercise which could be due to ineffective heat dissipation (Campbell et al. 1983). This suggests that while EHS and MH represent two distinct disorders, they are not mutually exclusive and may share a common causal factor.

Central core disease (CCD) is a genetic myopathy that has been linked to both recessive and dominant variants in *RYR1* leading to altered RyR1 function. CCD is diagnosed by histological examination of a muscle biopsy as type one muscle fibres vary greatly in size and contain a large central region or 'core' which lacks mitochondrial and oxidative enzyme activity, extending the length of the fibres (Dubowitz & Brooke 1973). Furthermore, individuals with CCD are considered to be susceptible to MH with RyR1 defects being the common causal factor (McCarthy et al. 2000).

Multiminicore disease (MmD) is similar to CCD as it is an early-onset myopathy diagnosed by the presence of multiple small regions or 'cores' of reduced mitochondrial activity in a histological stain which do not extend down the entire muscle fibre (Engel et al. 1971). MmD is a recessive disorder associated with variants in *RYR1* (Jungbluth et al. 2002, 2004, Monnier et al. 2003) and shows variable penetrance of several symptoms similar to CCD – the most common being muscle weakness. In addition to these similarities to CCD, some individuals with MmD have also experienced MH episodes (Koch et al. 1985).

King-Denborough syndrome (KDS) is another genetic myopathy with a similar phenotype to CCD that has been linked to *RYR1* variants (D'Arcy et al. 2008). It presents with skeletal abnormalities, but upon histological examination of a muscle biopsy, no cores are evident while variable fibre size is common (Dowling et al. 2011).

1.2.4.2 CAUSES OF RyR1 DYSFUNCTION

There are several theories for how *RYR1* mutations can cause a range of neuromuscular disorders, with a focus on four classes of RyR1 defects. The first class – the hyperactive channel – is associated with RyR1 proteins that are overly responsive to pharmacological stimuli and results in MH (Sei et al. 2002, Schiemann et al. 2014). The second class – the leaky channel – causes CCD and is associated with destabilisation of the closed state of the RyR1 channel (Lynch et al. 1999, Tilgen et al. 2001, Zorzato et al. 2003). This results in the slow leak of calcium into the cytoplasm, depleting the SR calcium stores and causing weak muscle contraction upon RyR1 activation. The EC-uncoupled channel is caused by the third class of *RYR1* mutations, associated with a lack of RyR1 response to activation by DHPR as the two proteins are uncoupled (Avila et al. 2001, Dirksen & Avila 2004, Kraeva et al. 2013). Consequently, little calcium is released from the SR which can lead to weak muscle contraction and CCD. The fourth class – RyR1 deficiency – is linked to CCD and MmD and can involve the monoallelic expression of a recessive mutation presenting as a homozygous mutant while being heterozygous at the genomic level (Zhou et al. 2007, Treves et al. 2008, Wilmshurst et al. 2010). Alternatively, the disruption of EC coupling may be caused by a depletion of RyR1 channels in the SR membrane (Attali et al. 2013). Low expression of RyR1 has been reported to result in the concomitant deficiency of DHPR channels and it was hypothesised that the stability of the EC coupling machinery requires the alignment and co-localisation of RyR1 and DHPR (Zhou et al. 2010, 2013).

The theory that a hypoactive RyR1 channel seen in myopathies such as CCD and MmD can become hyperactive in the presence of a trigger is seemingly contradictory; however, this may be partly explained by mutations causing instability of the EC coupling complex. Leaky RyR1, EC-uncoupling and RyR1 deficiency could all lead to the weakening of interactions between DHPR and RyR1 and therefore diminished EC

coupling activity, leading to the formation of cores in the muscle fibres. This is substantiated by the lack of RyR1, mitochondria and glycogen in the cores (Herasse et al. 2007). The RyR1 defect that causes the core phenotype could be hypersensitive to pharmacological stimuli, causing the MH phenotype. This has been seen in the combination p.S71Y+p.N2283H (GenBank accession NP_000531.2) variants in RyR1 seen in a patient with a core myopathy (Zhou et al. 2006). The channel was reported to be unstable as ryanodine binding (indicative of the open state of the channel) was significantly reduced in a heterologous system and myotubes from the patient had an MH-like response to agonists (Zhou et al. 2006).

1.3 CENTRAL CORE DISEASE

A congenital myopathy – later termed central core disease (Greenfield et al. 1958) – was discovered in a family with muscle weakness when a Gomori trichrome stain of their muscle biopsy showed no mitochondrial activity in the central regions of muscle cells (Shy & Magee 1956). CCD is a slowly-progressing or non-progressive myopathy with variable penetrance as the phenotype can range from no observable symptoms to a very severe phenotype, even within the same family (Lynch et al. 1999, Monnier et al. 2000). The disease presents with a wide range of clinical features that typically consist of delayed motor skill development and mild muscle weakness in the proximal muscles of the body that can continue into adulthood. In extreme cases, symptoms can include respiratory problems, skeletal abnormalities and greatly reduced muscle tone. Histological examination of a muscle biopsy of a nine year old patient displaying the classic CCD phenotype is shown in Figure 1.3. The large central cores found in type one muscle fibres as well as the variation in size of these fibres is apparent in Figure 1.3A while the deficiency of type two muscle fibres is apparent in Figure 1.3B. Histological examination of a normal phenotype would be expected to have uniformity in size and staining of type one muscle fibre and approximately equal amounts of the two muscle fibre types.

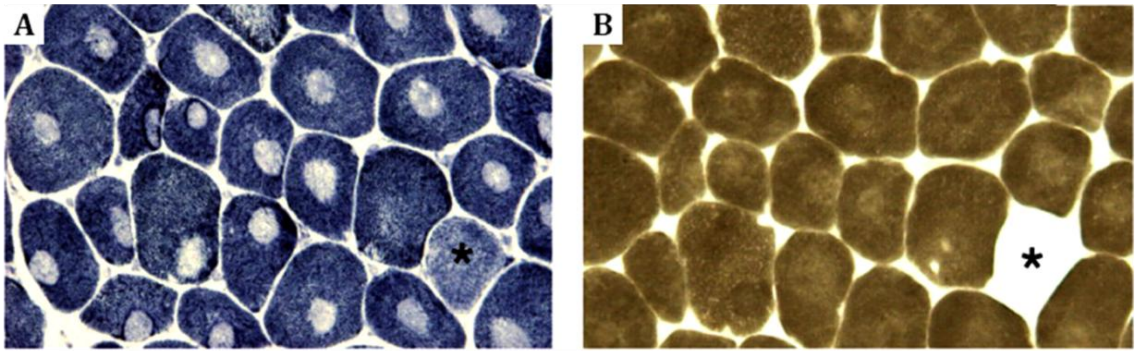

FIGURE 1.3 Histological examination of the classic CCD phenotype

A. The NADH-tetrazolium reductase stain was used to analyse mitochondrial activity. The endogenous mitochondrial enzyme, NADH-dehydrogenase, converts the colourless tetrazolium salt from the stain into an insoluble, coloured formazan compound which can be visualised using microscopy. **B.** Deficiency of type two muscle fibres (indicated by a star) shown by a myosin ATPase stain at pH 4.4. Under acidic conditions, the myosin ATPase of type two muscle fibres (and therefore the conversion of ATP to adenosine diphosphate and inorganic phosphate) is inhibited. This production of inorganic phosphate is indirectly coupled to the production of cobalt sulphide which can be viewed as a brown-black deposit by microscopy.

Central core disease is typically an autosomal dominant disorder, although recessive inheritance of the disease has been reported (Kossugue et al. 2007, Klein et al. 2012). The genetic cause of CCD has thus far been linked to variants in *RYR1* only, with a cluster of variants found in the final 17 exons of the coding sequence of the gene. Although mutations causing CCD have been found outside of this region, a study demonstrated that patients with C-terminal variants in RyR1 had more variable and severe phenotypes compared with those with variants outside the C-terminal region whose most severe symptom was a mild muscle weakness (Wu et al. 2006).

Muscle fibres of patients with amino acid changes in the C-terminal region of RyR1 usually have single cores that are centrally-located, in contrast to the presence of multiple cores per muscle fibre as well as cores on the edges of the muscle fibre seen in cases with amino acid changes in the N-terminal and central regions (Wu et al.

2006). Sewry et al. (2002) discussed two cases where the size and presence of cores seem to develop with age, contributing to the variable phenotype seen with CCD. The first case included two siblings with symptoms of the CCD phenotype, but only the three year old had visible cores under histological staining whereas the four month old had none; the second case was a mother whose cores were large and centrally located – as is the classic phenotype – while the children had much smaller cores. So far, however, no correlation has been found for the number of these cores and the extent of the disease phenotype (Avila et al. 2001, Sewry et al. 2002). This leads to the idea that the presentation of central core disease symptoms may not be a direct result of the presence of cores as previously thought.

1.4 MALIGNANT HYPERTHERMIA

1.4.1 CLINICAL FEATURES

Malignant hyperthermia was discovered as early as 1916, but it was first linked to anaesthesia in 1960 with a report describing a patient who survived an MH episode and had a family history of death as a result of exposure to anaesthesia which seemed to be inherited as a dominant trait (Denborough & Lovell 1960). Malignant hyperthermia (MH) is a pharmacogenetic disorder that predisposes patients to an episode triggered by exposure to depolarising muscle relaxants, volatile anaesthetics, or in rare cases, heat, exercise or stress in what have been termed 'awake episodes' (Groom et al. 2011). It is considered to be a rare disease, with estimates of incidence ranging from 1 in 2000 including all possible cases of MH (Monnier et al. 2002), to 1 in 250,000 including only the fulminant MH cases (Ording 1985). Crisis events resembling malignant hyperthermia have also been seen in animals species, namely pigs, horses and dogs (Rosenberg et al. 2007, Maclennan & Zvaritch 2011). Upon exposure of an MH-susceptible person to a triggering agent, the cytoplasm of the patient's skeletal muscle cells are flooded with calcium from the sarcoplasmic reticulum, causing a sustained muscle contraction. This creates a hypermetabolic state where the cell's reserves of ATP and oxygen are depleted, eventually leading to widespread organ failure and cardiac arrest.

Treatment of an MH episode must commence immediately upon recognition of the symptoms to avoid fatalities, and such an episode could occur both during, and in the period following, exposure to the trigger. Management of MH symptoms includes removing triggering agents, lowering the body temperature and administering dantrolene, a skeletal muscle relaxant. Dantrolene binds the ryanodine receptor in the cytoplasm to stabilise the interactions between the N-terminal and central domains in the closed state, preventing calcium release (Wang et al. 2011). Dantrolene remains the only clinical treatment for MH and has reduced the mortality rate from 80% to around 5% since it was first introduced (Kolb et al. 1982). The best defence against MH, however, is prevention, by identifying people at risk for MH susceptibility and subsequently avoiding known triggers.

1.4.2 DIAGNOSIS OF MALIGNANT HYPERTHERMIA

The symptoms of malignant hyperthermia are highly variable between individuals and similar to other complications from surgery which can lead to misdiagnosis. A standard clinical grading system was devised in 1994 (Larach et al. 1994) which compared the different criteria for diagnosis of MH with different weighting placed on each symptom. In addition to the variety of symptoms, MH has variable penetrance with patients exhibiting no symptoms in several surgeries before having an MH crisis in a subsequent surgery and a higher incidence rate has been reported in children compared to adults (Jurkat-Rott et al. 2000) likely due to their underdeveloped coping mechanisms. The majority of patients with MH have no observable changes in the morphology of their skeletal muscle (Ranklev et al. 1986) and consequently the diagnosis of this disease is problematic.

There are two widely-accepted methods for diagnosis of MH: the in vitro contracture test (IVCT) (EMHG: European Malignant Hyperpyrexia Group 1984, Ording et al. 1997) developed by the European Malignant Hyperthermia Group (EMHG) and the caffeine-halothane contracture test (CHCT) (Larach 1989) modified from the IVCT by the North American Malignant Hyperthermia Group. The IVCT involves a muscle biopsy taken from the patient suspected to have the disease, and the live tissue is then exposed to either caffeine or halothane in incremental doses. If the resultant muscle contracture

is below a certain threshold, the patient can be said to be malignant hyperthermia negative (MHN) and if both agonists cause muscle contracture above the threshold, the patient is characterised as malignant hyperthermia susceptible (MHS). Two additional criteria exist for the IVCT; these are MHS(h) (susceptible to halothane) if the threshold is reached only for halothane or MHS(c) (susceptible to caffeine) if the threshold is reached only for caffeine. Both are treated as MH-susceptible, however, for clinical purposes. Contractures above the threshold for either halothane or caffeine are both classified as MHS under the CHCT guidelines. When classifying a muscle biopsy, the IVCT protocol has 94% specificity and 99% sensitivity including the MHS(h) and MHS(c) classifications (Ording et al. 1997) while the CHCT protocol has a specificity of 78% and sensitivity of 97% (Allen et al. 1998). To avoid the potentially fatal error of classifying an MHS patient as MH negative, the tests are designed to produce a small number of false-positive results to err on the side of caution. IVCT is the gold-standard for diagnostic testing; however, results have been shown to contradict the presence of known MH-causative mutations in a very small number of cases. A study that investigated the concordance of genotypes with IVCT results found that in a cohort of 109 individuals, one false-negative result and two false-positive results were found (Brandt et al. 1999). Furthermore, the muscle biopsy requires minor surgery which is both invasive and expensive and the muscle removed does not grow back.

1.4.3 CHARACTERISATION OF VARIANTS

There are stringent criteria for classifying MH-causative mutations established by the European Malignant Hyperthermia Group. These include co-segregation of the disease and the variant in two independent pedigrees; absence of the variant in 100 MHN patients; and functional characterisation of the variant in an appropriate test system (Müller 2003).

1.4.3.1 IDENTIFICATION OF *RYR1* VARIANTS

To compensate for the large size of *RYR1*, different methods for the detection of variants have been utilised, the most recent being exome sequencing (Gonsalves et al. 2013, Kim et al. 2013). Whole exome sequencing can cover over 95% of the exons in the human genome while targeted exome sequencing covering a selected subset of

genes has been shown to yield significant results (Ku et al. 2012, Schiemann et al. 2013). Exome sequencing is a high-throughput method for the discovery of variants linked to any number of diseases and as a result, functionally uncharacterised variants in *RYR1* are often found in individuals whose MH susceptibility is unknown. This has little value in the diagnosis of MH due to the large number of variants of unknown significance that are identified. The increasing use of whole exome sequencing by clinicians with an incomplete understanding of the genetics and pathophysiology of MH/CCD and related disorders is likely to result in many individuals being labelled MH susceptible regardless of whether a variant has been shown to be causative of altered skeletal muscle calcium homeostasis. Because of this, results of exome analysis must be treated with appropriate caution. While there are a number of pathogenicity prediction programmes available, none have been trained on MH/CCD susceptibility, and at best provide only a rough estimate of the likelihood of a variant being pathogenic. It is therefore imperative that functional analysis of variants be carried out.

Other methods use polymerase chain reaction (PCR) to amplify the regions of DNA of interest followed by examination of the DNA, which can include: single strand conformation analysis, which is one of the simplest methods for the detection of variants (Girard et al. 2001, Ducreux et al. 2004); high resolution melting with which Broman et al. (2011) achieved 99.2% specificity and reduced the volume of sequencing by a reported 79%; and the screening of three mutation 'hotspots' contained within the N-terminal, central and C-terminal regions which are now thought to be the result of screening bias in those regions (McCarthy et al. 2000, Robinson et al. 2006).

1.4.3.2 METHODS TO DETECT RYR1 ACTIVITY

Once a variant is found to segregate with the disease, it is then tested in the presence of electrical stimuli or a pharmacological agent such as caffeine or 4-chloro-*m*-cresol to ensure the mutation is actually causing dysfunctional calcium homeostasis. Generally, mammalian cells containing RyR1 variants are exposed to incremental amounts of an agonist and the activity of the channel in the presence and absence of the agonist is measured and compared to that of cells containing wild type RyR1. As MH is thought

to be caused by a hyperactive calcium channel, it is expected that RyR1 carrying a causative amino acid change would activate at a lower concentration of agonist than a normally-functioning channel. Most systems measure the amount of calcium released using fluorescent calcium indicators which are highly specific and have a low level of background interference making them suitable for use in living cells, while alternative methods determine the conductivity of RyR1 itself. Ligands may be used to determine the state of the channel in response to agonists, such as radiolabeled ryanodine (Mickelson et al. 1990, Sato et al. 2010). Ryanodine preferentially binds the open state of RyR1 and so the degree to which RyR1 opens in response to an agonist can be determined by the size of the radioactive signal, although this can only be performed on extracted proteins *in vitro*. Another means to measure RyR1 activity is the patch-clamp method which measures a voltage signal transduced through the channel itself. This involves the incorporation of microsomal membranes containing RyR1 into a membrane separating two chambers; if upon addition of an agonist to one of the chambers, the channel opens, a voltage signal will be passed between the chambers which can be measured. This can be used to establish both the opening of the channel at different concentrations of agonist and the length of time the channel is open (O'Brien et al. 2002) although this system cannot be used for live cells as RyR1 is located intracellularly.

1.4.3.3 *EX VIVO* TESTING OF TISSUE SAMPLES

Tissue directly from the patient can be used to test for MH susceptibility *ex vivo*, which may be used in addition to or in lieu of contracture tests. *Ex vivo* tests can only be used when the results from patients of different pedigrees with the same variant can be compared as there are numerous variables in the genetic makeup of the patient which cannot be measured. SR microsomes from muscle biopsy are versatile and able to be used in a variety of tests, evidenced by their being the only preparation to be used in patch-clamp experiments *ex vivo*. They can be extracted from a range of tissue types and so their value is dependent on their tissue of origin (Diaz-Sylvester et al. 2008). Primary myotubes represent immature skeletal muscle fibres which contain all machinery required for skeletal muscle calcium release and are used to give the best estimation of the normal muscle cell environment (Gschwend et al. 1999). The use of

B-lymphoblastoid cells to test the function of RyR1 is relatively non-invasive, as they can be extracted from blood and immortalised (Tilgen et al. 2001). The major calcium storage organelle in B-lymphocytes is the ER rather than the SR and it contains two calcium release channels, RyR1 and the inositol triphosphate receptor (IP3R). Specificity for RyR1 function in this cell system can be determined using IP3R inhibitors. DHPR proteins have been shown to be expressed in other cells of the immune system but it is currently unknown if they are expressed in B-lymphocytes and therefore the mechanism of calcium release in this cell system remains obscure (Gomes et al. 2004, Vukcevic et al. 2008).

1.4.3.4 *IN VITRO* FUNCTIONAL ANALYSIS OF *RYR1* VARIANTS

Expression of recombinant mutant *RYR1* complementary DNA (cDNA) – either rabbit or human – in a cell line which lacks muscle proteins such as human embryonic kidney 293 (HEK-293) cells is a standard assay system. A mutant homozygous system can be used or the mutant *RYR1* cDNA can be co-expressed with the wild type *RYR1* cDNA to give a heterozygous system (Xu et al. 2008); a tetramer made of two different subunits could form in several different combinations, however, giving this method variability. In addition, the transfection and expression of two plasmids containing very large cDNA inserts in the same cell is technically challenging. The advantage of the heterologous system is the ability to directly compare the mutant and wild type RyR1 function without interference from the genetic background of the patient. However, the process of creating mutant cDNAs is lengthy and accessory proteins such as the DHPR which could provide a clearer understanding of any change to channel function are not present in this system. The expression of both endogenous skeletal and cardiac ryanodine receptors was found by western blotting and reverse-transcription PCR in a 1998 study which confirmed their ability to release calcium in the presence of caffeine (Querfurth et al. 1998). These findings were later rejected as the intracellular calcium release in response to caffeine was found to be independent of ryanodine receptor function in HEK-293 cells and the expression of RyR1 was found to be too low for detection by western blotting or ryanodine binding assays (Tong et al. 1999a). The non-muscle cell background has been used numerous times to produce reputable results (Tong et al. 1997, Kraeva et al. 2013, Sato et al. 2013). Functional

characterisation of the p.R2452W (GenBank accession NP_000531.2) RyR1 substitution by Roesl et al. (2014) reported the variant to be MH-causative in a heterologous *in vitro* system which confirmed the altered calcium homeostasis found in B-lymphocytes and myotubes from patients carrying the variant tested *ex vivo*. On rare occasions, however, studies in a non-muscle cell system can produce results that are divergent from that of studies that use muscle cell systems (Avila et al. 2001). *RYR1* cDNA expressed in dyspedic (*RYR1*-null) mouse myotubes is a more physiologically relevant system to test the behaviour of the protein compared to HEK-293 cells as they contain all machinery required for EC coupling excluding RyR1, although this system is considerably more technically challenging to use.

1.4.3.5 *IN VIVO* TESTING OF *RYR1* VARIANTS IN A MOUSE MODEL

The most physiologically relevant model of malignant hyperthermia when investigating RyR1 variants is currently the mouse model. Knock-in mice are created in an *RYR1*-null mouse (Takeshima et al. 1994) by introducing a variant form of *RYR1* into the genome of the mouse by targeted mutagenesis. Functional characterisation of RyR1 variants using knock-in mice is a valuable tool as the introduction of the variant *RYR1* allele is targeted to the location of endogenous *RYR1*, its expression levels and patterns are the same as the wild type allele it replaced. Dose-dependent phenotypes can also be examined as mice both heterozygous and homozygous for the variant *RYR1* allele can be created which could prove useful for studying the effects of recessive *RYR1* variants. For example, the R163C RyR1 mutation linked to MH has been created in the mouse model and used to analyse a variety of phenotypic characteristics (Yang et al., 2006). In this study, the sensitivities of the mutant mice to stimulants such as halothane and heat stress were tested in both heterozygous and homozygous models, as was the ability of dantrolene to negate these effects, providing a complete representation of the mutation in a physiological system (Yang et al. 2006). Despite these advantages, there are huge costs involved in creating a knock-in mouse, limiting the use of them as a diagnostic tool. As a result, there are presently only four RyR1 mutations that have been examined in this way and these include the R163C mutation mentioned earlier, Y522S, T4826I and I4898T.

The well-characterised I4898T RyR1 mutation has been linked solely to central core disease and has been observed to cause leakage of calcium in several cell systems, namely transfected HEK-293 cells (Lynch et al. 1999), B-lymphocytes extracted from heterozygous carriers of the mutation (Tilgen et al. 2001) and myotube cultures from individuals heterozygous for the mutation (Ducreux et al. 2004). These findings were partially confirmed by the *in vivo* analysis of I4898T knock-in mice, where heterozygous mice were observed to have reduced 4-C*m*C-stimulated and electrically-evoked calcium release compared with wild type mice despite the comparable levels of calcium observed in the sarcoplasmic reticulum (Loy et al. 2011). Homozygous mice, on the other hand, were non-viable which is a likely result of the loss of EC coupling function observed in cultured myotubes from these mice (Zvaritch et al. 2007). These mouse studies would suggest that the I4898T mutation is of the class of RyR1 mutation that causes CCD by reduced EC coupling, which is at odds with the phenotypes observed in previous studies. This is suggestive of not only the complex nature of CCD and MH but also of the care that must be taken when inferring the molecular basis of these neuromuscular disorders.

A dominant RyR1 mutation linked solely to malignant hyperthermia that was analysed in a mouse model was the T4826I mutation, with which mice demonstrated MH symptoms in response to heat stress and halothane exposure (Yuen et al. 2012). The severity of each MH response was not only dependent on whether the mice were heterozygous or homozygous for the mutation, which was as expected, but also was observed to be sex-dependent (Yuen et al. 2012) which was surprising as no link between severity of MH and gender has been observed in the human population as yet. The Y522S RyR1 mutation, linked to both dominant MH and CCD, was also examined in a mouse model in which heterozygous mice were found to be sensitive to both anaesthetics and heat stress (Chelu et al. 2005). Although no core myopathy was observed with histological analysis of muscle fibres from Y522S heterozygous mice, homozygous mice were found to have pronounced skeletal abnormalities (Chelu et al. 2005). The results of these two studies confirm the widely-held belief that a variety of factors, including RyR1 function, contribute to the phenotypes of MH and CCD to create highly-variable disorders.

1.5 PROJECT OUTLINE

1.5.1 SIGNIFICANCE OF PROJECT

Theoretically, a genetic test would be a non-invasive and relatively inexpensive alternative to contracture testing. The size of the *RYR1* gene is considerable, however, and a large array of accessory proteins play a role in calcium homeostasis of skeletal muscle, making a comprehensive genetic test both complicated and expensive. Over 300 variants in *RYR1* have been linked to MH through segregation analysis, accounting for around 70% of MHS patients. Currently, there are only two *CACNA1S* mutations and 34 *RYR1* mutations that have met the guidelines set by the EMHG for classification as being MH-causative and are therefore able to be used for DNA-based diagnosis of the disease. Six of those *RYR1* mutations correspond to amino acid changes in the C-terminal region of RyR1 which is significant as this region contributes less than 10% of the amino acid residues in the protein. This is likely due to the importance of the transmembrane region in the functionality of the channel, evidenced by its highly-conserved amino acid sequence. In addition, most variants linked to CCD are also located in the C-terminal region of RyR1 (Davis et al. 2003) and therefore the comparison of the genetic cause of these two neuromuscular disorders should be focused on variants found within this region. This research project aims to functionally characterise five C-terminal RyR1 variants, of which three are associated with CCD, one is linked to both MH and CCD and one is associated with an unclassified myopathy.

1.5.2 HYPOTHESIS OF STUDY

C-terminal *RYR1* variants – p.M4640I, p.V4849I, p.F4857S, p.R4861H, p.D4918N (GenBank accession NP_000531.2) – linked to malignant hyperthermia and/or central core disease or other myopathy alter calcium release from the endoplasmic reticulum in response to the RyR1-specific agonist 4-chloro-*m*-cresol.

1.5.3 AIMS OF STUDY

The key objectives of this project are as follows:

- Introduce variants into human *RYR1* cDNA and sub-clone into full-length *RYR1* cDNAs;
- Express *RYR1* cDNAs in a mammalian cell line;
- Confirm cDNA expression with microscopy and immunoblotting;
- Compare calcium release of wild type and variant-containing *RYR1*-transfected HEK-293T cells;
- Compare calcium release of B-lymphocytes from members of a family with a CCD-linked variant with the calcium release of the RyR1 variant in the recombinant system.

CHAPTER TWO: Materials and Methods

2.1 MATERIALS

TABLE 2.1 List of materials used and suppliers

SUPPLIER	MATERIAL
Anchor Fonterra Brands NZ Ltd Greenlane Auckland New Zealand	Trim milk powder.
Axygen Corning Life Sciences Union City California 94587 United States of America	T-200-Y pipette tips, T-1000-B pipette tips, T-300 pipette tips, 1.7 mL Eppendorf micro-centrifuge tubes and 0.6 mL Eppendorf micro-centrifuge tubes.
BD Biosciences San Jose California 95131 United States of America	Tuberculin syringes, Bacto Yeast Extract and Bacto Tryptone.
Bio-Rad Laboratories Ltd Albany Auckland New Zealand	40% Acrylamide/Bis solution, 29:1, Mini Protean 3 System, Precision Plus Protein Dual Colour Standards and DMSO (for PCR).
Carl Roth GmbH & Co. Schoemperlenstr. 1-5 76185 Karlsruhe Germany	HEPES.
ECP Ltd. Birkenhead Auckland 0746 New Zealand	Glacial acetic acid.
GE Healthcare Life Sciences Pittsburgh Pennsylvania 15264-3065 Unites States of America	3MM Whatman chromatography paper.
Gibco Life Technologies NZ Ltd. Penrose Auckland 1006 New Zealand	Opti-Mem I, Dulbecco's Modified Eagle's Medium, Foetal Bovine Serum and penicillin/streptomycin.

Gold Biotechnology St. Louis Missouri 63132 United States of America	Tris base.
Greiner Bio-One Maybachstr. 2 72636 Frickenhausen Germany	CellStar 50 mL Falcon tubes, CellStar 15 mL falcon tubes and Cryo-S cryotubes.
Invitrogen Life Technologies NZ Ltd. Penrose Auckland 1006 New Zealand	PureLink HiPure Plasmid Filter Midiprep kit, Fura-2 AM, ChargeSwitch Pro Plasmid Miniprep kit, PureLink Quick Gel Extraction kit, LB broth base, T4 DNA Ligase, 5x T4 DNA Ligase Buffer, 1 kb Plus DNA Ladder, ProLong Gold antifade reagent with DAPI and 10X gel loading dye.
Integrated DNA Technologies Coralville Iowa 52241 United States of America	Custom DNA oligonucleotides.
Jackson ImmunoResearch West Grove Pennsylvania 19390 United States of America	Anti-rabbit Tetramethylrhodamine isothiocyanate produced in goat (TRITC, Cat. No. 111-025-045).
Kapa Biosystems Wilmington Massachusetts 01887 United States of America	2x KAPA HiFi HotStart ReadyMix.
Kimberley-Clark Milsons Point New South Wales 1565 Australia	Kimtech Kimwipes.
Merck Kenilworth New Jersey 07033 United States of America	R-250 Coomassie Brilliant Blue, Glucose, KCl, Na_2HPO_4, KH_2PO_4, SDS and APS.
New England Biolabs Ipswich Massachusetts 01938-2723 United States of America	Purified BSA, Restriction endonucleases and restriction endonuclease buffers.
Pall Corporation Pukete Industrial Estate Hamilton 3200 New Zealand	BioTrace PVDF transfer membrane and AcroCap Filter Unit.

Promega Mt. Wellington Auckland New Zealand	FuGENE HD Transfection Reagent, Wizard SV Gel and PCR Clean-Up System, Wizard Genomic DNA Purification kit and HRP-conjugated anti-mouse antibody (Cat. No. W402B).
Pure Science Porirua 5022 New Zealand	99% Glycerol.
Roche Newmarket Auckland 1023 New Zealand	FuGENE 6 Transfection Reagent, BM Chemiluminescence Blotting Substrate (POD), cOmplete Mini EDTA-free protease inhibitor cocktail tablets, LightCycler 480 High Resolution Melting Master (Cat. No. 04909631001), Restriction endonucleases and restriction endonuclease buffers.
Sigma-Aldrich Auckland 1030 New Zealand	Ampicillin, $CaCl_2$, Pluronic F-127, Tween 20, Trypan blue solution, DMSO (for cell culture), EGTA, Bromophenol blue, $MgCl_2$, β-mercaptoethanol, TEMED, BSA, Triton X-100, Anti-Ryanodine Receptor antibody produced in mouse (34C, Cat. No. R129), Anti-Protein Disulphide Isomerase produced in rabbit (α-PDI, Cat. No. P7496), Anti-tubulin antibody produced in mouse (Cat. No. T9026), Anti-mouse Fluorescein isothiocyanate produced in goat (FITC, Cat. No. F8521), NaCl, $MgSO_4$, $NaHCO_3$, Greiner UV-Star 96 well plates and Poly-D-lysine hydrobromide.
Thermo Fisher Scientific Inc. Waltham Massachusetts 02451 United States of America	T25 Nunc flasks, T75 Nunc flasks, EDTA, Absolute Ethanol, Methanol, Petri dishes, Bacteriological Agar, Agarose, Glycine and Nunc Lab-Tek chamber slides.
VWR International Radnor Corporate Centre Radnor Pennsylvania United States of America	4-Chloro-*m*-cresol, Ethidium bromide and 0.2 mL PCR tubes.
Zymo Research Irvine California 92614 United States of America	Zymo Clean Gel DNA Recovery Kit and DNA Clean & Concentrator kit.

2.2 MOLECULAR CLONING OF *RYR1* VARIANTS

2.2.1 SITE-DIRECTED MUTAGENESIS

Mutagenesis was carried out by PCR-amplification of 70 ng of a 5.3 kb pBSH+ plasmid (appendix A) using the 2X Kapa HiFi HotStart Readymix diluted 4X supplemented with 3% dimethyl sulfoxide (DMSO). Complementary primer pairs from Integrated DNA Technologies (table 2.1) containing the variant to be introduced were used in a method based on the Stratagene QuikChange kit described by Papworth et al. (1996). Cycling conditions were 98°C for 30 seconds; 95°C for two minutes; 57°C for 30 seconds; 72°C for six minutes; 72°C for five minutes; and steps 2-4 were repeated 17 times. The PCR products were digested with ten units of restriction endonuclease DpnI (New England BioLabs) and buffer according to the manufacturer's instructions in a total volume of 30 µL to remove all methylated template DNA, creating a homogeneous mutant population.

TABLE 2.2 Mutagenic primers used for introduction of variants

VARIANT	FORWARD PRIMER SEQUENCE	REVERSE PRIMER SEQUENCE
c.14570T>C * **p.F4857S** †	5'-CACCGTGGTGGCCTCCAACTTC TTCCGC-3'	5'-CGCCTTCTTCAACCTCCGGTGG TGCCAC-3'
c.14582G>A * **p.R4861H** †	5'-CCTTCAACTTCTTCCACAAGTTC TACAACAA-3'	5'-TTGTTGTAGAACTTGTGGAAG AAGTTGAAGG-3'
c.14752G>A * **p.D4918N** †	5'-ACAGGGTGGTCTTCAACATCAC CTTCTTCTT-3'	5'-AAGAAGAAGGTGATGTTGAAG ACCACCCTGT-3'

* GenBank accession NM_000540.2.

† GenBank accession NP_000531.2.

2.2.2 ELECTROPHORESIS OF DNA FRAGMENTS

DNA fragments were separated by 0.7 % gel electrophoresis agarose for DNA fragments over 8 kb and 1% agarose for DNA fragments under 8 kb in TAE buffer (40 mM Tris-acetate, 1 mM EDTA, pH 8.0) containing 0.2 µg mL^{-1} ethidium bromide. DNA samples were loaded onto the agarose gel with 6x loading dye (New England BioLabs, Cat. No. B7024S) alongside 5 µL of 50 ng $µL^{-1}$ 1 kb+ DNA ladder as a size control and electrophoresis was carried out at 90 V for 1 hour in TAE buffer. The DNA was visualised under ultraviolet (UV) light.

2.2.3 SANGER SEQUENCING OF DNA

At each cloning step, sequencing was used to confirm the presence of the introduced variant. Sanger DNA sequencing was carried out on 400 ng plasmid DNA with 4 pmol primer using a capillary ABI3730 Genetic Analyzer with BigDye™ Terminator Version 3.1 chemistry at the Massey Genome Service in Palmerston North, New Zealand.

2.2.4 RESTRICTION ENDONUCLEASE DIGESTION

For both sub-cloning purposes and characterisation of plasmids, DNA was digested with restriction endonucleases (according to the manufacturer's instructions). This was usually carried out with 300 ng plasmid DNA, 10 units of each endonuclease and 2 µL 10x buffer in a volume of 20 µL for one hour at 37°C. DNA fragments were excised from the agarose gel and purified using the Wizard SV gel and PCR clean-up system when needed for subsequent cloning steps.

2.2.5 LIGATION OF DNA FRAGMENTS

Each cloning step required the insert containing the variant to be ligated into a pBluescript or pcDNA3.1+ vector using directional cloning. The molar ratio of insert DNA to vector DNA was between 3:1 and 6:1. Usually a total of 100 ng plasmid+insert DNA was ligated together with 1 unit ligase and 4 µL 5X ligase buffer in a total volume of 20 µL according to the manufacturer's instructions for 4 hours to overnight at 22°C.

2.2.6 TRANSFORMATION OF DNA INTO BACTERIA

DH5 alpha *Escherichia coli* (*E. coli*) grown in Luria Bertani (LB) broth (1% Peptone, 0.5% yeast extract, 0.5% NaCl) supplemented with 0.1 mg mL^{-1} ampicillin were made competent by incubation in ice-cold 0.1 M $CaCl_2$ overnight and then stored in 80 mM $CaCl_2$ containing 10% glycerol at -80°C. Plasmid DNA was added to 100 µL competent cells on ice and left for 20 minutes, before being heat-shocked at 42°C for 90 seconds. After a brief period on ice to recover, the cells were incubated with 900 µL of SOC medium (2% bacto-tryptone, 0.5% bacto-yeast extract, 10 mM NaCl, 2.5 mM KCl, 10 mM $MgCl_2$, 10 mM $MgSO_4$, 20 mM glucose) for 1 ½ hours at 37°C with agitation at 220 rpm. Cells were then collected by centrifugation at 2000 g for three minutes and grown on Luria Bertani-Agar plates containing 0.1 mg mL^{-1} ampicillin at 37°C overnight.

2.2.7 INOCULATION OF BROTH WITH BACTERIA

For the extraction of less than 10 µg of plasmid, single colonies were grown in 5 mL LB broth containing 0.1 mg mL^{-1} ampicillin at 37°C with agitation at 220 rpm for 16 hours. For the extraction of greater than 10 µg of plasmid, single colonies were grown in 100 mL LB broth containing 0.1 mg mL^{-1} ampicillin at 30°C with agitation at 220 rpm for 24 hours. Cell growth was observed visually through the glass tube or flask they were grown in. Plasmid DNA was prepared using either the Invitrogen ChargeSwitch-Pro Plasmid Miniprep Kit (Cat. No. CS30050) for restriction endonuclease digestion and DNA sequencing or the Invitrogen PureLink HiPure Plasmid Filter Midiprep Kit (Cat. No. K2100-14) for transfection of mammalian cells. These kits use an ion exchange mechanism to bind plasmid DNA to the column at a low pH and subsequently elute it with a solution with a higher pH. The DNA was then quantified by ultraviolet (A260) spectrophotometry using a Nanodrop 1000 spectrophotometer (Thermo Scientific).

2.3 HEK-293T CELLS

Human embryonic kidney 293 cells containing the SV40 large T-antigen (HEK-293T cells) were used to directly compare the activation of transiently expressed wild-type and mutant RyR1.

2.3.1 CRYOSTORAGE OF HEK-293T CELLS

Cells at 90% confluence were washed off the bottom of the T25 flask with foetal bovine serum (FBS) and collected by centrifugation at 200 g for five minutes. The pellet was resuspended in 1 mL FBS containing 10% DMSO and then dispensed into cryotubes. These were cooled slowly to -80°C before being stored long-term in liquid nitrogen.

2.3.2 REANIMATION OF HEK-293T CELLS

Cell lines stored in liquid nitrogen were thawed quickly at 37°C, resuspended in 5 mL complete Dulbecco's Modified Eagle Medium (complete DMEM: incomplete DMEM supplemented with 0.5% penicillin/streptomycin, 10% FBS) and then collected by centrifugation at 200 g for five minutes. Cell pellets were resuspended in 5 mL complete DMEM and grown in a T25 flask placed horizontally at 37°C in a humidified atmosphere containing 5% CO_2.

2.3.3 PASSAGING HEK-293T CELLS

Medium on proliferating cells was replaced every 2 – 3 days. When nearing confluence as measured by eye with an inverted optical microscope, cells were washed off the bottom of the flask with 5 mL complete DMEM. Half a mL of resuspended cells were seeded into a new T25 flask with 4.5 mL fresh complete DMEM which was placed horizontally at 37°C in a humidified atmosphere containing 5% CO_2.

2.3.4 ANALYSIS OF RyR1 EXPRESSION IN HEK-293T CELLS

HEK-293T cells were transiently transfected with pcRYR1 cDNA or empty pcDNA3.1+ plasmids for calcium release assays and the level of expression of each RyR1 variant in this cell line was determined by western blotting.

2.3.4.1 TRANSIENT TRANSFECTION FOR PROTEIN EXTRACTION

Cells were grown in a T25 flask horizontally to 90% confluence in 5 mL complete DMEM. Two hours prior to the transfection, the medium on the cells was replaced with 3 mL complete DMEM. A transfection mix of 6 µg plasmid DNA, 24 µL FuGENE HD

(formulated to work at high cell densities) and incomplete DMEM to a total volume of 300 µL was added to the flask after incubation at room temperature for 30 minutes and then the cells were left at 37°C in a humidified atmosphere containing 5% CO_2. Twenty four hours after transfection, 2 mL complete DMEM was added to the flask. Forty eight hours after transfection, the medium on the cells was replaced with 5 mL complete DMEM. The cells were ready for use 72 hours after transfection.

2.3.4.2 EXTRACTION OF TOTAL PROTEIN FROM HEK-293T

Three days after HEK-293T cells were transfected with plasmid DNA in a T25 flask, the cells were washed off the bottom of the flask with 5 mL PBS, collected by centrifugation at 200 g and then the pellet was resuspended in 150 µL cell lysis buffer (0.1M Tris-HCl pH 7.8, 0.5% Triton X-100) and 20 µL 7x cOmplete Mini EDTA-free protease inhibitor in a 1.7 mL micro-centrifuge tube. The mix was centrifuged at 16,000 g at 4°C for 30 minutes, the supernatant collected in a new micro-centrifuge tube and then centrifuged again at 16,000 g at 4°C for one hour. The supernatant was placed in a fresh tube, the concentration of protein was determined by UV spectrophotometry (A280) using a Nanodrop 1000 spectrophotometer (Thermo Scientific) and then the sample was kept at -80°C until use.

2.3.4.3 SDS POLYACRYLAMIDE GEL ELECTROPHORESIS (SDS-PAGE)

Sixteen µL of each total protein sample (~17 mg mL^{-1}) was mixed with 4 µL 5X sample buffer (60 mM Tris-HCl pH 6.8, 25% glycerol, 2% sodium dodecyl sulphate (SDS), 0.1% bromophenol blue, 5% β-mercaptoethanol) and loaded alongside 7 µL BioRad Precision Plus protein standard on a 4% SDS-PAGE stacking gel (4% acrylamide, 0.125 M Tris-HCl pH 6.8, 0.1% SDS, 0.1% ammonium persulfate (APS), 0.4% tetramethylethylenediamine (TEMED)). Proteins were resolved using a 7.5 % SDS-PAGE separating gel (7.55% acrylamide, 0.37 M Tris-HCl pH 8.8, 0.1% SDS, 0.1% APS, 0.1% TEMED). The protein gel was immersed in running buffer (25 mM Tris, 0.19 M Glycine, 0.1% SDS) and separated by electrophoresis for two hours at 120 V using the Mini PROTEAN electrophoresis system (Bio-Rad).

2.3.4.4 WESTERN BLOT ANALYSIS OF SDS-PAGE GEL

A polyvinylidene fluoride (PVDF) membrane (0.45 μM) trimmed to size was activated by immersion in methanol for 30 seconds and then rinsed in water for one minute. The PVDF membrane and an SDS polyacrylamide gel containing protein samples separated by electrophoresis were soaked in transfer buffer (15.6 mM Tris, 0.12 M Glycine, 10% MeOH) for ten minutes. The membrane was placed on top of the gel and both were sandwiched between four pieces of 3MM Whatman filter paper trimmed to size and two sponges in the blotting cassette and then immersed in ice-cold transfer buffer. The proteins contained within the SDS polyacrylamide gel were transferred to the PVDF membrane at 70 mA for 20 hours at 4°C. The amount of protein that successfully transferred to the membrane was visualised by staining the gel with Coomassie blue solution (1.2 mM Coomassie brilliant blue, 45% methanol, 10% glacial acetic acid) for five minutes followed by washing in destain solution (10% methanol, 10% glacial acetic acid) for three hours.

After the transfer, the membrane was blocked in 10 mL 5% skim milk in TBST (50 mM Tris, 0.15 M NaCl, 0.1% Tween-20, pH 7.6) for three hours at room temperature with gentle agitation before being cut in half to separate the 565 kDa RyR1 from the 50 kDa alpha tubulin (α-tubulin). The membrane section with the higher molecular weight proteins was incubated with mouse 34C primary antibody diluted 1:1000 in 5 mL 2.5% skim milk in TBST for detection of RyR1. The membrane section with the lower molecular weight proteins was incubated with mouse anti-α-tubulin primary antibody diluted 1:5000 in 5 mL 2.5% skim milk in TBST for detection of α-tubulin as a protein loading control. These were incubated for 16 hours at 4°C with gentle agitation and then twenty minutes at room temperature with agitation before being washed in 10 mL TBST. They were then incubated with horseradish peroxidase-conjugated anti-mouse secondary antibody diluted 1:5000 in 5 mL 2.5% skim milk in TBST for one hour at room temperature with gentle agitation before being washed in 10 mL TBST.

Roche chemiluminescence blotting substrate (Cat. No. 11 500 708 011) was prepared by mixing 5 mL Luminescence substrate solution A with 50 μL Starting solution B. This was applied to both membranes for one minute before being removed and the

membrane held between two transparent films. The proteins were visualised using an X-ray developer after exposing the X-ray film to the membrane for 15 – 30 seconds (dependent on signal strength).

2.3.5 ANALYSIS OF RyR1 LOCALISATION IN HEK-293T

HEK-293T cells were transiently transfected with pcRYR1 cDNA or pcDNA3.1+ plasmids for assays measuring calcium release from the ER and the localisation of each RyR1 variant in the cells was determined by immunofluorescence.

2.3.5.1 TRANSIENT TRANSFECTION OF HEK-293T

HEK-293T cells were grown to 20% confluence in a 4-chamber slide coated with 0.1 mg mL^{-1} poly-D-lysine in 1 mL complete DMEM. Two hours prior to the transfection, the medium on the cells was replaced with 600 µL complete DMEM. A transfection mix of 1 µg plasmid DNA, 3 µL FuGENE 6 (formulated to work at low cell densities) and incomplete DMEM to a total volume of 50 µL was added to each chamber after incubation at room temperature for 30 minutes and then the cells were left at 37°C in a humidified atmosphere containing 5% CO_2. Twenty four hours after transfection, 600 µL complete DMEM was added to each chamber. Forty eight hours after transfection, the medium on the cells was replaced with 1 mL complete DMEM. The cells were ready for use 72 hours after transfection.

2.3.5.2 IMMUNOFLUORESCENCE IMAGING OF HEK-293T CELLS

Three days after HEK-293T cells were transfected with plasmid DNA in a four-chamber slide, the medium was replaced with 200 µL phosphate-buffered saline (PBS: 137 mM NaCl, 2.7 mM KCl, 10 mM Na_2HPO_4, 1.8 mM KH_2PO_4). The cells were then fixed with 250 µL PBS containing 2% paraformaldehyde for 15 minutes which was then replaced with 200 µL PBS. Cells were washed twice more with 200 µL PBS. The cells were then permeabilised with 250 µL PBS containing 0.1% Triton-X-100 for five minutes which was then replaced with 200 µL PBS. Cells were washed twice more with 200 µL PBS. The chambers were blocked with 250 µL PBS containing 5% bovine serum albumin (BSA) and 0.5% Tween-20 for 30 minutes with gentle agitation before an overnight incubation with 250 µL PBS containing primary antibodies at 4°C for 16 hours. Each

chamber was incubated with mouse 34C antibody diluted 1:1000 for detection of RyR1 and mouse anti-protein disulfide isomerise (anti-PDI) antibody diluted 1:1000 for detection of the endoplasmic reticulum.

The antibodies were then replaced with 200 µL PBS and the cells washed twice with 200 µL PBS. The cells were then incubated with 250 µL PBS containing goat anti-mouse fluorescein isothiocyanate (FITC) secondary antibody (diluted 1:200) for detection of RyR1 and goat anti-rabbit tetramethylrhodamine (TRITC) secondary antibody (diluted 1:200) for detection of the endoplasmic reticulum. The antibodies were then replaced with 200 µL PBS and the cells were washed twice with 200 µL PBS. The chambers were removed from the slide and a coverslip applied with 7 µL ProLong Gold AntiFade mounting solution containing the fluorescent DNA stain DAPI (4',6-diamidino-2-phenylindole) for detection of nuclei. This was left to cure for 24 hours in the dark before the coverslip was sealed and the cells visualised using a Leica SP5 DM6000B Scanning Confocal Microscope at 1260 X magnification.

2.3.6 RyR1 ACTIVATION IN HEK-293T

2.3.6.1 TRANSIENT TRANSFECTION FOR CALCIUM RELEASE ASSAYS

HEK-293T cells were grown in a UV-transparent 96-well plate coated with 0.1 mg mL^{-1} poly-D-lysine to 90% confluence in 400 µL complete DMEM. Two hours prior to the transfection, the medium on the cells was replaced with 200 µL complete DMEM. A transfection mix of 300 ng plasmid DNA, 1 µL FuGENE HD (formulated to work at high cell densities) and incomplete DMEM to a total volume of 10 µL was added to each chamber after incubation at room temperature for 30 minutes and then the cells were left at 37°C in a humidified atmosphere containing 5% CO_2. Twenty four hours after transfection, aliquots of 200 µL complete DMEM were added to each chamber. Forty eight hours after transfection, the medium on the cells was replaced with 400 µL complete DMEM. The cells were ready for use 72 hours after transfection.

2.3.6.2 CALCIUM RELEASE ASSAYS IN HEK-293T CELLS

Three days after HEK-293T cells were transfected with DNA in a UV-transparent 96-well plate the medium on the cells was replaced with 100 µL balanced salt solution

(BSS) buffer (1 mM $MgCl_2$, 0.14 M NaCl, 2.8 mM KCl, 10 mM HEPES pH 7.3) containing 2 mM $CaCl_2$ at 37°C. These were then incubated in 100 µL BSS buffer containing 2 mM $CaCl_2$, 2 µM Fura2-AM and 0.01% Pluronic F-127 per well for one hour at 37°C in the dark. This was then replaced with 100 µL BSS buffer containing 2 mM $CaCl_2$ at 37°C which was then replaced with 100 µL BSS buffer at 37°C.

Activation of the RyR1 using 4-C*m*C as a specific agonist was measured by the change in the fluorescence emission ratio at 510 nm when excited by wavelengths 340 nm and 380 nm using an Olympus fluorescence microscope. Each well was assayed by establishing a fluorescence ratio baseline for each well using 100 µL BSS calcium-free buffer before adding 100 µL calcium-free BSS buffer containing 4-C*m*C. The final concentrations of 4-C*m*C used were 200, 300, 400, 600, 800, 1000 µM. As aliquots of 4-C*m*C were stored in DMSO, an assay was carried out on wild type *RYR1*-transfected HEK-293T cells with BSS buffer containing 1% DMSO, representative of the highest concentration of DMSO used in all assays.

2.4 LYMPHOBLASTOID B-CELLS

The lymphoblastoid B-cell lines used had been immortalised with the Epstein-Barr virus as described previously (Anderson et al. 2008) after being extracted from the blood of patients diagnosed with central core disease.

2.4.1 CRYOSTORAGE OF B-LYMPHOCYTE CELLS

Ten millilitres of cells (~1 x 10^6 cells mL^{-1}) were collected by centrifugation at 200 g for five minutes and then stored in cryotubes with 1 mL FBS containing 10% DMSO. They were cooled slowly to -80°C before being stored long-term in liquid nitrogen.

2.4.2 REANIMATION OF B-LYMPHOCYTES

Cell lines stored in liquid nitrogen were thawed quickly, resuspended in 5 mL complete Opti-MEM (Opti-minimum essential medium: 1% penicillin/streptomycin, 2% FBS) and then collected by centrifugation at 200 g for five minutes. Cell pellets were resuspended in 5 mL complete Opti-MEM in an upright T25 flask and grown at 37°C with 5% CO_2. The medium was supplemented daily with 1 – 2 mL complete Opti-mem

until it reached a volume of 10 mL. The cells were then transferred to a T75 flask where they were grown upright in ~15 mL complete Opti-MEM at 37°C in a humidified atmosphere containing 5% CO_2. Six mL of medium was replaced every day with 6 mL complete DMEM.

2.4.3 EXTRACTION OF GENOMIC DNA FROM B-LYMPHOCYTES

Genomic DNA (gDNA) was extracted from 1.5 mL (~1 x 10^6 cells mL^{-1}) immortalised B-lymphocyte cells for identification of their genotype. The Wizard genomic DNA purification kit (Promega) was used according to the manufacturer's instructions and the DNA resuspended in 50 µL TE buffer (10 mM Tris, 1 mM EDTA, pH 8.0).

2.4.4 HIGH RESOLUTION MELTING ANALYSIS

The gDNA extracted from immortalised B-lymphocyte cells was amplified by PCR using primers from Integrated DNA Technologies (table 2.3) designed to detect the variants of interest by high resolution melting (HRM) analysis in a total volume of 10 µL. This was carried out using the LightCycler 480 High Resolution Melting Master according to the manufacturer's instructions) in a LightCycler 480 instrument II (Roche). The region containing the g.38499670C>T mutation (Accession number ENSG00000196218.9) was amplified by PCR (0.2 µM forward and reverse primers and 3 mM $MgCl_2$) with the following cycling conditions: 95°C for ten minutes; 95°C for ten seconds; 65°C for ten seconds; 72°C for four seconds; and steps 2-4 were repeated 39 times. The region containing the g.38585048G>A mutation (Accession number ENSG00000196218.9) was amplified by PCR (0.3 µM forward and reverse primers and 4 mM $MgCl_2$) with the following cycling conditions: 95°C for ten minutes; 95°C for ten seconds; 65°C for ten seconds; 72°C for four seconds; and steps 2-4 were repeated 34 times. Both amplified regions were then heated to 95°C for one minute; cooled to 40°C for one minute; and then heated incrementally from 76°C to 92°C in the presence of a fluorescent dye that specifically binds double-stranded DNA. The decrease in fluorescence as the DNA melted was measured in the LightCycler 480 instrument II (Roche) using LightCycler 480 Gene Scanning software v1.5.

TABLE 2.3 Primer sequences for HRM analysis of B-lymphocyte gDNA

VARIANT	FORWARD PRIMER SEQUENCE	REVERSE PRIMER SEQUENCE
g.38499670C>T* **p.R2355W†**	5'-GAGAGCGTGGAGGAGAA-3'	5'- TGGCCTCTTCGATGGCA-3'
g.38585048G>A* **p.D4918N†**	5'- TGTACGTGGGTGTCCG-3'	5'- CCACTCCCAGCACTGA-3'

* Ensembl accession number ENSG00000196218.9

† GenBank accession NP_000531.2.

2.4.5 RyR1 ACTIVATION IN IMMORTALISED B-LYMPHOCYTES

Five µL resuspended cells were stained with 0.2% Trypan blue solution and observed at 100X magnification using an inverted optical microscope. A haemocytometer was used to count the number of living cells in the sample and ~1 x 10^7 cells were collected by centrifugation at 200 g for four minutes and resuspended in BSS buffer containing 2 mM $CaCl_2$ at 37°C. This procedure was repeated once. Cells were incubated in the dark in 1 mL BSS buffer containing 2 mM $CaCl_2$ with 4 µM Fura2-AM and 0.02% Pluronic F-127 for one hour at 37°C. They were then collected by centrifugation at 200 g for four minutes and resuspended in BSS buffer containing 2 mM $CaCl_2$ at 37°C, avoiding exposure to light. Cells were collected by centrifugation at 200 g for four minutes and resuspended in BSS buffer at 37°C; this procedure was repeated once.

Activation of RyR1 using 4-C*m*C was measured by the change in the ratio of fluorescence at 510 nm when excited by 340 nm and 380 nm wavelengths using a PerkinElmer LS50 spectrofluorometer. Each assay was carried out using ~6.7 x 10^5 cells mL^{-1} in calcium-free BSS buffer with the final concentrations of 150, 300, 450, 600, 750, 900, 1000, 1200 µM 4-C*m*C being added after a baseline was established. As aliquots of 4-C*m*C were stored in DMSO, an assay was carried out on wild type *RYR1*-transfected HEK-293T cells with BSS buffer containing 1% DMSO, representative of the highest concentration of DMSO used in all assays.

2.6 DATA ANALYSIS

2.6.1 MICROSCOPIC IMAGES

ImageJ software (Abramoff et al. 2004) was used to merge images taken using the confocal microscope and to add a scale bar.

2.6.2 CURVE FITTING

Calcium release assays to test the responsiveness of RyR1 to the specific agonist 4-C*m*C were carried out on lymphoblastoid B-cells and transiently transfected HEK-293T cells. The amount of calcium release at each concentration of 4-C*m*C was normalised to account for any differences in cell density for each assay and calculated as a percentage of the total calcium released with 1000 µM 4-C*m*C. A minimum of five biological replicates were carried out for each value of 4-C*m*C used in the assays in HEK-293T and a minimum of three biological replicates were carried out for each value of 4-C*m*C used in the assays in B-lymphocytes. The data were pooled and a sigmoidal curve fitted for each dataset with OriginLab Origin 8 software. Results were presented as the mean ± standard error of the mean (SEM) for each value of 4-C*m*C used.

2.6.3 STATISTICAL ANALYSIS

The data from calcium release assays using B-lymphoblastoid cell lines or transiently-transfected HEK-293T cells within each dataset were fitted with sigmoidal curves using OriginLab Origin 8 software. A minimum of eight analytical replicates were carried out for each *RYR1* variant expressed in HEK-293T cells and a minimum of five analytical replicates were used for each B-lymphocyte cell line. The half maximal effective concentration (EC_{50}) values were calculated from individual sigmoidal curves and then used to calculate the mean EC_{50} ± SEM for each *RYR1* variant expressed in HEK-293T cells or B-lymphocyte cell line. Statistical significance in the form of p-values was calculated with an unpaired Student's *t*-test using OriginLab Origin 8 software.

CHAPTER THREE: Results

3.1 PREPARATION OF *RYR1* MUTANT CDNAS

The overall aim of the research carried out for this thesis was to compare the activity of RyR1 variant channels in the presence of a RyR1-specific agonist, 4-C*m*C, to the activity of the wild type RyR1 channel under the same conditions. In order to do this, the substitutions had to be introduced into the *RYR1* cDNA which was then used to express RyR1 variant channels, the identities of which are p.M4640I, p.V4849I, p.F4857S, p.R4861H and p.D4918N. Two of these *RYR1* cDNA variants – c.13920G>C (p.M4640I) and c.14545G>A (p.V4849I) – had previously been created by Natisha Magan (Institute of Fundamental Sciences, Massey University, unpublished) prior to the start of this project. Therefore, only three of the variants investigated in the current study were produced in the *RYR1* cDNA during the course of the project. In addition, *RYR1* cDNAs for wild type and p.H4833Y (c.14497C>T) RyR1 channels, which had been created previously by Keisaku Sato (Sato et al. 2010), were used as controls for calcium release assays in the current study. The *RYR1* cDNA and RyR1 amino acid sequences referred to in this chapter are GenBank accessions NM_000540.2 and NP_000531.2, respectively.

3.1.1 CLONING STRATEGY

Site-directed mutagenesis was used to introduce a single variant of interest into the *RYR1* cDNA representing the C-terminal region of RyR1. As the entire human *RYR1* cDNA is over 15 kb in length, the variant was created in the pBSH+ plasmid (appendix A) containing a representative section of *RYR1* cDNA (Figure 3.1A, green region). The variant was then introduced into the full-length cDNA (Sato et al. 2010) in two sequential cloning steps – first into the pBSKX plasmid (appendix A) containing half the *RYR1* cDNA in the pBluescript II KS+ vector (Figure 3.1B) and then into the pcRYR1 plasmid (appendix A) containing the entire *RYR1* cDNA (Figure 3.1C) in a pcDNA3.1+ vector. This was due to constraints in available restriction endonuclease recognition sites (Figure 3.1).

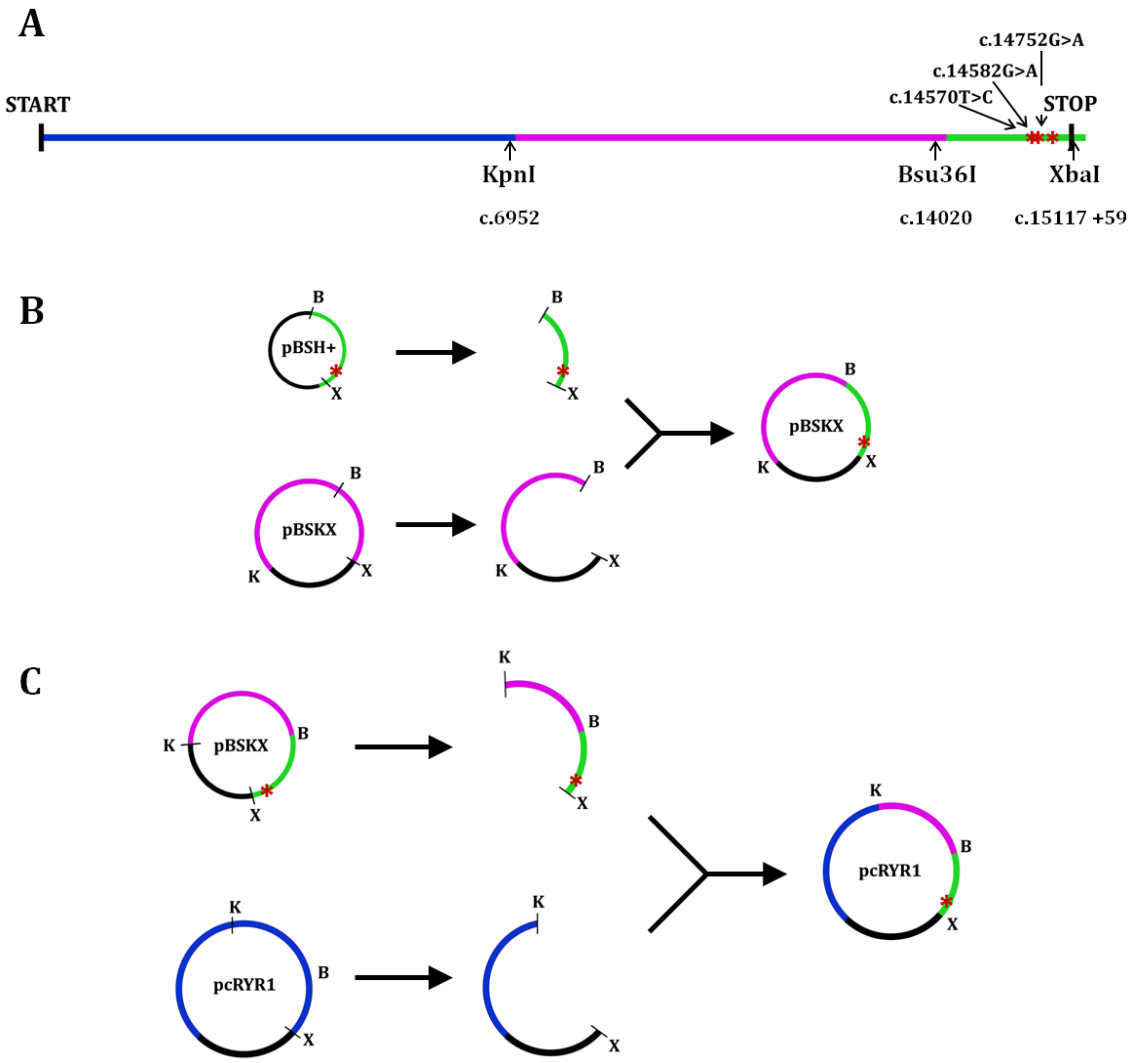

FIGURE 3.1 Schematic of the creation of *RYR1* variants

A. *RYR1* cDNA with the start and stop codon locations labelled and the locations of the three variants created indicated by red stars. The restriction endonuclease recognition sites used in sub-cloning are labelled with the nucleotide position in the cDNA indicated; XbaI is located 59 nucleotides beyond the stop codon. The cDNA component of each plasmid used in sub-cloning is indicated by colour: pBSH+ contains the green portion used for site-directed mutagenesis; pBSKX contains both the purple and green portions representing half of the full-length cDNA; and pcRYR1 contains the blue, purple and green portions, representing the complete coding sequence. **B.** Strategy used to sub-clone the 2.2 kb cDNA region (green) from pBSH+ into pBSKX using directional cloning. pBluescript II KS+ vector is shown in black; the approximate locations of the variants are indicated by a red star; and the restriction endonuclease sites are labelled K (KpnI), B (Bsu36I) or X (XbaI). **C.** Strategy used to sub-clone the 8.1 kb cDNA region (green and purple) from pBSKX into pcRYR1 using directional cloning.

3.1.2 MUTAGENESIS

The following variants were created in order to measure their effect on calcium release in the HEK-293T cell heterologous system: c.14570T>C (p.F4857S); c.14582G>A (p.R4861H); and c.14752G>A (p.D4918N). The first step was to introduce each variant into the *RYR1* cDNA by site-directed mutagenesis. As shown in Figure 3.2, this was carried out by PCR-amplification of a small plasmid (pBSH+) containing 2.3 kb of the most 3' *RYR1* cDNA (appendix A) with complementary mutagenic primer pairs; PCR with no template was used as a negative control. The PCR product was digested with the restriction endonuclease DpnI which digests DNA at *dam* methylation sites, effectively destroying the template DNA derived from bacteria *in vivo* leaving the PCR products synthesised *in vitro* intact.

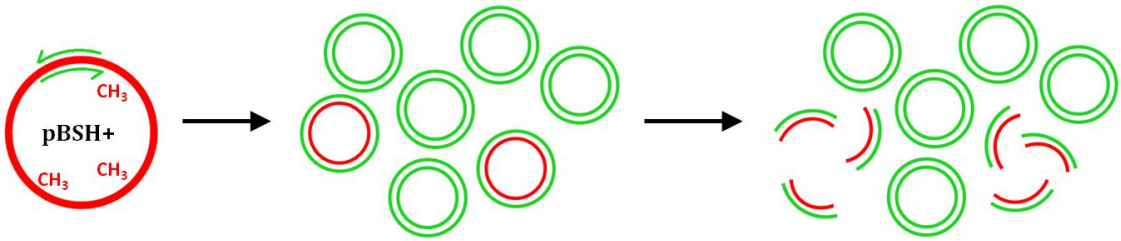

FIGURE 3.2 Strategy to introduce variants to *RYR1* cDNA

Mutagenic primers (green arrows) were used to introduce a variant of interest into the pBSH+ template plasmid (shown in red) by PCR. The resulting population of PCR products consists of both wild type (red) and variant-containing (green) plasmids. Upon treatment with the restriction endonuclease DpnI, all template plasmids should be digested while plasmids containing the variant should remain intact.

In order to determine that the plasmid was amplified correctly and the product was of the correct size, the PCR products were digested with restriction endonucleases SalI and XhoI alongside the original PCR template plasmid; these digests were analysed by gel electrophoresis (Figure 3.3A). The plasmid pBSH+ has one recognition site for SalI and two recognition sites for XhoI; the digests were expected to yield a linear DNA fragment 5.3 kb in length for SalI and two DNA fragments 2.3 kb and 3 kb in length for

XhoI. The undigested pBSH+ plasmid was produced *in vivo* and as a result could be seen as two bands on the agarose gel which can be identified as the relaxed and supercoiled forms of the plasmid, while the undigested PCR product was in the 'nicked' form as a result of the PCR process. Both digests produced the expected DNA fragment sizes indicating that the correctly-sized plasmid had been produced and the negative PCR control sample shows no amplification of DNA as expected. The products of mutagenesis PCR also included excess primers which could be seen near the bottom of the gel most prominently in the sample of undigested PCR product as well as the negative control sample.

After being propagated in *E. coli* and extracted with the Invitrogen Miniprep Kit, each plasmid containing a different variant was then sent for Sanger sequencing (primer sequences in appendix B) to confirm the presence of the variant that had been introduced (Figure 3.3B). In addition, this sequencing was carried out to ensure no other polymorphisms or mutations were introduced by the DNA polymerase during amplification of the plasmid that would change the amino acid sequence of the protein product (appendix B).

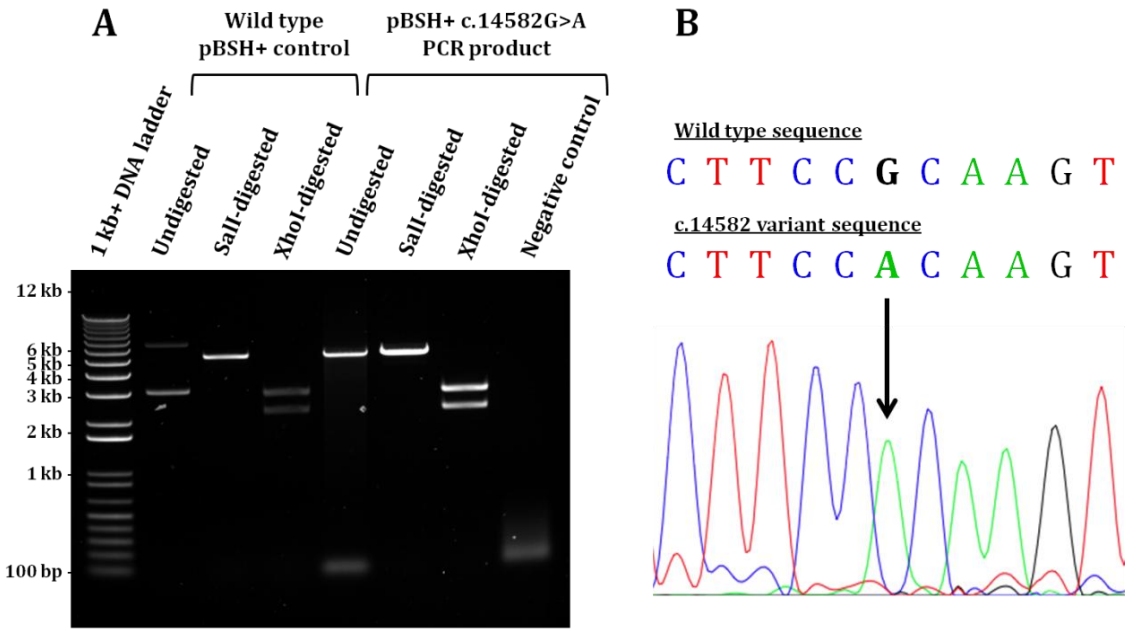

FIGURE 3.3 Confirmation of site directed mutagenesis

A. The pBSH+ plasmids (original template and after PCR mutagenesis) were digested with restriction endonucleases, analysed by gel electrophoresis in a 1% agarose gel at 90 V alongside a 1kb+ DNA ladder and visualised using UV (A_{260}) light. Shown is a representative image from the mutagenesis of the c.14582G>A (p.R4861H) variant. The 2.3 and 3 kb bands in lane 4 may be difficult to perceive in this image. **B.** Shown is a representative chromatogram from Sanger sequencing of the region containing the c.14582G>A variant, where the green peak indicated by the arrow represents the adenine nucleotide introduced at that site.

3.1.3 SUB-CLONING VARIANTS INTO pBSKX PLASMID

Because of the lack of unique recognition sites of restriction endonucleases in the *RYR1* cDNA, the variants to be created were first sub-cloned into a plasmid containing the 3' half of the *RYR1* cDNA, pBSKX (appendix A). The pBSH+ plasmid containing *RYR1* cDNA with the variant of interest was digested with two restriction endonucleases – Bsu-36I and XbaI – as was the pBSKX plasmid containing the wild type residue at that site (Figure 3.1B). The products of these restriction endonuclease digests were analysed by gel electrophoresis (Figure 3.4). The two bands in the undigested pBSKX sample were identified as the relaxed and supercoiled forms of a plasmid produced *in vivo.* The digest of pBSKX produced two bands, approximately 1.1 kb and 10 kb in

length; the 1.1 kb fragment contained the most 3' *RYR1 c*DNA with the wild type residue at the location of the variant to be introduced while the 10 kb fragment contained the pBluescript II KS+ vector and the remaining *RYR1* cDNA. The digest of pBSH+ produced a 1.1 kb and a 4.2 kb band; the 1.1 kb fragment contained the most 3' *RYR1 c*DNA with the variant while the 4.2 kb fragment contained the pBluescript II KS+ vector and the remaining *RYR1* cDNA.

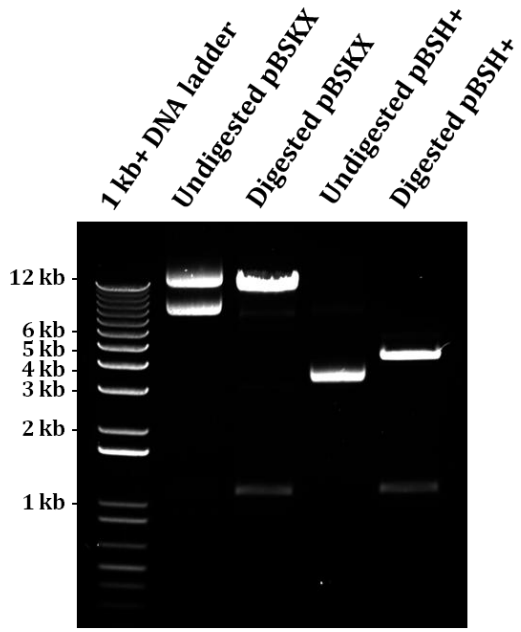

FIGURE 3.4 Digest of plasmids for sub-cloning into pBSKX

The digests of wild type pBSKX, pBSH+ containing each variant of interest and their respective undigested controls were separated by electrophoresis in a 1% agarose gel at 90 V alongside a 1kb+ DNA ladder and visualised using UV (A260) light. Shown is a representative digest of the c.14582G>A (p.R4861H) variant. The 1.1 kb bands in lanes 3 and 5 may be difficult to perceive in this image.

The DNA bands corresponding to the 10 kb wild type DNA fragment from the pBSKX plasmid and the 1.1 kb DNA fragment containing the variant of interest from the pBSH+ plasmid were excised from the agarose gel. These were purified using the Gel DNA Recovery kit according to the manufacturer's instructions and then ligated

together using T4 DNA ligase to produce the pBSKX plasmid containing the variant of interest. *E. coli* DH5α were transformed with the product of that ligation and allowed to grow, after which the plasmids were extracted using the Invitrogen Miniprep Kit. In order to determine that the DNA fragments had ligated correctly and the product was of the correct size, plasmids containing each variant were digested with restriction endonucleases NotI and XhoI alongside the original wild type pBSKX plasmid. These digests were analysed by gel electrophoresis (Figure 3.5A). The restriction endonuclease NotI has two recognition sites in pBSKX and was expected to give two DNA fragments 2.3 kb and 8.8 kb in length while the restriction endonuclease XhoI has three recognition sites in pBSKX and was expected to give three DNA fragments 2.3 kb, 4.3 kb and 4.5 kb in length. In both the wild type and variant-containing form of the plasmid, the undigested pBSKX+ showed two bands which were identified as the relaxed and supercoiled forms of the plasmid produced *in vivo*. Both restriction endonuclease digests produced the expected fragments indicating that the correctly-sized plasmid had been produced; the 4.3 kb and 4.5 kb bands from the XhoI digest run as a doublet and cannot be distinguished by 0.7% agarose gel electrophoresis. Each pBSKX variant was then sent for Sanger sequencing (appendix B, primer D) to confirm the presence of the variant that had been introduced (Figure 3.5B).

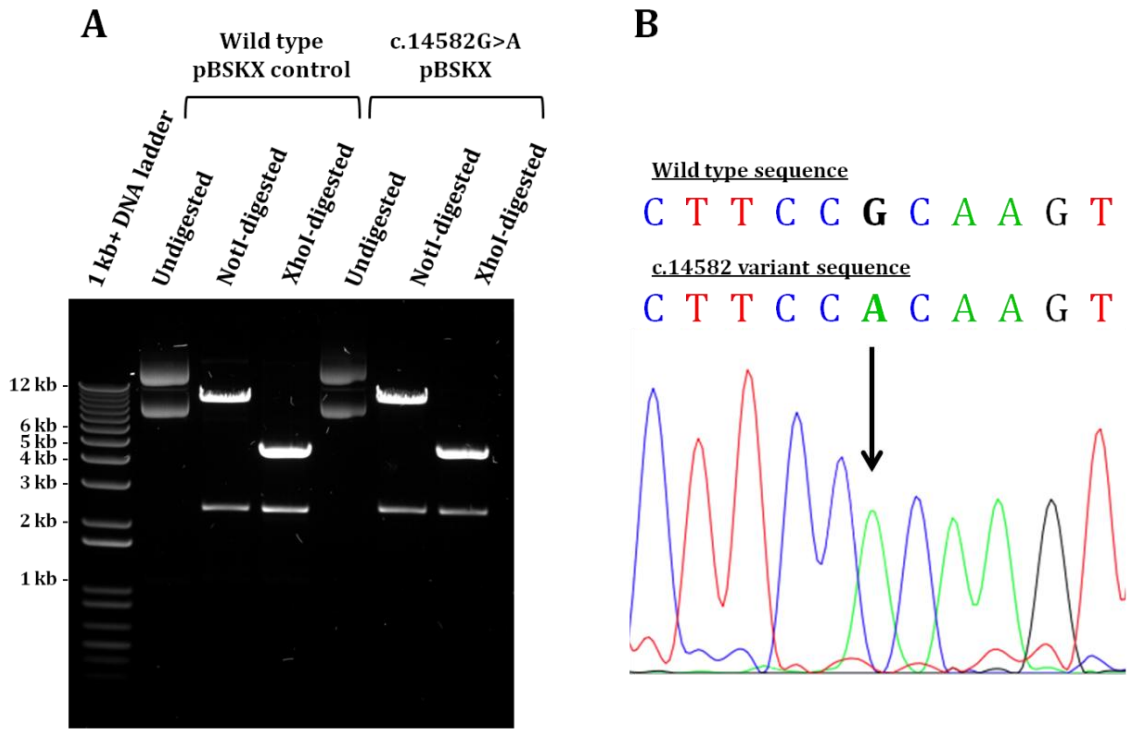

FIGURE 3.5 Confirmation of ligation of variants into pBSKX

A. The pBSKX wild type plasmid and the variant-containing pBSKX plasmids were digested with restriction endonucleases, analysed by gel electrophoresis in a 0.7% agarose gel at 90 V alongside a 1kb+ DNA ladder and visualised using UV (A_{260}) light. Shown is a representative image from the cloning of the c.14582G>A (p.R4861H) variant **B.** Shown is a representative chromatogram from Sanger sequencing of the region containing the c.14582G>A variant, where the green peak indicated by the arrow represents the adenine nucleotide at that site.

3.1.3 SUB-CLONING VARIANTS INTO PCRYR1 PLASMID

After being sub-cloned into the pBSKX plasmid, the 3' half of the *RYR1* cDNA containing the variant of interest was then sub-cloned into a plasmid containing the entire *RYR1* cDNA, pcRYR1 (appendix A). The pBSKX plasmid containing *RYR1* cDNA with the variant of interest was digested with two restriction endonucleases – KpnI and XbaI – as was the pcRYR1 plasmid containing the wild type residue at that site (Figure 3.1C). The products of these restriction endonuclease digests were analysed by gel electrophoresis (Figure 3.6). The two bands seen in both undigested samples could be identified as the relaxed and supercoiled forms of a plasmid produced *in vivo*. The

digest of pcRYR1 produced two bands, approximately 8.2 kb and 12.4 kb in length; the 8.2 kb fragment contained the 3' half of *RYR1* cDNA with the wild type residue at the location of the variant to be introduced while the 12.4 kb fragment contained the pcDNA3.1+ vector and the remaining *RYR1* cDNA. The digest of pBSKX produced two bands, approximately 2.9 kb and 8.2 kb in length; the 2.9 kb fragment contained the 3' half of *RYR1* cDNA with the variant of interest while the 8.2 kb fragment contained the pBluescript II KS+ vector and the remaining *RYR1* cDNA.

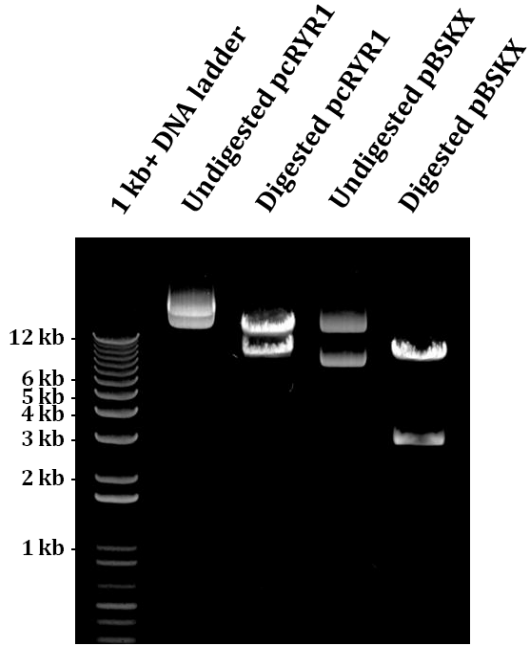

FIGURE 3.6 Digest of plasmids for sub-cloning into pcRYR1

The digests of pcRYR1 and pBSKX and their undigested controls were separated by electrophoresis on an agarose gel in a 0.7% agarose gel at 90 V alongside a 1kb+ DNA ladder and visualised using UV (A_{260}) light. Shown is a representative digest of the c.14582G>A (R4861H) variant.

The DNA bands corresponding to the 12.4 kb wild type DNA fragment from the pcRYR1 plasmid and the 8.2 kb DNA fragment containing the variant of interest from the pBSKX plasmid were excised from the agarose gel. These were purified using the Gel DNA Recovery kit according to the manufacturer's instructions and then ligated

together with T4 DNA ligase to produce the pcRYR1 plasmid containing the variant of interest. *E. coli* DH5α were transformed with the product of that ligation and allowed to grow, after which the plasmids were extracted using the Invitrogen Miniprep Kit. This final sub-cloning step was carried out by a colleague (Mrs. Lili Rhodes, Institute of Fundamental Sciences, Massey University) for two of the three variants – c.14570T>C (p.F4857S) and c.14752G>A (p.D4918N) – created in this way. In order to determine that the DNA fragments had ligated correctly and the product was of the correct size, plasmids containing each variant were digested with restriction endonucleases SalI and XhoI alongside the wild type pcRYR1 plasmid and analysed by gel electrophoresis. The restriction endonuclease SalI has four recognition sites in pcRYR1 and was expected to give four DNA fragments 1.5 kb, 2.2 kb, 2.3 kb and 14.6 kb in length while the restriction endonuclease XhoI has five recognition sites in pcRYR1 and was expected to give five DNA fragments 2.1 kb, 2.3 kb, 4 kb, 4.3 kb and 7.9 kb in length. Both restriction endonuclease digests produced the expected fragment sizes indicating that the correctly-sized plasmid had been produced for all three of the variants (appendix C). Each pcRYR1 variant was also sent for Sanger sequencing (appendix B, primer D) to confirm the presence of the variant that was introduced (appendix C). These verifications were also carried out for the pcRYR1 variants to be characterised in the present study that were created by Natisha Magan prior to this project: c.13920G>C (p.M4640I) and c.14545G>A (p.V4849I) (appendix C). In addition, the restriction endonuclease digests were carried out on two pcRYR1 plasmids created by Keisaku Sato (Sato et al. 2010) – wild type and c.14497C>T (p.H4833Y) pcRYR1 –that were used as negative and positive controls respectively in calcium release assays (appendix C).

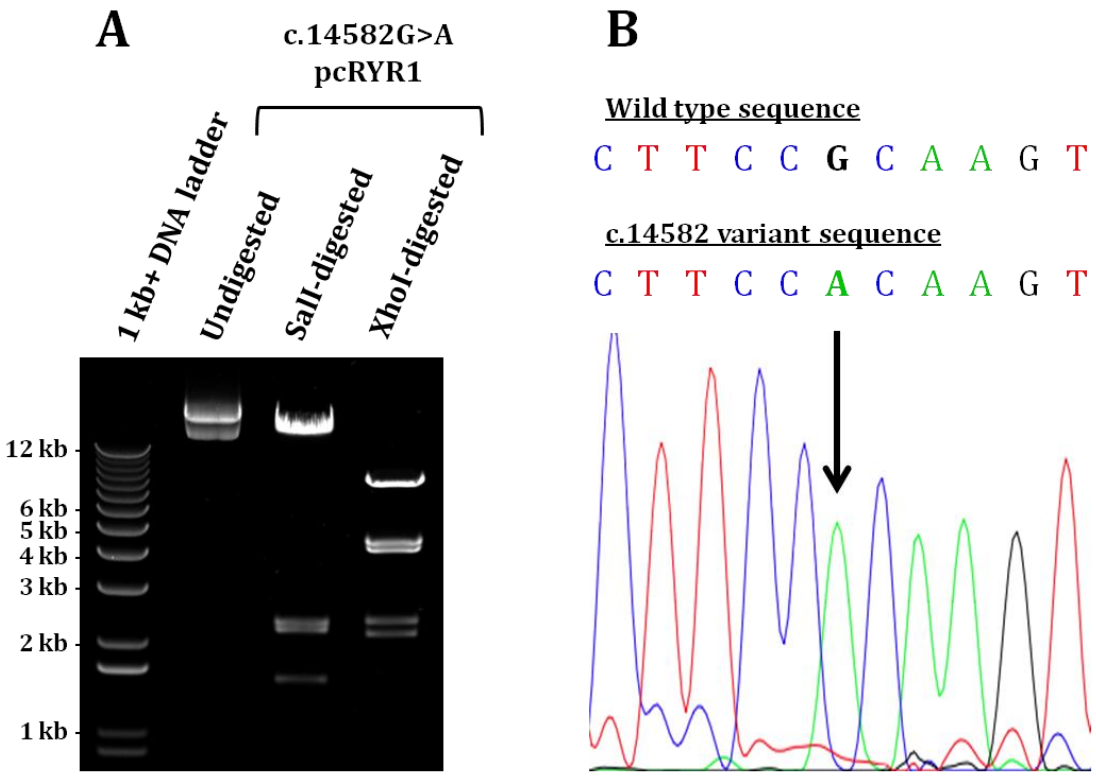

FIGURE 3.7 Confirmation of pcRYR1 variants

A. The pcRYR1 variants were digested with restriction endonucleases, analysed by gel electrophoresis in a 0.7% agarose gel at 90 V alongside a 1kb+ DNA ladder and visualised using UV (A_{260}) light. Shown is a representative image from the cloning of the c.14582G>A (p.R4861H) variant. The 1.5 kb band in lane 3 may be difficult to perceive in this image. **B.** Shown is a representative chromatogram from Sanger sequencing of the region containing the c.14582G>A variant, where the green peak indicated by the arrow represents the adenine nucleotide at that site.

3.2 CHARACTERISATION OF RyR1 VARIANTS IN A HETEROLOGOUS SYSTEM

Wild type and M4640I, H4833Y, V4849I, F4857S, R4861H and D4918N variant RyR1 were expressed in the HEK-293T cell line (HEK-293 cell line containing the *Simian virus 40* large T antigen) after transient transfection to compare the functional effects of the variants and the wild type channel. HEK-293T cells do not normally express RyR1 at detectable levels or in a functional form (Tong et al. 1999a) and are therefore often used to investigate directly the impact that *RYR1* substitutions have on the function of RyR1 as a calcium channel (Zhou et al. 2006, Kraeva et al. 2013, Roesl et al. 2014).

3.2.1 CONFIRMATION OF RyR1 EXPRESSION

Wild type RyR1 and RyR1 variants must be expressed at approximately equal levels in order to be able to compare the functional effects of the variants. For that reason, the level of RyR1 expression in HEK-293T cells was measured by western blotting (Figure 3.8). The total protein of transiently transfected HEK-293T was extracted and separated by SDS-PAGE alongside the Precision Plus Protein Dual Colour Standard protein ladder. The separated proteins were then transferred to a PVDF membrane and analysed by immunoblotting where the intensity of the RyR1 protein signal indicated the level of protein expressed in the cell line.

The 50 kDa α-tubulin protein bands were evident in all samples and were approximately the expected size when compared with the 50 kDa band in the protein ladder (not seen on the blot). The RyR1 protein bands were prominent in all pcRYR1-transfected samples and were approximately the correct size of 565 kDa as they migrated more slowly than the highest molecular weight marker in the protein ladder, which was 250 kDa. Although some non-specific binding of the antibodies to other proteins from the total protein samples was evident, the level of RyR1 protein expressed from the transfection of HEK-293T cells with each variant *RYR1* cDNA was comparable to the level of RyR1 protein in the wild type *RYR1* cDNA-transfected cells. In addition, there was no RyR1 protein detected in the vector-only sample; this represents protein extracted from HEK-293T cells transiently transfected with the empty pcDNA3.1+ vector (appendix A) as a negative control.

The level of α-tubulin in each sample was detected to ensure the amount of protein loaded was equal between samples. Alpha-tubulin is one of two polypeptides that make up tubulin, a globular protein that forms microtubules as part of the cell cytoskeleton and whose protein expression should be unaffected by the expression of RyR1. To facilitate the migration of the large 565 kDa RyR1 monomer into the resolving gel, electrophoresis was continued until the tubulin band reached the end of the gel, causing the tubulin bands to be less intense than expected as the transfer of proteins from the edge of the protein gel to the PVDF membrane was inefficient. In addition, the tubulin signal was weaker than RyR1 because RyR1 was overexpressed in the HEK-

293T cell line and therefore the level of RyR1 appeared to be high compared to the endogenous proteins in the sample.

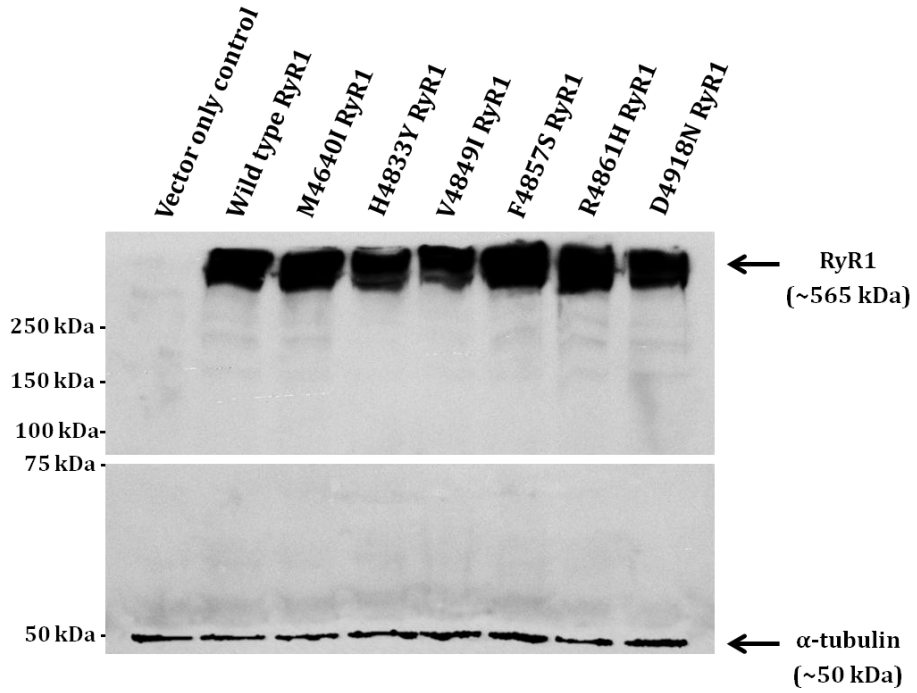

FIGURE 3.8 RyR1 variants are present at approximately equal levels

Total protein (~270 µg) samples extracted from pcDNA3.1+- and *RYR1*-transfected HEK-293T cells were separated by electrophoresis alongside the Precision Plus protein standard ladder (labelled) at 120 V in a SDS-polyacrylamide gel (4% stacking gel and 7.5% resolving gel). Resolved proteins were transferred to a PVDF membrane at 70 mA and then detected using primary antibodies specific for RyR1 and α-tubulin and secondary antibodies conjugated to horseradish peroxidase. Variants are indicated by their amino acid change.

3.2.2 CONFIRMATION OF RyR1 LOCALISATION

The presence of RyR1 in the membrane of calcium storage organelles is essential for their function as calcium channels and for this reason the cellular localisation of RyR1 proteins expressed in HEK-293T cells was analysed by immunofluorescence. If any of the variants were found to be mislocalised, it might have been the cause of any subsequent loss of function observed in the calcium release assays rather than any intrinsic functional change in the channel's activity. The fluorescent stain DAPI was used to visualise the nuclei of each cell as it fluoresces brightly when bound to AT-rich

regions of DNA while fluorescently-labelled antibodies were used for visualisation of RyR1 and protein disulfide isomerase (PDI) – an ER-specific protein. Because of its size, the rate of transfection of the *RYR1* cDNA construct in HEK-293T cells was very low, subsequently causing the majority of cells to have no observable RyR1. While calculating the transfection efficiency of each construct was unfeasible due to the large number of cells growing in multiple layers, all *RYR1* constructs were seen to be expressed in approximately the same number of cells. Moreover, the images in figure 3.9 are representative of hundreds of cells observed to express and localise RyR1 to the ER. PDI and RyR1 co-localised completely in the HEK-293T cells that expressed the wild type and variant *RYR1* cDNAs, suggesting that the RyR1 channels were correctly located in the ER of these cells. In addition, HEK-293T cells were transfected with empty pcDNA3.1+ vector as a negative control where no RyR1 was detected.

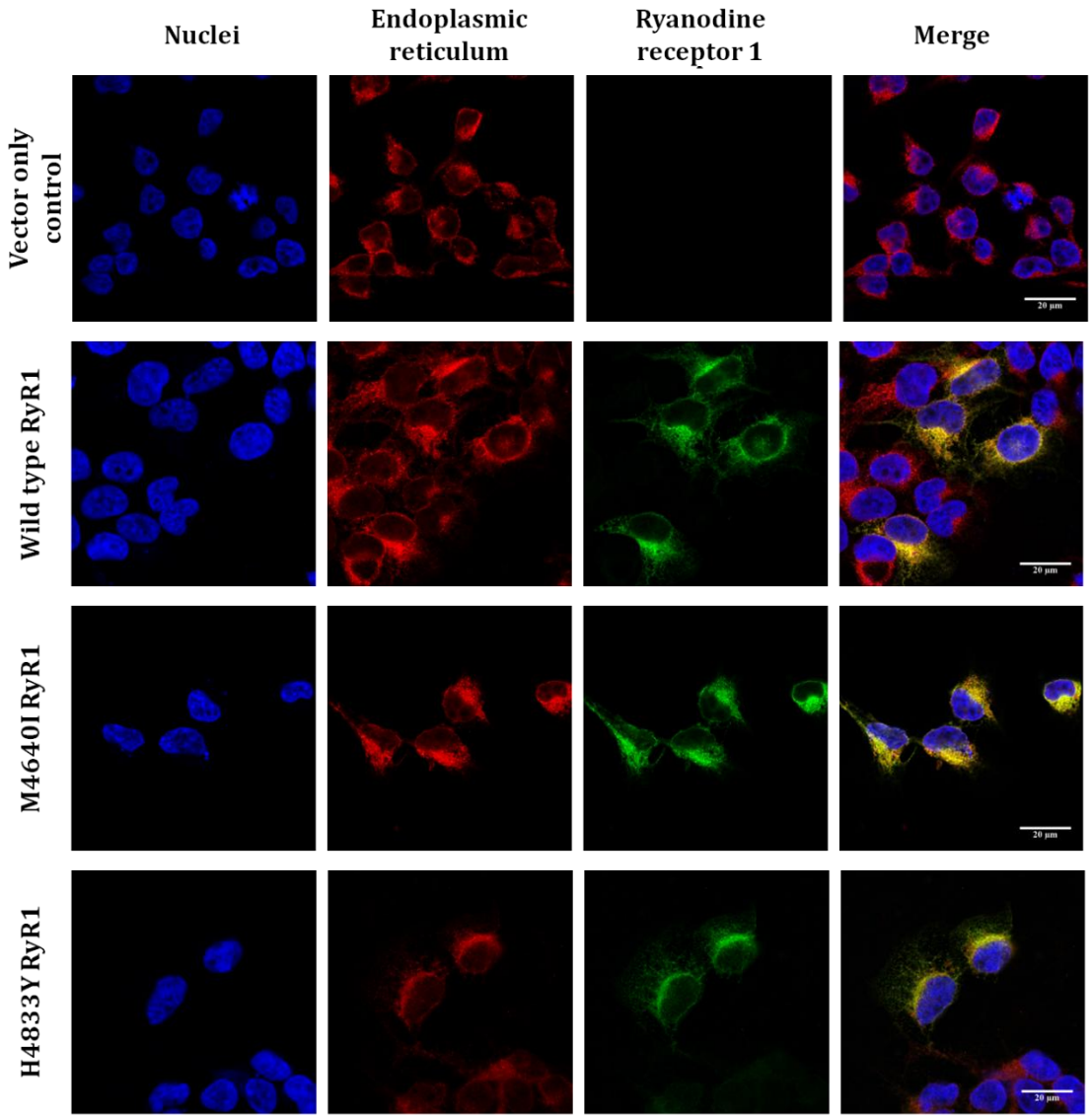

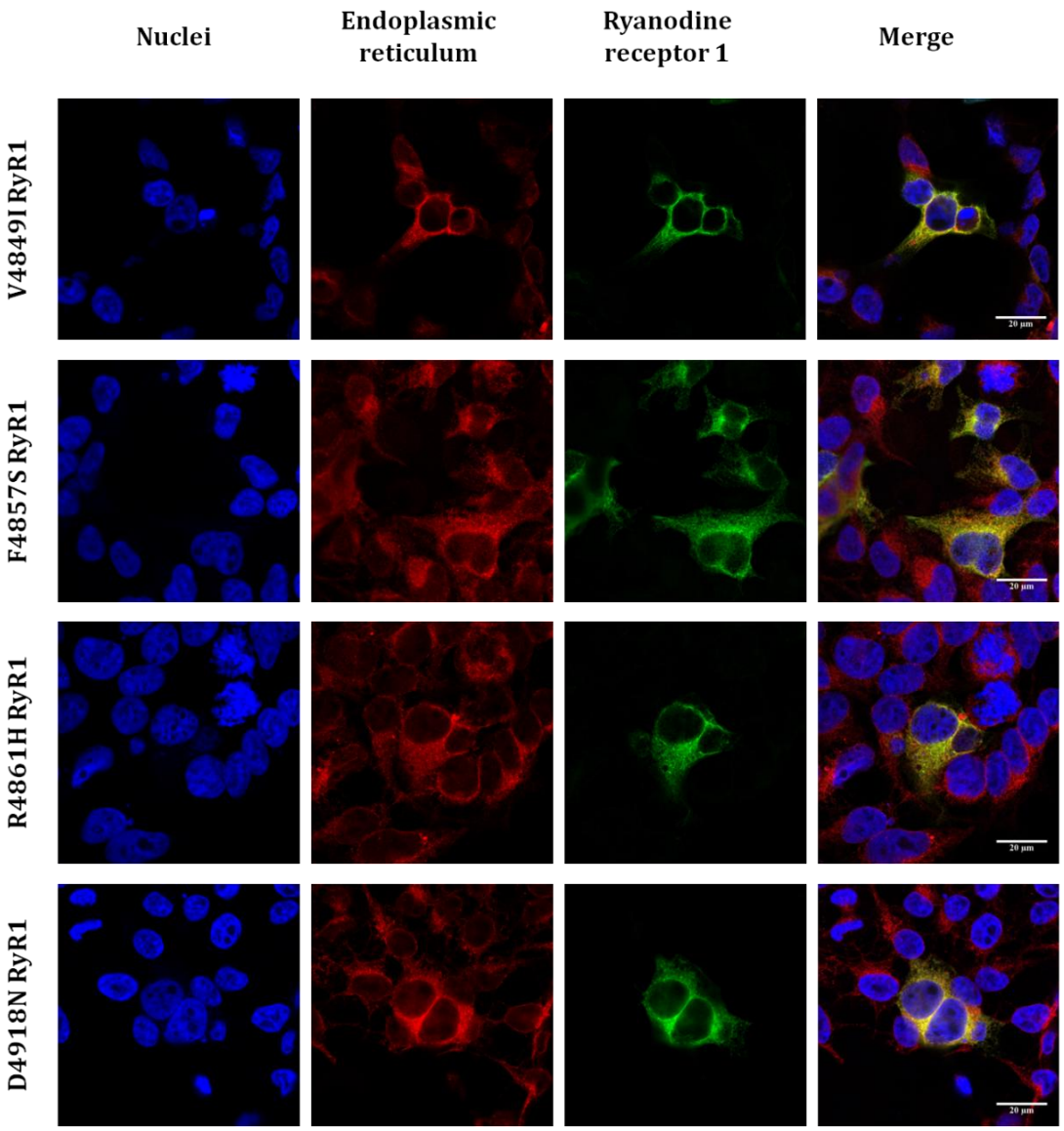

FIGURE 3.9 RyR1 localises to the ER of HEK-293T cells

HEK-293T cells at low confluence were transiently transfected with 1 µg empty pcDNA3.1+ vector, wild type pcRYR1 or pcRYR1 variant plasmids on a microscope slide. Variants are indicated by their amino acid change. Primary antibodies that specifically recognise RyR1 (34C) and PDI as well as fluorescently-labelled secondary antibodies FITC (green) and TRITC (red) were used to visualise RyR1 and the PDI respectively, while nuclei were visualised by staining the cells with DAPI (blue). Cells were examined by confocal fluorescence microscopy at a magnification of 1260 X; the scale bar in each merged image represents a length of 20 microns.

3.2.3 ANALYSIS OF RyR1 ACTIVITY IN HEK-293T CELLS

The activities of variant RyR1 channels in the ER of HEK-293T cells were compared with the activity of the wild type RyR1 channels using calcium release assays under the same conditions. The increase in intracellular calcium was measured after the addition of incremental doses of the RyR1-specific agonist 4-C*m*C to the cells and then calculated as a percentage of total calcium release. Total calcium release was defined as the increase in intracellular calcium in the presence of 1000 µM 4-C*m*C. Intracellular calcium levels were measured using the ratiometric dye, Fura-2. The dye in esterified form, Fura-2AM, is able to cross plasma membranes, after which the acetoxymethyl (AM) group is removed by cellular esterases and Fura-2 binds free calcium located in the cytoplasm. Fura-2 can be excited at both 340 nm and 380 nm with emission at 510 nm for both excitation wavelengths. When Fura-2 binds to calcium, the emission at 510 nm from the 340 nm excitation is higher than when unbound. Conversely, the emission at 510 nm is lower from the 380 nm excitation when bound to calcium. As a consequence, the 340 nm / 380 nm excitation ratio of fluorescence is an accurate measure of relative levels of calcium as when intracellular calcium increases it causes an increase of the 340 nm excitation signal and an equal decrease of the 380 nm excitation signal. A minimum of five biological replicates were carried out for each concentration of 4-C*m*C used in the assays. The data from all assays for each variant were pooled and a sigmoidal curve was fitted to the data using OriginLab software. These curves were plotted on a graph (Figure 3.10) with the mean ± SEM values for each concentration of 4-C*m*C tested for each variant.

As the DMSO in which 4-C*m*C is stored is known to be toxic to living cells in high doses, HEK-293T cells were exposed to DMSO in the absence of 4-C*m*C as a negative control. Another negative control used was HEK-293T cells transiently-transfected with the empty pcDNA3.1+ vector and exposed to 4-C*m*C. As expected, neither negative control produced discernible changes in the intracellular calcium levels of HEK-293T cells.

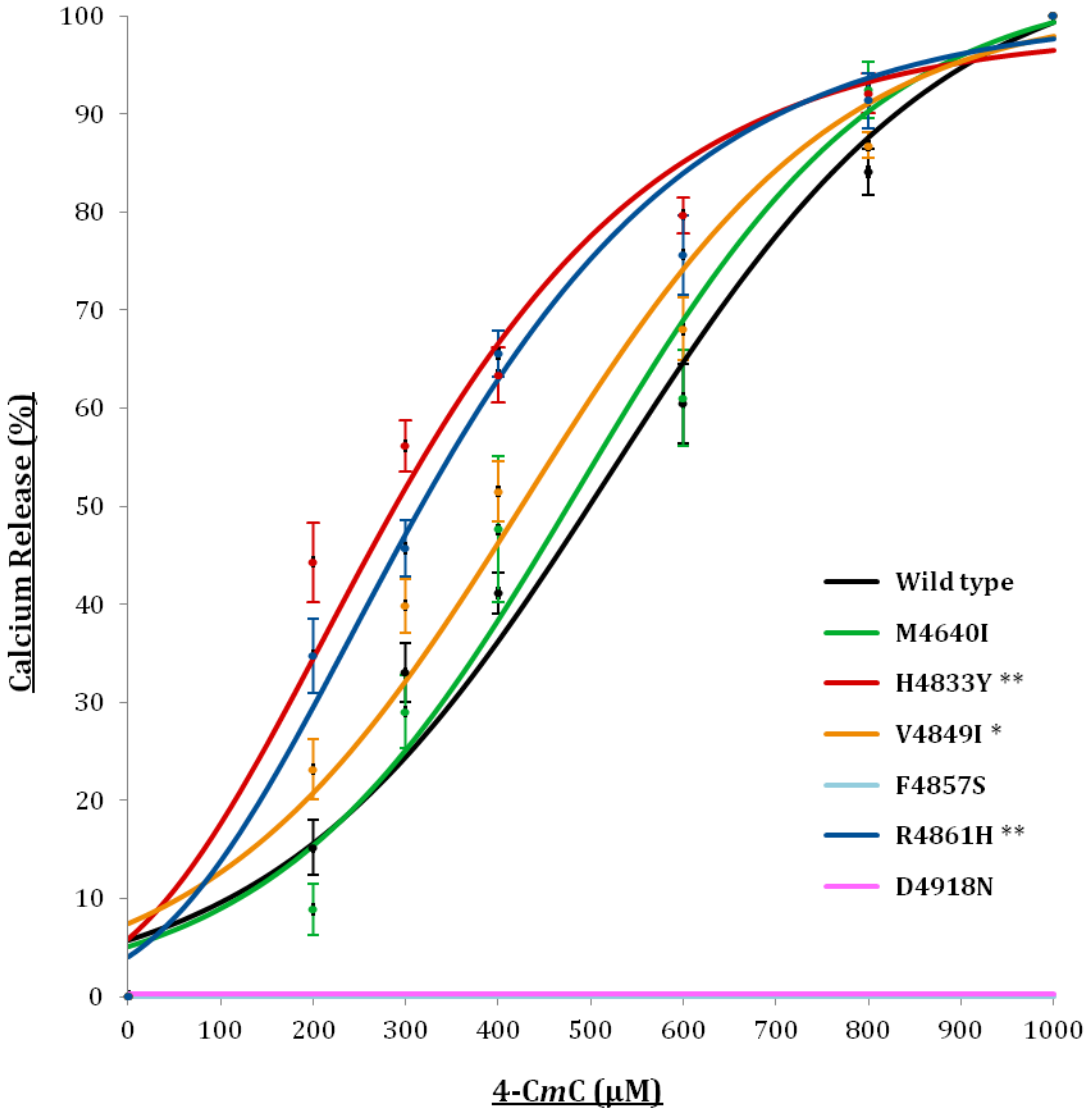

FIGURE 3.10 Calcium release in HEK-293T cells by RyR1 channels

HEK-293T cells transfected with wild type or variant *RYR1* cDNAs in a UV-transparent 96-well plate were exposed to incremental doses of the RyR1-specific agonist 4-C*m*C in the presence of the ratiometric indicator, Fura-2. Increases in intracellular calcium upon introduction of the agonist were measured using a fluorescent microscope and normalised to 100% calcium release with 1000 µM 4-C*m*C. Each dataset was presented as the mean ± SEM and fitted with a sigmoidal curve. Variants shown represent the amino acid change in the RyR1 protein expressed and statistical significance is denoted by * ($P < 0.05$, ≥95% confidence) and ** ($P < 0.01$, ≥99% confidence).

For each assay carried out, a sigmoidal curve was fitted to the data using OriginLab software and the half maximal effective concentration (EC_{50}) was calculated from the

curve. The mean ± SEM values were then calculated from the EC_{50} values of all assays carried out for each RyR1 variant and statistical significance was calculated using an unpaired student t test (table 3.1).

TABLE 3.1 EC_{50} values and statistical significance of each RyR1 variant

VARIANT	EC_{50} ± SEM (µM 4C*m*C)	P-VALUE	CONFIDENCE
Wild type	468.8 ± 17.2		
M4640I	487.2 ± 28	0.582	42%
H4833Y	290.2 ± 11.5	2.85×10^{-8} **	100%
V4849I	411.6 ± 18.5	0.039 *	96%
F4857S	0	7.65×10^{-15} **	100%
R4861H	322.4 ± 19.7	4.81×10^{-5} **	100%
D4918N	0	7.65×10^{-15} **	100%

All variants show the amino acid change, GenBank accession NP_000531.2.

** Statistical significance, P < 0.01

* Statistical significance, P < 0.05

The RyR1 variants p.H4833Y and p.R4861H both had considerably increased sensitivities to 4-C*m*C as indicated by their curves in Figure 3.10 which were shifted to the left when compared to the wild type RyR1 curve. In addition, both variants had EC_{50} values that differed from the wild type RyR1 EC_{50} with strong statistical significance (100%). The RyR1 variant p.V4849I also showed an increased sensitivity to the RyR1 agonist when compared to the wild type RyR1 curve and had an EC_{50} value that differed from the wild type RyR1 EC_{50} with statistical significance (96%). The RyR1 variant p.M4640I showed no significant difference in calcium release in response to

agonist when compared to the wild type RyR1. The RyR1 variants p.F4857S and p.D4918N both showed no measurable change in intracellular calcium levels in the presence of any concentrations of 4-C*m*C used in the calcium release assays and can therefore be identified as inactive channels.

3.3 D4918N RyR1 VARIANT ANALYSED IN B-LYMPHOBLASTOID CELLS

In addition to being tested in an *in vitro* system, the p.D4918N variant was able to be tested in immortalised B-lymphoblastoid cells *ex vivo*. Members of a family with a history of CCD were tested for a number of known RyR1 variants, one of which – p.D4918N – was shown to segregate with the disease. This variant corresponds to c.14752G>A in the cDNA sequence and is one of the *RYR1* variants tested in the recombinant system. Blood samples from family members were then used to extract B-lymphocytes as described previously (Anderson et al. 2008) which were then immortalised and grown *ex vivo*. The response of these cells to the RyR1 agonist 4-C*m*C was measured for family members both with and without the variant of interest. In addition, non-family members known to be MH-susceptible and MH negative were used as positive and negative controls, respectively.

The family members tested in the calcium release assays are shown in figure 3.11. Individuals III:3,4,6 and IV:5 had been diagnosed with CCD and were found to be heterozygous for the g.38585048G>A (Genomic accession number ENSG00000196218.9) variant in *RYR1* which corresponds to the p.D4918N variant in RyR1. Individuals III:1 and IV:1 were the only family members to be tested for MH susceptibility by IVCT and were found to be MHS(h). Neither individual carries D4918N variant. The family member V1 has a history of EHS, but neither her nor her mother (IV:4) carry the D4918N variant.

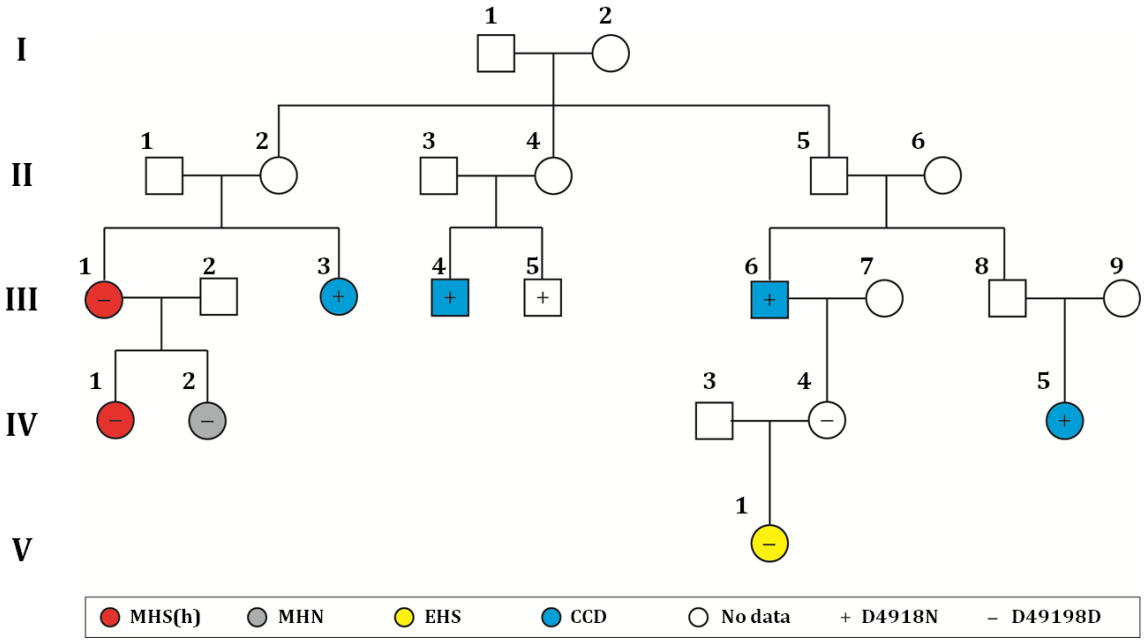

FIGURE 3.11 Pedigree of family with CCD-linked p.D4918N variant

Five generations of a family with D4918N-linked central core disease. Letters indicate generations and numbers indicate individuals. Phenotypes and genotypes are indicated by colours and symbols.

The positive control for MH-susceptibility used in the calcium release assays in B-lymphocytes was from an individual with the p.R2355W mutation. This mutation has been shown to segregate with MH and cause an increase in calcium release in both B-lymphocytes (Schiemann et al. 2014) and myotubes (Wehner et al. 2004) in response to 4-C*m*C, caffeine and halothane. The MH negative control used in B-lymphocytes was from an individual who tested negative for MH in IVCT and has been used as a negative control for MH susceptibility in a previous report (Schiemann et al. 2014).

3.3.1 HRM ANALYSIS OF B-LYMPHOCYTES

The presence of the p.R2355W mutation (g.38499670C>T: Genomic accession number ENSG00000196218.9) in the gDNA extracted from the B-lymphocytes from the individual used as an MHS positive control in calcium release assays was confirmed by HRM analysis. Genomic DNA samples were used as positive (mutation present) and negative (mutation absent) controls. The genotype of the R2355W gDNA sample was determined by comparing its melting curve (plotted as the change in fluorescence over

time versus temperature) with that of the positive and negative controls using LightCycler 480 Gene Scanning software (Roche). In Figure 3.12, the positive control represented by a red melting curve showed two peaks corresponding to the two alleles present – one wild type and one mutant. These peaks were at relatively lower temperatures compared to the negative control represented by a blue melting curve which showed one peak as it was homozygous wild type. The R2355W gDNA sample also represented by a red curve had a similar set of melting peaks to the positive control, and therefore can be confirmed to contain the p.R2355W mutation.

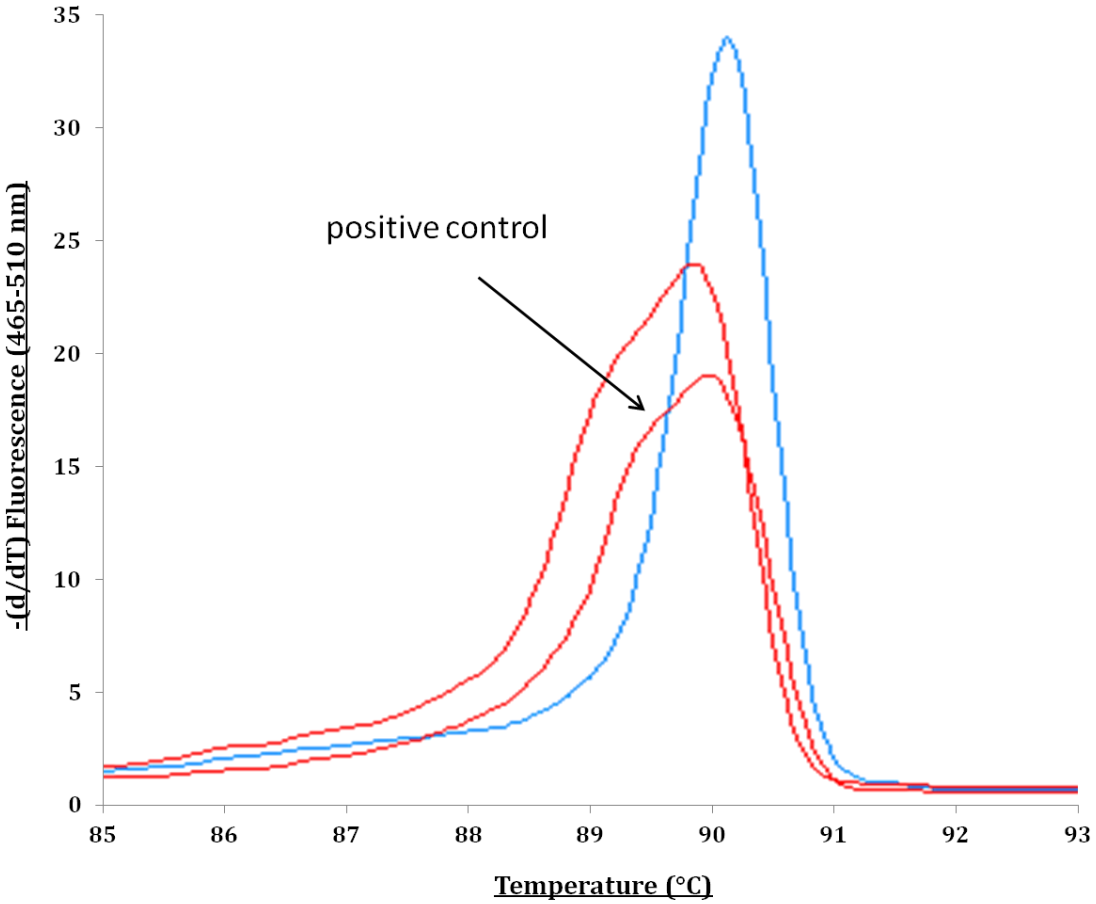

FIGURE 3.12 Confirmation of p.R2355W mutation

High resolution melting analysis was carried out on the gDNA extracted from B-lymphocytes of the R2355W individual as well as positive and negative gDNA controls for the genotype encoding the p.R2355W mutation. The melting curves were plotted as the decrease in fluorescence over time (-(d/dT) fluorescence) at 465 – 510 nm versus temperature (degrees Celsius) using the LightCycler 480 Gene Scanning software (Roche). Positive and negative controls are shown as red and blue melting curves, respectively.

HRM analysis was carried out on the genomic DNA extracted from B-lymphocytes of a family in which the p.D4918N variant (g.38585048G>A: Genomic accession number ENSG00000196218.9) was found to segregate with CCD. Genomic DNA samples were used as positive (variant present) and negative (variant absent) controls. The genotypes of the gDNA samples from each family member were determined by comparing the melting curve with those of the positive and negative controls. In Figure 3.13, the positive control represented by a red melting curve showed two peaks corresponding to the two alleles present – wild type and variant. The peaks were at relatively lower temperatures than the negative control represented by a blue melting curve which showed one peak, corresponding to the homozygous wild type genotype. Three family members – III:3,4 and IV:5 – had similar melting peaks (red) to the positive control and therefore can be confirmed to contain the p.D4918N variant. Two family members – III:1 and V:1 – as well as both the MHS and MHN gDNA controls had similar melting peaks (blue) to the negative control and therefore can be confirmed not to contain the p.D4918N variant.

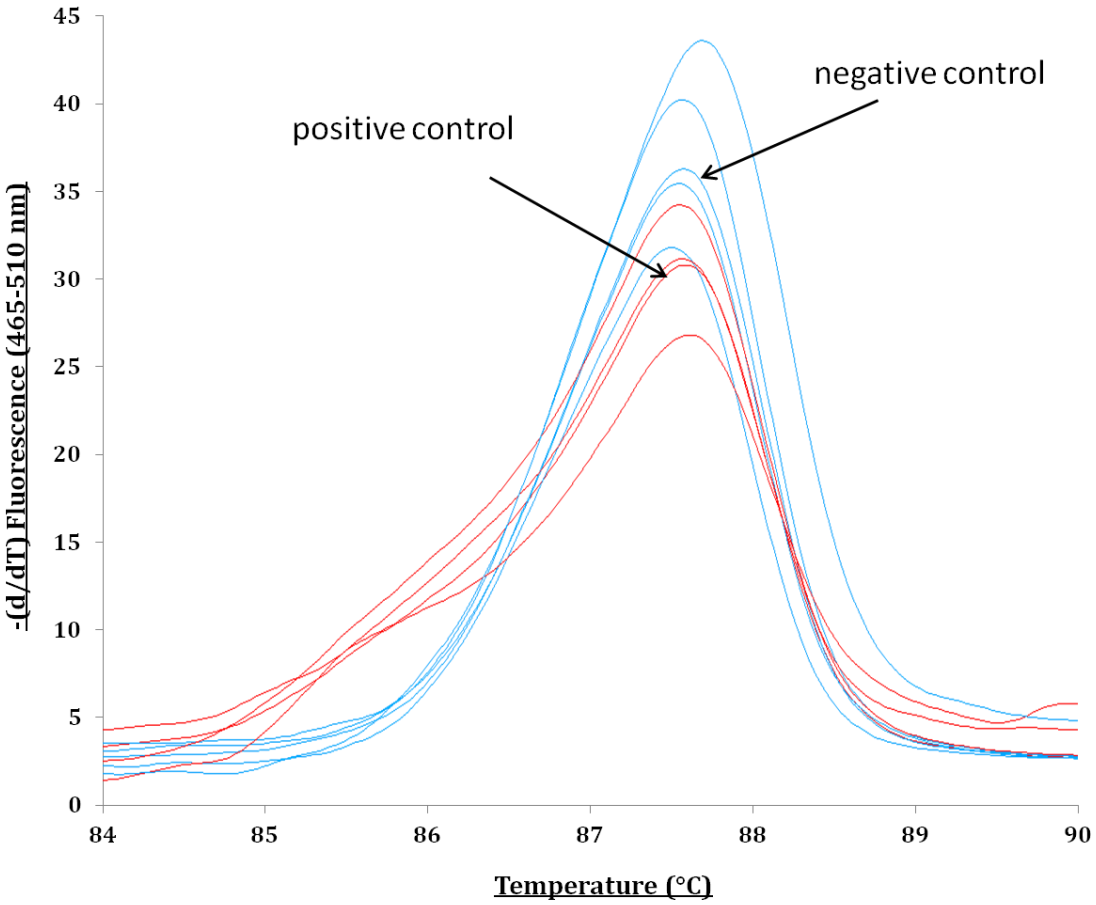

FIGURE 3.13 Confirmation of p.D4918N variant

High resolution melting analysis was carried out on gDNA extracted from B-lymphocytes of individuals of a family in which the p.D4918N variant was found to segregate with CCD. HRM analysis was also carried out on the gDNA from MHS and MHN controls for calcium release assays and the positive and negative gDNA controls for the genotype encoding the p.D4918N mutation. The melting curves were plotted as the decrease in fluorescence over time (-(d/dT) fluorescence) at 465 – 510 nm versus temperature (degrees Celsius) using the LightCycler 480 Gene Scanning software (Roche). Positive and negative controls are shown as red and blue melting curves, respectively.

3.3.2 ANALYSIS OF D4918N RyR1 ACTIVITY *EX VIVO*

The ability of the RyR1 calcium channel of B-lymphocyte cells to release calcium from the endoplasmic reticulum into the cytoplasm was detected by spectrofluorometry using the ratiometric dye Fura-2 that fluoresces when bound to intracellular calcium, as described in section 3.2.3. The increase in intracellular calcium was measured after the addition of incremental doses of the RyR1-specific agonist 4-C*m*C to the cells and then calculated as a percentage of total calcium release. Total calcium release was defined as the increase in intracellular calcium in the presence of 1000 µM 4-C*m*C. A minimum of three biological replicates (separate preparations of the immortalised B-lymphocytes from each individual) were carried out for each concentration of 4-C*m*C used in the assays. The data from all assays for each variant were pooled and a sigmoidal curve was fitted to the data using OriginLab software. These curves were plotted on a graph (Figure 3.14) with the mean ± SEM values for each concentration of 4-C*m*C tested for each variant.

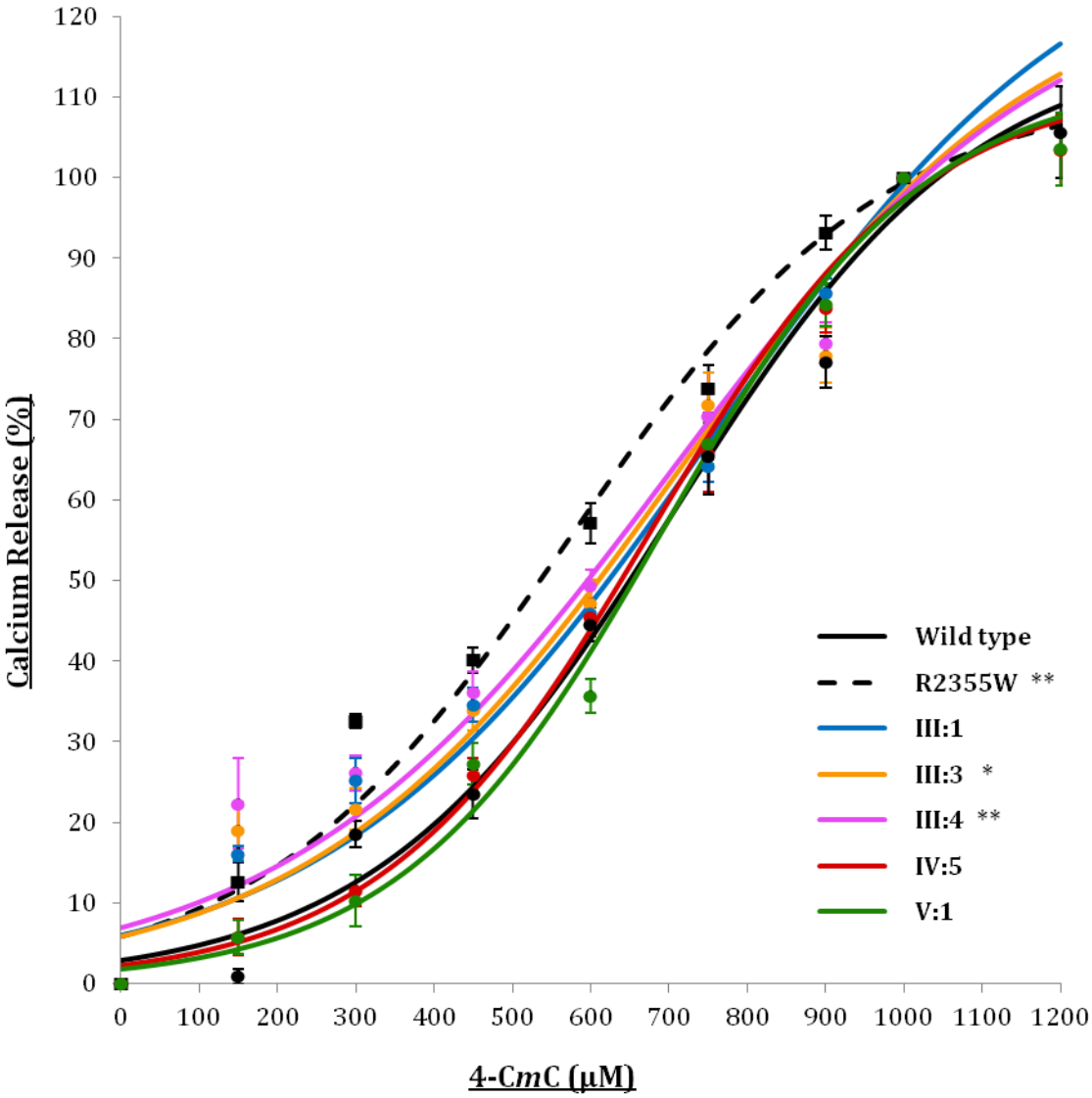

FIGURE 3.14 Calcium release activity of RyR1 in B-lymphocytes

Incremental doses of the RyR1-specific agonist 4-C*m*C were introduced into B-lymphocytes of individuals of a family in which the p.D4918N variant was found to segregate with CCD. The level of calcium release at each concentration of 4-C*m*C was normalised to 100% calcium release with 1000 µM 4-C*m*C. Data points represent the mean ± SEM and statistical significance is denoted by * ($P < 0.05$, ≥95% confidence) and ** ($P < 0.01$, ≥99% confidence).

In addition, for each assay carried out, a sigmoidal curve was fitted to the data using OriginLab software and the half maximal effective concentration (EC_{50}) was calculated from the curve. The mean ± SEM values were then calculated from the EC_{50} values of

all assays carried out for each B-lymphocyte cell line and statistical significance was calculated using an unpaired Student's t-test (table 3.2).

TABLE 3.2 EC_{50} values of B-lymphocytes tested *ex vivo*

INDIVIDUAL	EC_{50} ± SEM (µM 4-C*m*C)	P-VALUE	CONFIDENCE
Wild type	650.9 ± 11		
R2355W	533.7 ± 9.5	3.46×10^{-6} **	100%
III:1	623.1 ± 10.9	0.113	89%
III:3	612.5 ± 11.3	0.032 *	97%
III:4	580.6 ± 7.3	6.73×10^{-4} **	100%
IV:5	656.7 ± 4.8	0.652	35%
V:1	645.2 ± 11.6	0.730	27%

* Statistical significance, $P < 0.01$

** Statistical significance, $P < 0.05$

Calcium release assays carried out on B-lymphocytes from individuals IV:5 and V:1 both had very similar calcium release curves compared to the wild type control which was reflected in their low statistical significance values of 0.65 and 0.73, respectively. The B-lymphocytes from family members III:1,3 and 4 showed a slightly increased sensitivity to the RyR1-agonist as their calcium release curves were shifted slightly to the left when compared to the wild type RyR1 curve. Although the EC_{50} values for only two of these curves were found to be statistically significant, III:1 had a very similar calcium release curve to the other two individuals and was found to be 89% significant, which is still a high level of confidence. However, when examined visually, the shape of their curves are not dissimilar to the wild type control unlike the relatively large difference seen in the curve of the positive control (R2355W) and therefore these results are inconclusive.

CHAPTER FOUR: Discussion

The main objective of the current study was to determine the effect of C-terminal variants on the function of the skeletal muscle calcium channel, RyR1. The variants selected for the present study were chosen for their association with either central core disease or malignant hyperthermia (two neuromuscular disorders that are often found to coincide in patients), or a non-specific myopathy that may be central core disease. Five RyR1 variants– p.M4640I, p.V4849I, p.F4857S, p.R4861H, p.D4918N (GenBank accession NP_000531.2) – were examined in a heterologous system *in vitro*; one of which, the p.D4918N variant, was also able to be examined in immortalised B-lymphocytes *ex vivo*. All five variants were cloned into the full-length human *RYR1* cDNA (GenBank accession NM_000540.2) in a pcDNA3.1+ vector previously constructed by Sato et al. (2010). Variant *RYR1* cDNAs were then used to transiently-transfect HEK-293T cells, which are a useful cell system to compare the effects of RyR1 variants in a homogeneous background. The level of RyR1 expression and the localisation of the RyR1 channels in HEK-293T cells were confirmed by western blotting (Figure 3.8) and immunofluorescence (Figure 3.9) respectively, where all RyR1 variants were expressed at similarly high levels and observed to localise to the endoplasmic reticulum. The sensitivity of RyR1 to the specific agonist 4-C*m*C was measured in transiently-transfected HEK-293T cells and immortalised B-lymphocytes using a ratiometric fluorescent calcium indicator in calcium release assays. The data from these assays were then used to compare the activities of the variant RyR1 channels with that of the wild type RyR1 channel and statistically significant differences were then estimated using a Student's *t*-test. In this chapter, all RyR1 variants are referred to by their amino acid change in the human RyR1 sequence – GenBank accession NP_000531.2 – unless stated otherwise.

As a positive control for MH susceptibility, the previously-characterised H4833Y mutation located in exon 100 of *RYR1* was also tested under the same conditions. This substitution was first identified in 2008 where it was shown to segregate with MH (Anderson et al. 2008). B-lymphocytes from patients with the variant were more sensitive to 4-C*m*C than negative controls (Anderson et al. 2008). This mutation was

confirmed as being MH-causative when HEK-293T cells expressing H4833Y RyR1 were significantly more sensitive to 4-C*m*C than their wild type counterparts (Sato et al. 2010), resulting in this mutation being accepted as MH-causative by the European Malignant Hyperthermia Group (2014).

4.1 CHARACTERISATION OF M4640I RyR1

The substitution of a methionine for an isoleucine at residue 4640 was found by DNA sequencing in a patient with central core disease who was diagnosed as MHS by IVCT; the individual was heterozygous for this variant. The single nucleotide change, located in exon 95 of *RYR1*, is contained in an evolutionarily-conserved region of the gene and no amino acid substitutions at the corresponding residue were observed in a number of ryanodine receptor isoforms, including RyR2 from human and RyR1 from mouse, pig, rabbit and cow (Figure 4.1). 'Polymorphism Phenotyping' version two (PolyPhen-2) and 'Sorting Tolerant from Intolerant' (SIFT) are algorithms that determine the likelihood that a variant amino acid will impact the structure and function of the protein in which it is located (Kumar et al. 2009, Adzhubei et al. 2010). PolyPhen-2 predicted that the M4640I substitution would be damaging to the protein, with a probability of 0.969; the probability scores range from 0 – 1 with a score of zero assigned to benign substitutions and a score of 1 assigned to likely damaging substitutions. This prediction had a false-positive rate of 0.77, however, and a true-positive rate of 0.95, which are not convincing statistics. SIFT predicted this substitution would be tolerated in the protein with a SIFT score of 0.06 which is close to the threshold; this score ranges from 0 – 1 and anything below 0.05 is determined to be damaging. These results indicated that, although unlikely, this variant could potentially have some damaging effect on the function of the protein. In addition, the model for RyR1 structure by Yan et al. (2015) places the M4640 residue at the luminal edge of the S2 transmembrane helix (Figure 1.1B) where the substitution to an isoleucine residue is unlikely to have a significant effect on the function of the channel as it is structurally-similar to methionine.

Human RyR1 NP_000531.2	E	S	T	G	Y	M	E	P	A	L	R
Human RyR2 NP_001026.2	E	S	**S**	G	Y	M	E	P	**T**	L	R
Mouse RyR1 NP_033135.2	E	S	T	G	Y	M	E	P	A	L	R
Pig RyR1 NP_001001534.1	E	S	T	G	Y	M	E	P	A	L	R
Rabbit RyR1 P11716.1 *	E	S	T	G	Y	M	E	P	A	L	**C**
Cow RyR1 NP_001193706.1	E	S	T	G	Y	M	E	P	A	L	R

FIGURE 4.1 The M4640 residue is evolutionarily conserved

The amino acid sequences of human (*Homo sapiens*) RyR1, human RyR2, mouse (*Mus musculus*) RyR1, pig (*Sus scrofa*) RyR1, rabbit (*Oryctolagus cuniculus*) RyR1 and cow (*Bos Taurus*) RyR1 were compared at residues corresponding to 4635 – 4645 in the human RyR1 sequence. Variants are indicated in bold and the M4640 residue in each sequence is indicated by the red box. All accession numbers are GenBank sequences unless specified. * Indicates a UniProt sequence.

The residues flanking this amino acid are highly-conserved (Figure 4.1) and have been linked to central core disease almost exclusively, with only one variant found as yet – R4645Q – associated with MH (Davis et al. 2003, Shepherd et al. 2004, Wu et al. 2006, Robinson et al. 2006). Two RyR1 substitutions at the same residue – M4640V and M4640R – have also been identified in individuals with central core disease (Dulhunty et al. 2012, Kraeva et al. 2013) but only the M4640V variant has been functionally characterised as yet. In a study by Dulhunty et al. (2012), dyspedic mouse myotubes were transfected with rabbit *RYR1* cDNA containing the variant *in* vitro and the expressed M4640V RyR1 was observed to have no effect on EC coupling compared with the wild type channel when stimulated by 4-C*m*C and caffeine. The results of the present study support this research as the M4640I variant showed normal calcium release in response to the RyR1 agonist, 4-C*m*C, when compared to the wild type RyR1 channel using the HEK-293T heterologous system (Figure 3.10). Therefore it seems from this evidence that this variant is unlikely to have an effect on calcium release through RyR1 *in vivo*. It is important to note, however, that MH and CCD are complex disorders that are likely caused by a number of genetic factors and the effect of the

variant on other protein interactions that may modulate RyR1 activity cannot be ruled out as HEK-293T cells do not express the full complement of skeletal muscle proteins. Therefore it is possible that the M4640I variant is indeed the cause of central core disease in the patient, but it is also possible that the IVCT result was a false-positive. The *RYR1* and *CACNA1S* genes belonging to the individual in whom the variant was originally found were completely sequenced and no other variants were identified, therefore if the IVCT result was not in fact a false positive, another gene could also be involved.

4.2 CHARACTERISATION OF V4849I RyR1

The substitution of a valine to an isoleucine at residue 4849 was first discovered in 2001 in a study investigating *RYR1* variants in CCD patients, but was disregarded as a control individual was heterozygous for the variant (Monnier et al. 2001). Since then, however, numerous patients with CCD (Monnier et al. 2005, 2008, Kossugue et al. 2007) and MH after diagnosis by CHCT or IVCT (Sambuughin et al. 2005, Broman et al. 2011) have been found to be homozygous for the variant. If the V4849I RyR1 substitution is indeed causative of a disorder, it is likely to be through recessive inheritance as the CCD and MH phenotypes have only been observed in individuals homozygous for the variant. In one case, a child with CCD inherited an *RYR1* allele containing the V4849I variant from their mother and a truncated (predicted to be non-functional) *RYR1* allele from their father (Monnier et al. 2005). Both parents had normal phenotypes and so it seemed that monoallelic expression of the *RYR1* allele containing the recessive V4849I substitution revealed the CCD phenotype. The V4849I variant was originally thought to be linked to recessively-inherited MmD as histological analysis of a muscle biopsy taken from a patient homozygous for the variant revealed a phenotype indicative of MmD rather than CCD (Jungbluth et al. 2002). The gradual development of large central cores may be common to recessive inheritance of CCD, as evidenced by reports of another recessive myopathy that segregated with an *RYR1* variant. This family was initially diagnosed as MmD but later found to be CCD after the patients reached adulthood (Ferreiro et al. 2002). This may be a point of difference

between dominantly- and recessively-inherited CCD that could assist in the search for causative mutations.

The single nucleotide change, located in exon 101 of *RYR1*, is contained in an evolutionarily-conserved region of the gene and no amino acid substitutions at the corresponding residue were observed in a number of ryanodine receptor isoforms, including RyR2 from human and RyR1 from mouse, pig, rabbit and cow (Figure 4.2). Variants in the region surrounding the V4849 residue have been linked to both CCD and MH (Oyamada et al. 2002, Wu et al. 2006, Robinson et al. 2006, Bharucha-Goebel et al. 2013), although these variants have been observed to be inherited in a dominant manner. The substitution of the valine to the larger isoleucine residue at the V4849 site – located in the middle of the S5 transmembrane helix (Figure 1.1B) – may have an effect on the hypothesised interaction between the S5 and S6 helices that are proposed to make up the calcium pore (Yan et al. 2015). This may result in altered calcium conductance through the channel and therefore a disease phenotype. PolyPhen-2 predicted that the V4849I substitution would be damaging to the protein, with a probability of 0.999. This prediction had a false-positive rate of 0.14 and a true-positive rate of 0.99, supporting the reliability of this prediction. SIFT predicted this substitution would be tolerated in the protein as it has a SIFT score of 0.1, which is relatively low and yet above the threshold to be considered damaging. These results indicate that this variant may have some damaging effect on the function of the protein, although this effect is unlikely to be severe.

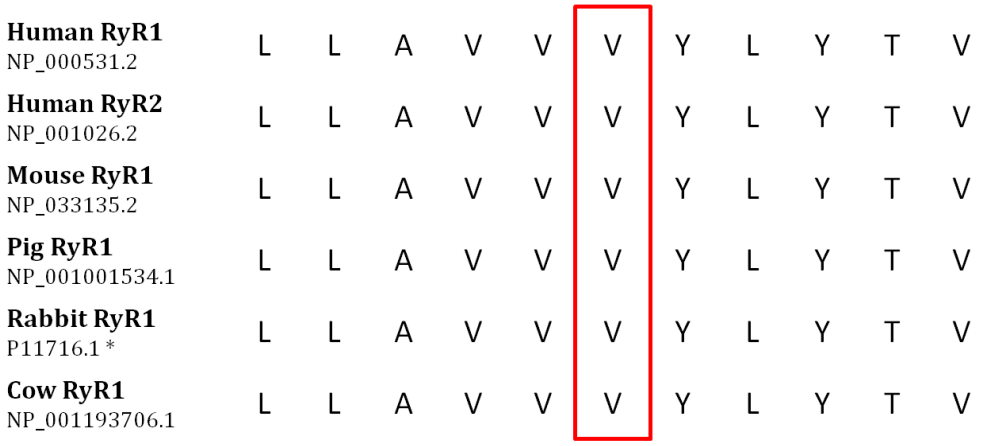

FIGURE 4.2 The V4849 residue is evolutionarily conserved

The amino acid sequences of human (*Homo sapiens*) RyR1, human RyR2, mouse (*Mus musculus*) RyR1, pig (*Sus scrofa*) RyR1, rabbit (*Oryctolagus cuniculus*) RyR1 and cow (*Bos Taurus*) RyR1 were compared at residues corresponding to 4844 – 4854 in the human RyR1 sequence. The V4849 residue in each sequence is indicated by the red box. All accession numbers are GenBank sequences unless specified. * Indicates a UniProt sequence.

The V4849I RyR1 variant expressed in HEK-293T cells was shown in the current study to release higher than normal levels of calcium into the cytoplasm of the cells when stimulated by 4-C*m*C (Figure 3.10). The variant had a significantly lower EC_{50} than its wild type counterpart, meaning the RyR1 channel was activated at significantly lower concentrations of agonist. This finding suggests that the V4849I variant may confer MH susceptibility to individuals that carry it. Tong et al. (1999b) proposed that both MH and some cases of CCD are caused by hyperactive RyR1 channels. MH is thought to be caused by spontaneous calcium release under stimulating conditions causing a crisis event while CCD is thought to be caused by spontaneous calcium release which is not so easily corrected by the cell and leads to a phenotype characterised by weak muscle action. In these cases, leakage of calcium in resting conditions was thought to lead to a constant state of altered calcium homeostasis in the centre of skeletal muscle cells and a relatively normal state of calcium homeostasis on the periphery of cells where extracellular pathways such as ECCE and SOCE might play a role. These events were proposed in the study by Tong et al. (1999b) to be the cause of the classical CCD

phenotype of centralised cores in muscle fibres lacking cellular activity. In this way, a defective channel that causes the CCD phenotype could also be a hyperactive channel that displays the MH phenotype with pharmacological or environmental stimulation.

A similar finding to that of the present research was also found in a study that examined the effect that human RyR1 containing the V4849I variant expressed in HEK-293 cells would have on calcium release in response to stimulation by caffeine (Merritt 2013). The V4849I RyR1 channels examined in this study released significantly more calcium than the wild type channel in the presence of low concentrations of caffeine. This suggested that this variant was causative of MH, although the calcium release curve of this variant was significantly more sensitive to agonist in the study by Merritt (2013) than that of the variant tested in the present research. Fluo-4 was used as a calcium indicator, however, which is a non-ratiometric dye which can be affected by variables such as uneven loading of cells and therefore may have been the cause of the slightly disparate results between the two studies. In disagreement with those results, a study by Ducreux et al. (2006) examined the effect this variant had on the calcium homeostasis of B-lymphocytes from a patient with CCD who was homozygous for the V4849I substitution in RyR1 and their asymptomatic parents who were both heterozygous for V4849I. The B-lymphocytes from all three individuals showed no difference in calcium release from the endoplasmic reticulum in response to 4-C*m*C or caffeine when compared with control individuals (Ducreux et al. 2006). This contradicts the results from the current study, although it may be the result of the different experimental systems used or the genetic makeup of the individuals tested, as only three closely-related people were examined.

Although the system used in the present study does not differentiate between dominant and recessive mutations, the fact that the EC_{50} of the V4849I RyR1 channel was intermediate between the wild type RyR1 and the MHS control RyR1 could be indicative of the recessive nature of this variant. When RyR1 channels consisting of wild type monomers as well as monomers containing dominant RyR1 mutations were expressed and analysed in HEK-293 cells by Tong et al. (1999b), they were observed to have sensitivity to caffeine midway between homotetrameric wild type and mutant channels. Individuals homozygous for MH or CCD mutations are rare and thus when

RyR1 variants that are usually in a heterotetrameric state *in vivo* are analysed in a homozygous system, their phenotypes are likely to be extreme versions of that which would be expected of a heterotetramer channel. It may be that the calcium release curve of the V4849I variant observed in the present study was more indicative of its respective phenotype than the MH-positive control (H4833Y) *in vivo.* This is beacause any phenotype observed in HEK-293T cells transfected with a single *RYR1* allele would be representative of the phenotype of a homozygous individual and the H4833Y mutation, along with the majority of MH-causative mutations, has only been observed in heterozygous form.

4.3 CHARACTERISATION OF F4857S RyR1

The *de novo* substitution of a phenylalanine to a serine at residue 4857 was found by Sanger sequencing of selected regions of the *RYR1* gene in a patient presenting with a non-specific myopathy. The variant was not found in either parent, both of whom were asymptomatic. The single nucleotide change, located in exon 101 of *RYR1*, is contained in an evolutionarily-conserved region of the gene and no amino acid substitutions at the corresponding residue were found in a number of ryanodine receptor isoforms, including RyR2 from human and RyR1 from mouse, pig, rabbit and cow (Figure 4.3). PolyPhen-2 predicted that the F4857S substitution would be damaging to the protein, with a probability of 0.999; this prediction had a false-positive rate of 0.14 and a true-positive rate of 0.99. SIFT predicted this substitution would be damaging to the protein as it has a SIFT score of 0. These results indicated that this variant would likely have a very damaging effect on the function of the protein.

Human RyR1 NP_000531.2	Y	T	V	V	A	F	N	F	F	R	K
Human RyR2 NP_001026.2	Y	T	V	V	A	F	N	F	F	R	K
Mouse RyR1 NP_033135.2	Y	T	V	V	A	F	N	F	F	R	K
Pig RyR1 NP_001001534.1	Y	T	V	V	A	F	N	F	F	R	K
Rabbit RyR1 P11716.1 *	Y	T	V	V	A	F	N	F	F	R	K
Cow RyR1 NP_001193706.1	Y	T	V	V	A	F	N	F	F	R	K

FIGURE 4.3 The F4857 residue is evolutionarily conserved

The amino acid sequences of human (*Homo sapiens*) RyR1, human RyR2, mouse (*Mus musculus*) RyR1, pig (*Sus scrofa*) RyR1, rabbit (*Oryctolagus cuniculus*) RyR1 and cow (*Bos Taurus*) RyR1 were compared at residues corresponding to 4852 – 4862 in the human RyR1 sequence. The F4857 residue in each sequence is indicated by the red box. All accession numbers are GenBank sequences unless specified. * Indicates a UniProt sequence.

Variants of the residues surrounding F4857 have been mostly linked to central core disease (Monnier et al. 2001, Robinson et al. 2006, Bharucha-Goebel et al. 2013); however, the A4856G and N4858D substitutions of the residues adjacent to F4857 have been linked to MH and CCD, respectively (Wu et al. 2006, Robinson et al. 2006). In the current study, HEK-293T cells were transiently-transfected with *RYR1* cDNA containing the variant encoding the F4857S amino acid substitution. Although western blotting and immunofluorescence analysis confirmed the expression and localisation of RyR1 proteins to the ER, no calcium release was detected upon stimulation by the RyR1-agonist 4-C*m*C (figure 3.10). These results suggest that the F4857S RyR1 protein is a non-functional calcium channel which would likely produce a very severe – if not lethal – phenotype in a homozygous individual. According to the model by Yan et al. (2015), the F4857 residue is located in the S5 transmembrane helix, near the luminal side (Figure 1.1B). The substitution of a large, hydrophobic phenylalanine residue to a small, polar serine residue at the 4857 residue would likely have an effect on the interaction between the S5 and S6 helices that make up the calcium pore. As the

individual with the *de novo* F4857S variant was identified as being heterozygous for the variant, it is likely that the RyR1 channels of this individual were tetramers comprised of both variant and wild type monomers. In these heterotetramers, the F4857S RyR1 monomers may inhibit the gating of RyR1 channels, causing reduced calcium conductance during their activation. This may result in hypoactive RyR1 channels *in vivo* considered to be the cause of some CCD cases.

4.4 CHARACTERISATION OF R4861H RyR1

The substitution of arginine to histidine at residue 4861 was found in two studies in 2001 to segregate with central core disease (Monnier et al. 2001, Tilgen et al. 2001). It has since been linked to CCD in numerous reports (Monnier et al. 2001, Quinlivan et al. 2003, Shepherd et al. 2004, Kossugue et al. 2007, Brandom et al. 2013, Gu et al. 2014), leading to its inclusion in the list of *RYR1* mutations accepted by the EMHG as being causative of MH (EMHG, 2014). Moreover, the substitution of arginine to a cysteine at the same site has also been linked to CCD (Bharucha-Goebel et al. 2013) as have substitutions in the region surrounding R4861 (Quinlivan et al. 2003, Wu et al. 2006, Robinson et al. 2006). It was because of these findings that R4861H was used in the present research as a positive control for a RyR1 mutation that is known to be causative of CCD. Because there currently exists no functional assay to test RyR1 variants for CCD, most variants are categorized as being 'linked' to CCD while very few are determined to have sufficient evidence to be labelled as CCD mutations.

The single nucleotide change, located in exon 95 of *RYR1*, is contained in an evolutionarily-conserved region of the gene and no amino acid substitutions at the corresponding residue were found in a number of ryanodine receptor isoforms, including RyR2 from human and RyR1 from mouse, pig, rabbit and cow (Figure 4.4). PolyPhen-2 predicted that the R4861H substitution would be damaging to the protein, with a probability of 1; this prediction had a false-positive rate of 0 and a true-positive rate of 1. SIFT predicted this substitution would be damaging to the protein as it has a SIFT score of 0. These results indicated that this mutation would be almost certain to have a damaging effect on the function of the protein.

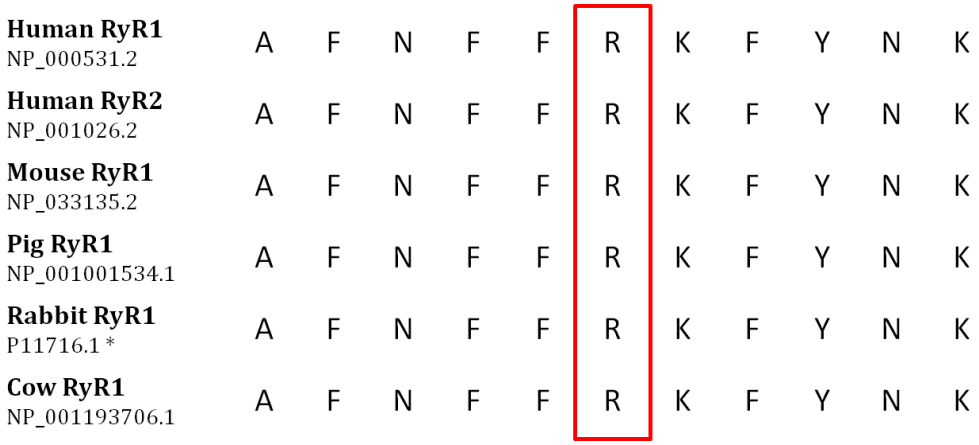

FIGURE 4.4 The R4861 residue is evolutionarily conserved

The amino acid sequences of human (*Homo sapiens*) RyR1, human RyR2, mouse (*Mus musculus*) RyR1, pig (*Sus scrofa*) RyR1, rabbit (*Oryctolagus cuniculus*) RyR1 and cow (*Bos Taurus*) RyR1 were compared at residues corresponding to 4856 – 4866 in the human RyR1 sequence. The R4861 residue in each sequence is indicated by the red box. All accession numbers are GenBank sequences unless specified. * Indicates a UniProt sequence.

In the current study, the R4861H mutation produced RyR1 channels that were significantly more sensitive to 4-C*m*C than wild type channels (table 3.1). The calcium release curve of the mutant RyR1 channel was strikingly similar to the MHS positive control RyR1 mutant, H4833Y (figure 3.10), suggesting that this mutation is causative of MH. This supports the finding by Davis et al. (2003) of an individual with the R4861H RyR1 mutation that was diagnosed with both MH by IVCT and CCD. The R4861 residue is situated at the luminal edge of the transmembrane helix S5 where electronegative hairpin loops located above the selectivity filter are believed to attract cations to the channel for their subsequent transport out into the cytoplasm (Yan et al. 2015). The function of the large, positively-charged arginine residues in these loops is unknown; however, the substitution to an uncharged, more hydrophobic residue at that position may result in an increase in the overall negative charge of the highly-dynamic luminal loops. This may cause an increase in the transport of calcium across the membrane and thus produce a phenotype typical of a hyperactive RyR1 channel. As was likely the

case for the V4849I variant, this hyperactive RyR1 channel was indicative of the class of CCD-causing mutation the R4861H mutation belongs to.

Although the assay system used in the present study was not used to measure physiological changes that could be attributed to a leaky calcium channel, based on prior evidence, it is probable that the R4861H RyR1 channels are leaky, constantly releasing calcium and disturbing the calcium homeostasis of the cell. Another study that used B-lymphocytes from CCD patients with the R4861H mutation to examine the functional properties of the RyR1 mutant channels partially confirms this theory (Tilgen et al. 2001). These RyR1 channels were shown to continuously leak calcium into the cytoplasm of the lymphocytes thereby altering the delicate balance of calcium homeostasis in the B-lymphocytes (Tilgen et al. 2001). This leakage is hypothesised to result in the formation of cores in the centre of skeletal muscle fibres that are reduced in cellular activity and thus cause weak muscle action and the CCD symptoms. It may be that this hyperactive channel also results in the spontaneous and uncontrollable release of calcium when stimulated by pharmacological or environmental triggers, additionally causing the MH phenotype.

However, contrary to the results of the present study, it was suggested by Tilgen et al. (2001) that this SR leak resulted in the reduced calcium release upon activation by 4-C*m*C, indicating that this mutation would not confer MH susceptibility but rather cause only CCD. As only one patient was tested in that study, however, the genetic background of the patient may have been a contributing factor. For instance, this was likely the case for the variant p.R163C which was reported to segregate with both MH and CCD in one pedigree and MH alone in another unrelated pedigree (Quane et al. 1993). It is likely that other factors, in addition to RyR1, contribute to the presentation of malignant hyperthermia and central core disease as both have a large amount of phenotypic heterogeneity and there are so many protein modulators involved in EC coupling. An example of this is the variation in JP-45 function (mentioned in chapter 1.2.3) which is hypothesised to contribute to the variable penetrance typical of MH by reducing EC coupling by a small but not insignificant amount (Yasuda et al. 2013).

4.5 CHARACTERISATION OF D4918N RyR1

The substitution of aspartic acid to asparagine at residue 4918 was found to segregate with central core disease in a family. The single nucleotide change, located in exon 95 of *RYR1*, is contained in an evolutionarily-conserved region of the gene and no amino acid substitutions at the corresponding residue were observed in a number of ryanodine receptor isoforms, including RyR2 from human and RyR1 from mouse, pig, rabbit and cow (Figure 4.5). PolyPhen-2 predicted that the D4918N substitution would be damaging to the protein, with a probability of 1; this prediction had a false-positive rate of 0 and a true-positive rate of 1. SIFT predicted this substitution would be damaging to the protein as it has a SIFT score of 0. These results indicated that this variant would be almost certain to have a damaging effect on the function of the protein. Variants in the region surrounding this residue have also been linked to central core disease (Monnier et al. 2001, Davis et al. 2003, Wu et al. 2006), suggesting that this region may be important for the proper conductance of calcium through the channel.

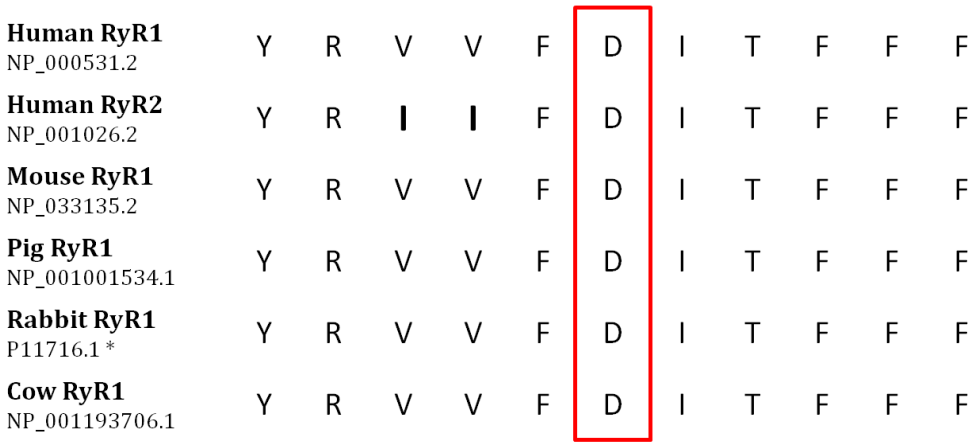

FIGURE 4.5 The D4918 residue is evolutionarily conserved

The amino acid sequences of human (*Homo sapiens*) RyR1, human RyR2, mouse (*Mus musculus*) RyR1, pig (*Sus scrofa*) RyR1, rabbit (*Oryctolagus cuniculus*) RyR1 and cow (*Bos Taurus*) RyR1 were compared at residues corresponding to 4913 – 4923 in the human RyR1 sequence. Variants are indicated in bold and the D4918 residue in each sequence is indicated by the red box. All accession numbers are GenBank sequences unless specified. * Indicates a UniProt sequence.

4.5.1 CHARACTERISATION IN A HETEROLOGOUS SYSTEM

The effect of the D4918N variant on the function of RyR1 was investigated in the research carried out for this thesis using a heterologous system involving the transient transfection of HEK-293T cells with human *RYR1* cDNA containing the variant. Previously, HEK-293 cells transiently-transfected with rabbit *RYR1* cDNA containing a similar variant – corresponding to D4918A in human RyR1 protein – were tested for the function of RyR1 which was found to be an inactive channel (Gao et al. 2000). The RyR1 channels containing the variant were unresponsive to caffeine treatment, releasing no calcium when measured with Rhod-2, a non-ratiometric dye (Gao et al. 2000). Moreover, no ryanodine binding was observed for this RyR1 variant in HEK-293 cells (Gao et al. 2000), suggesting this substitution causes the RyR1 channel to be totally unresponsive to activation by agonists. In support of these findings, a recent study reported the D4918N RyR1 to be an inactive channel also, based on the activity of the variant in two cell systems transiently-transfected with rabbit *RYR1* cDNA (Kraeva et al. 2013). No caffeine-induced calcium release was detected in HEK-293 cells containing the variant in this study, nor was any electrically- or 4-C*m*C-induced calcium release detected in transfected dyspedic mouse myotubes containing the variant (Kraeva et al. 2013).

The results of the current study support these findings, where calcium release upon stimulation by 4-C*m*C was measured in HEK-293T cells transiently-transfected with human *RYR1* cDNA. Using this system, no calcium release was observed from the D4918N RyR1 channels when RyR1-agonist was introduced (figure 3.10). The expression and localisation of RyR1 proteins to the ER was confirmed by western blotting and immunofluorescence analysis and therefore the lack of response to the agonist can be attributed to the change in the protein function rather than a lack of RyR1 channels in the ER membrane. The loss of RyR1 activity with this variant is likely due to the substitution of a negatively-charged amino acid to an uncharged amino acid, as aspartate and asparagine are similar in both size and hydrophobicity. Similarly, the variant characterised by Gao et al. (2000) which was also reported to confer a loss of activity to the RyR1 channel involves the substitution to an uncharged, hydrophobic

alanine residue. D4918 is located within the S6 transmembrane helix which forms the major part of the ion conducting pathway (Yan et al. 2015).

It is probable that the D4918N variant would be lethal in the homozygous form and therefore individuals that have been identified as being heterozygous for the variant would have RyR1 channels comprised of both variant and wild type monomers. In these heterotetramers, the D4918N RyR1 monomers may inhibit the gating of RyR1 channels, causing reduced calcium conductance during their activation. This may result in hypoactive RyR1 channels *in vivo* considered to be the cause of some CCD cases. The results from the research presented here as well as the previous studies mentioned earlier indicate the negative charge at the 4918 site is likely to be an essential component of the S6 helix involved in the attraction and rapid conductance of cations through the pore, and therefore the transport of calcium across the SR membrane.

4.5.2 THE D4918N VARIANT IN B-LYMPHOBLASTOID CELLS

The use of B-lymphocytes taken from patients in whom a certain RyR1 variant segregates with a disease phenotype is a useful tool for the purposes of characterising RyR1 variants in a physiologically relevant system. As people suffering from CCD are assumed to have MH when undergoing anaesthesia, they are rarely tested by IVCT for their MH susceptibility. Because of this, there was a lack of information in this regard for the family examined in the current research. This pedigree was included in the current study after the D4918N variant was found by sequencing selected regions of the RyR1 gene in all family members suffering from central core disease (figure 3.10). One family member (individual III:5 in section 3.3, figure 3.11) was found to be a carrier of the D4918N variant but was asymptomatic. Although this individual was not tested by muscle biopsy, a diagnosis of CCD could be excluded on the basis of a lack of observable symptoms alone. B-lymphocytes from selected family members were made available and were subsequently immortalised using the Epstein-Barr virus as described previously (Anderson et al. 2008) and tested for abnormal calcium release as described in section 2.4.5.

While none of the B-lymphocyte cell lines demonstrated the classical MH response observed with the R2355W positive control, abnormal calcium release was observed in

three of the five cell lines when stimulated with 4-C*m*C (table 3.2). The level of calcium released in the B-lymphocytes of individuals III:1,3,4 at lower concentrations of agonist was much higher than the MHN control and other family members, while at higher concentrations of agonist the calcium release was observed to be similar to the control sample (figure 3.14). This is suggestive of perhaps a RyR1 channel which opens inappropriately at low levels of activation, which is the opposite of what one might expect of an inactive calcium channel. Individuals III:3 and III:4 were both confirmed as being carriers of the D4918N variant (figure 3.13) and exhibit central core disease, while individual III:1 was confirmed as being negative for the D4918N variant and positive for MH by IVCT with halothane. A CCD diagnosis cannot be ruled out for this individual as no histological tests were performed, although they were observed to be asymptomatic. Despite the fact that statistical significance ($P<0.05$) was not achieved for this individual, the calcium release was calculated to be different from the MHN control with 89% confidence, and had a similar curve to the two family members that were found to be different from the control with statistical significance – III:3 and III:4.

The two descendants of individual III:1 (IV:1 and IV:2) were both negative for the D4918N variant, one of which was MHS(h) by IVCT (figure 3.10). This suggests the presence of at least one other genetic factor causing a neuromuscular disorder in this family. This may be present in the entire extended family or it may have been introduced paternally to the pedigree by individual II:1 and be limited to direct descendants of this person. It is possible that this same genetic defect is the cause of the EHS in individual V:1 as this person was found to be negative for the D4918N variant (figure 3.13). The B-lymphocytes of this individual were found to have a normal calcium release, however, (table 3.2) and so this person is likely to be MHN. It is probable therefore that the EHS phenotype observed in individual V:1 was caused by an unrelated factor such as ineffective heat dissipation or extreme environmental conditions. The B-lymphocytes from the other individual observed to have no significantly different calcium release when stimulated with 4-C*m*C – IV:5 – was positive for both central core disease and the D4918N variant (figure 3.10). This indicates the significantly-increased calcium release in the presence of agonist observed for individuals III:3 and III:4 were unlikely to be a result of the D4918N

variant. It is feasible that these individuals are carriers of the alternative genetic defect hypothesised to cause the MHS(h) phenotype in individuals III:1 and IV:1 as individuals III:1 and III:3 are siblings and individual III:4 is their first maternal cousin.

The results from the calcium release assays carried out on B-lymphocytes from members of the pedigree examined in this research do not corroborate the findings discussed in section 4.5.1. When expressed in homozygous state in HEK-293T cells, the D4918N RyR1 channel was unresponsive to stimulation by 4-C*m*C when calcium release was measured. This type of inactive channel would be expected to cause a decrease in calcium conductance when expressed alongside the wild type RyR1 in a heterozygous system as in the family members tested in the present study. Contrary to this theory, B-lymphocytes from D4918N carriers were observed to have no change in calcium release when compared to the MHN control; some individuals were even found to have hyperactive calcium channels. The D4918N variant did not segregate with any specific calcium release phenotype in the B-lymphocytes tested and therefore no conclusions can be made from the results of these assays without further information.

CHAPTER FIVE: Final Summary

In this research, five C-terminal RyR1 variants – M4640I, V4849I, F4857S, R4861H and D4918N (GenBank accession NP_000531.2) – were characterised using a heterologous system, one of which was also tested in B-lymphocytes taken from carriers of the D4918N variant. An interesting observation from the current study was that the three C-terminal variants – M4640I, R4861H and D4918N – linked solely to central core disease produced three completely divergent calcium release profiles in HEK-293T cells transfected with *RYR1* cDNA containing the variants of interest. Normal calcium release was observed for M4640I RyR1 channels stimulated with agonist; R4861H RyR1 was found to be a hyperactive channel similar to the MHS control channel, H4833Y; while the D4918N channel was observed to be unresponsive to stimulation by 4-C*m*C. The individual carrying the *de novo* F4857S RyR1 variant had been diagnosed with a non-specific myopathy which can now be hypothesised to be central core disease as it produced an inactive channel in HEK-293T cells comparable to the relatively well-characterised D4918N variant. Of note is the phenotype seen in the HEK-293T cells transfected with the V4849I RyR1 variant which was linked to both CCD and MH and was hypothesised to be a recessive *RYR1* allele as individuals were asymptomatic unless homozygous for the variant. This was observed to be a hyperactive channel in transiently-transfected HEK-293T cells, supporting the findings of a report using a similar method (Merritt 2013).

Although the D4918N variant was found to be unresponsive to the agonist used in the present study, this was not supported by the results of the calcium release assays carried out in the B-lymphocytes of the pedigree carrying the variant. The results of these assays in B-lymphocytes indicated that this variant does not consistently produce hyperactive or hypoactive RyR1 channels; however, the abnormal calcium release phenotype did not segregate with CCD either. No valid argument can be made for the divergent results of the D4918N RyR1 channel between these two physiological systems, except that the complement of accessory proteins varies greatly between the two types of cell systems and the genetic background of the B-lymphocytes is a confounding factor. Phenotypes produced by RyR1 variants can vary greatly between

physiological systems and two examples of this were found in the present study. The V4849I found to be a hyperactive channel in the current study was observed to confer normal calcium release in the heterozygous or homozygous state when compared to MHN controls (Ducreux et al. 2006). The R4861H RyR1 variant also observed to be a hyperactive channel in the current research was reported to be a 'leaky' channel in B-lymphocytes with a reduced response to agonist (Tilgen et al. 2001). As was the case in the current study, the B-lymphocytes of carriers of the V4849I and R4861H variants from these two studies were from a single pedigree and therefore genetic background may have been an issue (Tilgen et al. 2001, Ducreux et al. 2006). Further investigation into the pedigree examined in the present study is needed before conclusions may be drawn.

5.1 FUTURE DIRECTIONS

5.1.1 LIMITATIONS OF THIS RESEARCH

In order to strengthen the findings reported in this thesis, further exploration of the phenotypes conferred by the C-terminal RyR1 variants included in the current study is required. While the results of the present study indicate that the M4640I RyR1 variant is not likely to be causative of a neuromuscular disorder, expression of the variant in a more physiologically relevant system such as dyspedic myotubes may produce more physiologically relevant results.

The two CCD variants observed to have an increased sensitivity to agonist compared with wild type RyR1 were V4849I and R4861H. The well-characterised, CCD-causative R4861H mutation was found to produce a hyperactive channel in this study, therefore supporting the theory of the hyperactive channel altering calcium homeostasis and producing the CCD phenotype. As no functional test exists presently to characterise RyR1 variants as being causative of CCD, the functional characterisation of a known CCD mutation such as R4861H in RyR1 is beneficial to the understanding of the physiological changes that take place at the cellular level that lead to the CCD phenotype. More information is required before any conclusions may be drawn – specifically the characterisation of a R4861H/wild type RyR1 heterotetramer which

may demonstrate more clearly the phenotype of a heterozygous individual as well as the analysis of the intracellular calcium levels during both stimulation and resting states which may elucidate the cause of CCD in patients with the R4861H variant.

An interesting hypothesis emerging from this research is the theory that there may be difference in the severity of the abnormal calcium release observed between dominant and recessive RyR1 variants. Single-channel recordings of the action of the V4849I RyR1 channel may elucidate how this recessive variant caused a reduced form of the MH response in HEK-293T cells. Additionally, the comparison of the function of RyR1 channels homozygous and heterozygous for recessive *RYR1* variants would provide valuable information as to the reason for the recessive nature of these variants. This may assist in the identification of recessive *RYR1* variants which might normally be disregarded due to their presence in MHN control individuals, as was the case initially with the V4849I variant.

More information is required about the myopathy observed in the patient with the *de novo* F4857S variant before assumptions can be made regarding the function of this channel in causing this particular myopathy, when expressed in heterozygous form. Analysis of this variant, as well as the inactive D4918N RyR1 channel, in a more physiologically relevant system such as transfected dyspedic mouse myotubes should clarify their roles in their respective myopathies. In addition, as neither variant has been observed in a homozygous state in a patient as it is potentially a lethal genotype, the functional analysis of RyR1 heterotetramers containing both wild type and either the F4857S or D4918N variant RyR1 monomers would be valuable. Of particular interest was the lack of segregation between abnormal calcium release profiles of B-lymphocytes and either the presence of the D4918N variant or the CCD phenotype in the pedigree examined in this research. Abnormal calcium release was observed for some individuals of the family; however, this is likely due to a genetic anomaly independent of the D4918N variant and CCD status of the individuals.

5.1.2 ALTERNATIVE RESEARCH METHODOLOGY

The creation of RyR1 variants currently requires site-directed mutagenesis (SDM) of *RYR1* cDNA – either human or rabbit in origin – which is fifteen kilobases in length.

While the Kapa HiFi PCR kit has reportedly the highest-fidelity DNA polymerase currently commercially available (Kapa Biosystems), the issue of the introduction of errors during the PCR amplification of the *RYR1* cDNA persists. Because of this, mutagenesis is performed on a relatively small representative section of *RYR1* cDNA and subsequently sub-cloned into the full-length cDNA. This is a convoluted and often challenging process due to the lack of unique restriction endonuclease recognition sites in the cDNA sequence. Therefore a system which eliminates the need for sub-cloning steps by removing the PCR amplification aspect of SDM would be advantageous. The site-specific splicing of DNA using endonucleases and the subsequent repair of that DNA is a relatively new technique for the precise introduction of nucleotide changes. Transcription activator-like effector nucleases, clustered regulatory interspaced short palindromic repeats and zinc finger nucleases are three methods that have been used successfully for the introduction of sequence variations into various genomes (Urnov et al. 2010, Joung & Sander 2013, Hwang et al. 2013). These technologies may be used for the direct introduction of variants to the genome of model organisms for the characterisation of variants *in vivo* and could potentially be engineered for the high-throughput creation of full-length *RYR1* cDNAs as well as the cDNA of other candidate genes. This should reduce both the time and the costs of this process compared to the methods currently in use.

Functional characterisation of RyR1 variants is a relatively labour-intensive process as assays are currently performed individually and the analysis of samples is repeated several times in order to have sufficient biological replicates for data analysis. It is because of this that adopting a high throughput system to assay many samples simultaneously would be an efficient alternative to the methods currently in use. An example of such a system is the range of plate readers currently available from Seahorse Bioscience (North Billerica, Massachusetts, United States of America) which can measure the oxygen consumption and extracellular acidification of 96 samples simultaneously (Klingler et al. 2002). While these instruments are versatile in that they are able to analyse several types of samples including adherent cells such as HEK-293 cells and non-adherent cells such as B-lymphocytes, they are very expensive and the analysis would be made more informative if another parameter such as intracellular

calcium was also able to be measured. A relatively inexpensive alternative to this is the selection of products currently offered by Luxcel Biosciences (County Cork, Ireland) which assess metabolic changes such as oxygen consumption and extracellular acidification of samples in a standard fluorescence plate reader; however, only one parameter may be measured per assay, making this approach less efficient. What is clear is that unless a high-throughput system is put in place to characterise the many variants linked to neuromuscular disorders, progress into the understanding of these diseases will continue to be slow.

5.1.3 FUNCTIONAL ASSAYS TO COMPARE MH AND CCD

As the findings of the present study have shown, there are a variety of RyR1 phenotypes that lead to neuromuscular disorders. In order to elucidate the similarities and differences that exist between MH and CCD, the transport of calcium in cells representative of these disorders under different physiological conditions needs to be examined. One way of doing this would be to measure the concentration of intracellular calcium in the cells – any cell system could be used – at a resting state and a stimulated state. There are a number of intracellular calcium indicators which can be used for specific tasks, for example the low affinity dye Mag-Fluo-4AM from Invitrogen may be used to detect high calcium levels in the ER or SR of living cells while the high affinity, ratiometric dye Fura-2AM may be used to detect small calcium levels in the cytoplasm of cells (Life Technologies: Invitrogen 2010). The use of these calcium indicators could reveal the changes in the levels of the calcium store and the cytoplasmic calcium between the resting state and stimulated states which may help in understanding the relationship between MH and CCD phenotypes. As it has been theorised that CCD is caused by lower muscle activity under normal conditions whereas MH is asymptomatic in these conditions, a full grasp on the CCD phenotype during the resting state is essential to differentiating these related neuromuscular disorders.

It has been proposed that a combination of a low affinity dye and a high affinity dye for the detection of ER and cytoplasmic calcium, respectively, may be used for the direct comparison of the concentration of calcium in these stores in real time (Life

Technologies: Invitrogen 2010). These systems may be challenging to combine as the specific detection of ER calcium usually requires the removal of the dye from the cytoplasm by way of a method such as dialysis. It may prove useful, however, for the investigation of the roles that SOCE and ECCE play in the complex EC coupling pathways in MH and CCD patients. In some cases of CCD it is thought the normally hypoactive calcium channel that causes the CCD phenotype can become a hyperactive channel under specific stimulating conditions such as after exposure to inhalational anaesthesia. This intriguing paradox could in fact be due to the various extracellular calcium pathways compensating for the loss-of-function phenotype of CCD under resting conditions. This may explain the apparent MH phenotypes observed with some RyR1 variants such as the R4861H mutation examined in the present study.

5.1.4 OTHER FACTORS CONTRIBUTING TO MH AND CCD

Causative mutations for MH have thus far been characterised in the genes for RyR1 and the α1 subunit of DHPR only (EMHG, 2014); however, malignant hyperthermia is a genetically heterogeneous disease with several other genetic loci linked to MH susceptibility. The variable penetrance of both MH and CCD – even between patients carrying the same RyR1 mutation – suggests the action of as yet unknown mutations in multiple genes that act in concert to produce a specific phenotype. It has been reported that while variants at certain genetic loci may not cause a condition individually, they may contribute minor changes to the disease manifestation when combined with other variants (Robinson et al. 2000, 2003). The reason for this is that excitation-contraction coupling in skeletal muscle involves a complex interplay of protein channels and signalling proteins, each with their own specific regulatory mechanisms. The detection of variants could be carried out by a method such as exome sequencing in population-wide screens as was the case for the JP-45 variants discovered by Althobiti et al. (2009). The identification of alleles that are involved in the presentation of neuromuscular disorders would be not only beneficial to the understanding of these disease phenotypes, but would contribute to the overall understanding of skeletal muscle calcium homeostasis. The functional analysis of variants is essential to this understanding as many minor variants involved in MH or CCD phenotypes may not segregate exclusively with disease.

5.2 FINAL CONCLUSION

The majority of muscle tissue in the human body is represented by skeletal muscle and the proper regulation of intracellular calcium is essential to the normal functioning of this muscle. Two neuromuscular disorders caused by changes in calcium homeostasis, central core disease and malignant hyperthermia, have been linked to dysfunctional RyR1 channels. The research presented in this thesis identified RyR1 variants that are likely causative of CCD and/or MH with two distinct aetiologies while the characterisation of one variant (p.M4640I) was inconclusive. Two RyR1 variants linked to CCD (p.V4849I and p.R4861H) were observed in a heterologous system to produce hyperactive RyR1 channels – one of which was a recessive allele – and thus confirm the theory that centralised cores in muscle fibres and muscle weakness in some cases of CCD is a result of hyperactive and leaky channels. This theory is based on the idea that with these RyR1 variants, calcium homeostasis is altered so dramatically in the cell that the muscle has reduced function while the area of the cell closer to the membrane compensates through the use of extracellular pathways to maintain calcium homeostasis in these regions. Conversely, two RyR1 variants (p.F4857S and p.D4918N) linked to core myopathies – either one or both of which are CCD – were observed to have a complete lack of EC coupling in the homozygous form in a heterologous system. These variants would likely result in reduced function of the tetramer and therefore a hypoactive calcium channel when in the heterozygous form in which they were identified in the patients. In addition to this, one of these inactive channels was also analysed in B-lymphocytes extracted from the tissue of participants with the variant that also suffer from CCD, but the results were inconclusive. No clear pattern could be ascertained from the results of this analysis, demonstrating the complex nature of these disorders. Altogether, the findings of this research are a valuable contribution to the current body of work, with some confirmations of previous ideas and some novel findings.

References

Abramoff, M. D., Magalhaes, P. J., & Ram, S. J. (2004). Image Processing with ImageJ. *Biophotonics International*, *11*(7), 36–42.

Adzhubei, I. A., Schmidt, S., Peshkin, L., Ramensky, V. E., Gerasimova, A., Bork, P., Kondrashov, A. S., & Sunyaev, S. R. (2010). A method and server for predicting damaging missense mutations. *Nature methods*, *7*(4), 248–249.

Allen, G. C., Larach, M. G., & Kunselman, A. R. (1998). The sensitivity and specificity of the caffeine-halothane contracture test: a report from the North American Malignant Hyperthermia Registry. The North American Malignant Hyperthermia Registry of MHAUS. *Anesthesiology*, *88*(3), 579–588.

Althobiti, M., Booms, P., Fiszer, D., Halsall, P. J., Shaw, M. A., & Hopkins, P. M. (2009). Sequencing the *JSPR1* gene in patients susceptible to malignant hyperthermia and identification of two novel genetic variants. *British Journal of Anaesthesia*, *103*(2), 321–321.

Anderson, A. A., Altafaj, X., Zheng, Z., Wang, Z.-M., Delbono, O., Ronjat, M., Treves, S., & Zorzato, F. (2006). The junctional SR protein JP-45 affects the functional expression of the voltage-dependent Ca^{2+} channel Cav1.1. *Journal of Cell Science*, *119*(10), 2145–2155.

Anderson, A. A., Brown, R. L., Polster, B., Pollock, N., & Stowell, K. M. (2008). Identification and biochemical characterization of a novel ryanodine receptor gene mutation associated with malignant hyperthermia. *Anesthesiology*, *108*(2), 208–215.

Anderson, A. A., Treves, S., Biral, D., Betto, R., Sandonà, D., Ronjat, M., & Zorzato, F. (2003). The novel skeletal muscle sarcoplasmic reticulum JP-45 protein. Molecular cloning, tissue distribution, developmental expression, and interaction with alpha 1.1 subunit of the voltage-gated calcium channel. *The Journal of Biological Chemistry*, *278*(41), 39987–39992.

Attali, R., Aharoni, S., Treves, S., Rokach, O., Becker Cohen, M., Fellig, Y., Straussberg, R., Dor, T., Daana, M., Mitrani-Rosenbaum, S., & Nevo, Y. (2013). Variable myopathic presentation in a single family with novel skeletal *RYR1* mutation. *PloS One*, *8*(7), e69296.

Avila, G., O'Brien, J. J., & Dirksen, R. T. (2001). Excitation--contraction uncoupling by a human central core disease mutation in the ryanodine receptor. *Proceedings of the National Academy of Sciences of the United States of America*, *98*(7), 4215–4220.

Balshaw, D., Gao, L., & Meissner, G. (1999). Luminal loop of the ryanodine receptor: a pore-forming segment? *Proceedings of the National Academy of Sciences of the United States of America*, *96*(7), 3345–3347.

Bannister, R. A., Pessah, I. N., & Beam, K. G. (2009). The skeletal L-type Ca^{2+} current is a major contributor to excitation-coupled Ca^{2+} entry. *The Journal of General Physiology*, *133*(1), 79–91.

Beam, K. G., Tanabe, T., & Numa, S. (1989). Structure, function, and regulation of the skeletal muscle dihydropyridine receptor. *Annals of the New York Academy of Sciences*, *560* 127–137.

Bharucha-Goebel, D. X., Santi, M., Medne, L., Zukosky, K., Zukosky, K., Dastgir, J., Shieh, P. B., Winder, T., Tennekoon, G., Finkel, R. S., Dowling, J. J., Monnier, N., & Bönnemann, C. G. (2013). Severe congenital *RYR1*-associated myopathy: the expanding clinicopathologic and genetic spectrum. *Neurology*, *80*(17), 1584–1589.

Bhat, M. B., & Ma, J. (2002). The transmembrane segment of ryanodine receptor contains an intracellular membrane retention signal for $Ca^{(2+)}$ release channel. *The Journal of Biological Chemistry*, *277*(10), 8597–8601.

Bhat, M. B., Zhao, J., Takeshima, H., & Ma, J. (1997). Functional calcium release channel formed by the carboxyl-terminal portion of ryanodine receptor. *Biophysical Journal*, *73*(3), 1329–1336.

Boncompagni, S., Thomas, M., Lopez, J. R., Allen, P. D., Yuan, Q., Kranias, E. G., Franzini-Armstrong, C., & Perez, C. F. (2012). Triadin/Junctin double null mouse reveals a differential role for Triadin and Junctin in anchoring CASQ to the jSR and regulating $Ca^{(2+)}$ homeostasis. *PloS One*, *7*(7), e39962.

Bouchama, A., & Knochel, J. P. (2002). Heat stroke. *The New England Journal of Medicine*, *346*(25), 1978–1988.

Brandom, B. W., Bina, S., Wong, C. A., Wallace, T., Visoiu, M., Isackson, P. J., Vladutiu, G. D., Sambuughin, N., & Muldoon, S. M. (2013). Ryanodine receptor type 1 gene variants in the malignant hyperthermia-susceptible population of the United States. *Anesthesia and Analgesia*, *116*(5), 1078–1086.

Brandt, A., Schleithoff, L., Jurkat-Rott, K., Klingler, W., Baur, C., & Lehmann-Horn, F. (1999). Screening of the ryanodine receptor gene in 105 malignant hyperthermia families: novel mutations and concordance with the *in vitro* contracture test. *Human Molecular Genetics*, *8*(11), 2055–2062.

Broman, M., Heinecke, K., Islander, G., Schuster, F., Glahn, K., Bodelsson, M., Treves, S., & Müller, C. (2011). Screening of the ryanodine 1 gene for malignant hyperthermia causative mutations by high resolution melt curve analysis. *Anesthesia and Analgesia*, *113*(5), 1120–1128.

Campbell, I. T., Ellis, F. R., Evans, R. T., & Mortimer, M. G. (1983). Studies of body temperatures, blood lactate, cortisol and free fatty acid levels during exercise in human subjects susceptible to malignant hyperpyrexia. *Acta Anaesthesiologica Scandinavica*, *27*(5), 349–355.

Capacchione, J. F., Sambuughin, N., Bina, S., Mulligan, L. P., Lawson, T. D., & Muldoon, S. M. (2010). Exertional rhabdomyolysis and malignant hyperthermia in a patient with ryanodine receptor type 1 gene, L-type calcium channel alpha-1 subunit gene, and calsequestrin-1 gene polymorphisms. *Anesthesiology*, *112*(1), 239–244.

Chelu, M. G., Goonasekera, S. A., Durham, W. J., Tang, W., Lueck, J. D., Riehl, J., Pessah, I. N., Zhang, P., Bhattacharjee, M. B., Dirksen, R. T., & Hamilton, S. L. (2005). Heat- and anesthesia-induced malignant hyperthermia in an RyR1 knock-in mouse. *The FASEB Journal*, *20*(2), 329–330.

Cherednichenko, G., Hurne, A. M., Fessenden, J. D., Lee, E. H., Allen, P. D., Beam, K. G., & Pessah, I. N. (2004). Conformational activation of Ca^{2+} entry by depolarization of skeletal myotubes. *Proceedings of the National Academy of Sciences of the United States of America*, *101*(44), 15793–15798.

D'Arcy, C. E., Bjorksten, A., Yiu, E. M., Bankier, A., Gillies, R., McLean, C. A., Shield, L. K., & Ryan, M. M. (2008). King-denborough syndrome caused by a novel mutation in the ryanodine receptor gene. *Neurology*, *71*(10), 776–777.

Davis, M., Brown, R., Dickson, A., Horton, H., James, D., Laing, N., Marston, R., Norgate, M., Perlman, D., Pollock, N., & Stowell, K. (2002). Malignant hyperthermia associated with exercise-induced rhabdomyolysis or congenital abnormalities and a novel *RYR1* mutation in New Zealand and Australian pedigrees. *British Journal of Anaesthesia*, *88*(4), 508–515.

Davis, M., Haan, E., Jungbluth, H., Sewry, C., North, K., Muntoni, F., Kuntzer, T., Lamont, P., Bankier, A., Tomlinson, P., Sánchez, A., Walsh, P., Nagarajan, L., Oley, C., Colley, A., Gedeon, A., Quinlivan, R., Dixon, J., James, D., Müller, C. R., & Laing, N. G. (2003). Principal mutation hotspot for central core disease and related myopathies in the C-terminal transmembrane region of the *RYR1* gene. *Neuromuscular disorders*, *13*(2), 151–157.

Denborough, M. A., & Lovell, R. R. (1960). Anaesthetic deaths in a family. *Lancet*, *2*(45),.

Diaz-Sylvester, P. L., Porta, M., & Copello, J. A. (2008). Halothane modulation of skeletal muscle ryanodine receptors: dependence on Ca^{2+}, Mg^{2+}, and ATP. *American Journal of Physiology. Cell Physiology*, *294*(4), 1103–1112.

Dietze, B., Bertocchini, F., Barone, V., Struk, A., Sorrentino, V., & Melzer, W. (1998). Voltage-controlled Ca^{2+} release in normal and ryanodine receptor type 3 (RyR3)-deficient mouse myotubes. *The Journal of Physiology*, *513*(1), 3–9.

Dirksen, R. T., & Avila, G. (2004). Distinct effects on Ca^{2+} handling caused by malignant hyperthermia and central core disease mutations in RyR1. *Biophysical Journal*, *87*(5), 3193–3204.

Dowling, J. J., Lillis, S., Amburgey, K., Zhou, H., Al-Sarraj, S., Buk, S. J. A., Wraige, E., Chow, G., Abbs, S., Leber, S., Lachlan, K., Baralle, D., Taylor, A., Sewry, C., Muntoni, F., & Jungbluth, H. (2011). King-Denborough syndrome with and without mutations in the skeletal muscle ryanodine receptor (*RYR1*) gene. *Neuromuscular disorders*, *21*(6), 420–427.

Dubowitz, V., & Brooke, M. H. (1973). Muscle biopsy: a modern approach. W. B. Saunders.

Ducreux, S., Zorzato, F., Ferreiro, A., Jungbluth, H., Muntoni, F., Monnier, N., Müller, C. R., & Treves, S. (2006). Functional properties of ryanodine receptors carrying three amino acid substitutions identified in patients affected by multi-minicore disease and central core disease, expressed in immortalized lymphocytes. *Biochemical Journal*, *395*(2), 259–266.

Ducreux, S., Zorzato, F., Müller, C., Sewry, C., Muntoni, F., Quinlivan, R., Restagno, G., Girard, T., & Treves, S. (2004). Effect of ryanodine receptor mutations on interleukin-6 release and intracellular calcium homeostasis in human myotubes from malignant hyperthermia-susceptible individuals and patients affected by central core disease. *The Journal of Biological Chemistry*, *279*(42), 43838–43846.

Du, G. G., Sandhu, B., Khanna, V. K., Guo, X. H., & MacLennan, D. H. (2002). Topology of the Ca^{2+} release channel of skeletal muscle sarcoplasmic reticulum (RyR1). *Proceedings of the National Academy of Sciences of the United States of America*, *99*(26), 16725–16730.

Dulhunty, A. F., Wium, E., Li, L., Hanna, A. D., Mirza, S., Talukder, S., Ghazali, N. A., & Beard, N. A. (2012). Proteins within the intracellular calcium store determine cardiac RyR channel activity and cardiac output. *Clinical and Experimental Pharmacology & Physiology*, *39*(5), 477–484.

Eltit, J. M., Ding, X., Pessah, I. N., Allen, P. D., & Lopez, J. R. (2013). Nonspecific sarcolemmal cation channels are critical for the pathogenesis of malignant hyperthermia. *FASEB journal: official publication of the Federation of American Societies for Experimental Biology*, *27*(3), 991–1000.

EMHG: European Malignant Hyperpyrexia Group. (1984). A protocol for the investigation of malignant hyperpyrexia (MH) susceptibility. *British Journal of Anaesthesia*, *56*(11), 1267–1269.

EMHG: European Malignant Hyperthermia Group. (2014). Genetics in malignant hyperthermia.

Engel, A. G., Gomez, M. R., & Groover, R. V. (1971). Multicore disease. A recently recognized congenital myopathy associated with multifocal degeneration of muscle fibers. *Mayo Clinic Proceedings*, *46*(10), 666–681.

Ferreiro, A., Monnier, N., Romero, N. B., Leroy, J.-P., Bönnemann, C., Haenggeli, C.-A., Straub, V., Voss, W. D., Nivoche, Y., Jungbluth, H., Lemainque, A., Voit, T., Lunardi, J., Fardeau, M., & Guicheney, P. (2002). A recessive form of central core disease, transiently presenting as multi-minicore disease, is associated with a homozygous mutation in the ryanodine receptor type 1 gene. *Annals of Neurology*, *51*(6), 750–759.

Fessenden, J. D., Perez, C. F., Goth, S., Pessah, I. N., & Allen, P. D. (2003). Identification of a key determinant of ryanodine receptor type 1 required for activation by 4-chloro-*m*-cresol. *The Journal of Biological Chemistry*, *278*(31), 28727–28735.

Gao, L., Balshaw, D., Xu, L., Tripathy, A., Xin, C., & Meissner, G. (2000). Evidence for a role of the lumenal M3-M4 loop in skeletal muscle $Ca^{(2+)}$ release channel (ryanodine receptor) activity and conductance. *Biophysical Journal*, *79*(2), 828–840.

Girard, T., Urwyler, A., Censier, K., Mueller, C. R., Zorzato, F., & Treves, S. (2001). Genotype-phenotype comparison of the Swiss malignant hyperthermia population. *Human Mutation*, *18*(4), 357–358.

Gomes, B., Savignac, M., Moreau, M., Leclerc, C., Lory, P., Guery, J.-C., & Pelletier, L. (2004). Lymphocyte calcium signaling involves dihydropyridine-sensitive L-type calcium channels: facts and controversies. *Critical Reviews in Immunology*, *24*(6), 425–447.

Gonsalves, S. G., Ng, D., Johnston, J. J., Teer, J. K., Stenson, P. D., Cooper, D. N., Mullikin, J. C., Biesecker, L. G., & NISC Comparative Sequencing Program. (2013). Using exome data to identify malignant hyperthermia susceptibility mutations. *Anesthesiology*, *119*(5), 1043–1053.

Goonasekera, S. A., Beard, N. A., Groom, L., Kimura, T., Lyfenko, A. D., Rosenfeld, A., Marty, I., Dulhunty, A. F., & Dirksen, R. T. (2007). Triadin binding to the C-terminal luminal loop of the ryanodine receptor is important for skeletal muscle excitation contraction coupling. *The Journal of General Physiology*, *130*(4), 365–378.

Gouadon, E., Schuhmeier, R. P., Ursu, D., Anderson, A. A., Treves, S., Zorzato, F., Lehmann-Horn, F., & Melzer, W. (2006). A possible role of the junctional face protein JP-45 in modulating Ca^{2+} release in skeletal muscle. *The Journal of Physiology*, *572*(1), 269–280.

Greenfield, J., Cornman, T., & Shy, G. (1958). The Prognostic Value of the Muscle Biopsy in the Floppy Infant. *Brain*, *81*(4), 461–&.

Groom, L., Muldoon, S. M., Tang, Z. Z., Brandom, B. W., Bayarsaikhan, M., Bina, S., Lee, H.-S., Qiu, X., Sambuughin, N., & Dirksen, R. T. (2011). Identical *de novo* mutation in the type 1 ryanodine receptor gene associated with fatal, stress-induced malignant hyperthermia in two unrelated families. *Anesthesiology*, *115*(5), 938–945.

Gschwend, M. H., Rüdel, R., Brinkmeier, H., Taylor, S. R., & Föhr, K. J. (1999). A transient and a persistent calcium release are induced by chlorocresol in cultivated mouse myotubes. *Pflügers Archiv: European Journal of Physiology*, *438*(1), 101–106.

Gu, M., Zhang, S., Hu, J., Yuan, Y., Wang, Z., Da, Y., & Wu, S. (2014). Novel *RYR1* missense mutations in six Chinese patients with central core disease. *Neuroscience Letters*, *566* 32–35.

Györke, S., & Terentyev, D. (2008). Modulation of ryanodine receptor by luminal calcium and accessory proteins in health and cardiac disease. *Cardiovascular Research*, *77*(2), 245–255.

Herasse, M., Parain, K., Marty, I., Monnier, N., Kaindl, A. M., Leroy, J.-P., Richard, P., Lunardi, J., Romero, N. B., & Ferreiro, A. (2007). Abnormal distribution of calcium-handling proteins: a novel distinctive marker in core myopathies. *Journal of Neuropathology and Experimental Neurology*, *66*(1), 57–65.

Hwang, W. Y., Fu, Y., Reyon, D., Maeder, M. L., Tsai, S. Q., Sander, J. D., Peterson, R. T., Yeh, J.-R. J., & Joung, J. K. (2013). Efficient genome editing in zebrafish using a CRISPR-Cas system. *Nature Biotechnology*, *31*(3), 227–229.

Jayaraman, T., Brillantes, A. M., Timerman, A. P., Fleischer, S., Erdjument-Bromage, H., Tempst, P., & Marks, A. R. (1992). FK506 binding protein associated with the calcium release channel (ryanodine receptor). *The Journal of Biological Chemistry*, *267*(14), 9474–9477.

Joung, J. K., & Sander, J. D. (2013). TALENs: a widely applicable technology for targeted genome editing. *Nature Reviews. Molecular Cell Biology*, *14*(1), 49–55.

Jungbluth, H., Davis, M. R., Müller, C., Counsell, S., Allsop, J., Chattopadhyay, A., Messina, S., Mercuri, E., Laing, N. G., Sewry, C. A., Bydder, G., & Muntoni, F. (2004). Magnetic resonance imaging of muscle in congenital myopathies associated with *RYR1* mutations. *Neuromuscular disorders: NMD*, *14*(12), 785–790.

Jungbluth, H., Müller, C. R., Halliger-Keller, B., Brockington, M., Brown, S. C., Feng, L., Chattopadhyay, A., Mercuri, E., Manzur, A. Y., Ferreiro, A., Laing, N. G., Davis, M., Roper, H. P., Dubowitz, V., Bydder, G., Sewry, C. A., & Muntoni, F. (2002). Autosomal recessive inheritance of *RYR1* mutations in a congenital myopathy with cores. *Neurology*, *59*(2), 284–287.

Jurkat-Rott, K., McCarthy, T., & Lehmann-Horn, F. (2000). Genetics and pathogenesis of malignant hyperthermia. *Muscle & Nerve*, *23*(1), 4–17.

Kim, J. H., Jarvik, G. P., Browning, B. L., Rajagopalan, R., Gordon, A. S., Rieder, M. J., Robertson, P. D., Nickerson, D. A., Fisher, N. A., & Hopkins, P. M. (2013). Exome sequencing reveals novel rare variants in the ryanodine receptor and calcium channel genes in malignant hyperthermia families. *Anesthesiology*, *119*(5), 1054–1065.

Klein, A., Lillis, S., Munteanu, I., Scoto, M., Zhou, H., Quinlivan, R., Straub, V., Manzur, A. Y., Roper, H., Jeannet, P.-Y., Rakowicz, W., Jones, D. H., Jensen, U. B., Wraige, E., Trump, N., Schara, U., Lochmuller, H., Sarkozy, A., Kingston, H., Norwood, F., Damian, M., Kirschner, J., Longman, C., Roberts, M., Auer-Grumbach, M., Hughes, I., Bushby, K., Sewry, C., Robb, S., Abbs, S., Jungbluth, H., & Muntoni, F. (2012). Clinical and genetic findings in a large cohort of patients with ryanodine receptor 1 gene-associated myopathies. *Human Mutation*, *33*(6), 981–988.

Klingler, W., Baur, C., Georgieff, M., Lehmann-Horn, F., & Melzer, W. (2002). Detection of proton release from cultured human myotubes to identify malignant hyperthermia susceptibility. *Anesthesiology*, *97*(5), 1059–1066.

Koch, B. M., Bertorini, T. E., Eng, G. D., & Boehm, R. (1985). Severe multicore disease associated with reaction to anesthesia. *Archives of Neurology*, *42*(12), 1204–1206.

Köchling, A., Wappler, F., Winkler, G., & Schulte am Esch, J. S. (1998). Rhabdomyolysis following severe physical exercise in a patient with predisposition to malignant hyperthermia. *Anaesthesia and Intensive Care*, *26*(3), 315–318.

Kolb, M. E., Horne, M. L., & Martz, R. (1982). Dantrolene in human malignant hyperthermia. *Anesthesiology*, *56*(4), 254–262.

Kossugue, P. M., Paim, J. F., Navarro, M. M., Silva, H. C., Pavanello, R. C. M., Gurgel-Giannetti, J., Zatz, M., & Vainzof, M. (2007). Central core disease due to recessive mutations in *RYR1* gene: is it more common than described? *Muscle & Nerve*, *35*(5), 670–674.

Kraeva, N., Zvaritch, E., Rossi, A. E., Goonasekera, S. A., Zaid, H., Frodis, W., Kraev, A., Dirksen, R. T., MacLennan, D. H., & Riazi1, S. (2013). Novel excitation-contraction uncoupled *RYR1* mutations in patients with central core disease. *Neuromuscular disorders*, *23*(2), 120–132.

Ku, C.-S., Cooper, D. N., Polychronakos, C., Naidoo, N., Wu, M., & Soong, R. (2012). Exome sequencing: dual role as a discovery and diagnostic tool. *Annals of Neurology*, *71*(1), 5–14.

Kumar, P., Henikoff, S., & Ng, P. C. (2009). Predicting the effects of coding non-synonymous variants on protein function using the SIFT algorithm. *Nature Protocols*, *4*(7), 1073–1081.

Larach, M. G. (1989). Standardization of the caffeine halothane muscle contracture test. North American Malignant Hyperthermia Group. *Anesthesia and Analgesia*, *69*(4), 511–515.

Larach, M. G., Localio, A. R., Allen, G. C., Denborough, M. A., Ellis, F. R., Gronert, G. A., Kaplan, R. F., Muldoon, S. M., Nelson, T. E., & Ording, H. (1994). A clinical grading scale to predict malignant hyperthermia susceptibility. *Anesthesiology*, *80*(4), 771–779.

Lee, J. M., Rho, S.-H., Shin, D. W., Cho, C., Park, W. J., Eom, S. H., Ma, J., & Kim, D. H. (2004). Negatively charged amino acids within the intraluminal loop of ryanodine receptor are involved in the interaction with triadin. *The Journal of Biological Chemistry*, *279*(8), 6994–7000.

Life Technologies: Invitrogen. (2010). Reagents for reporting changes in calcium concentrations. *BioProbes Journal of Cell Biology Applications*, *63* 20–21.

Liou, J., Kim, M. L., Heo, W. D., Jones, J. T., Myers, J. W., Ferrell, J. E., & Meyer, T. (2005). STIM is a Ca^{2+} sensor essential for Ca^{2+}-store-depletion-triggered Ca^{2+} influx. *Current biology: CB*, *15*(13), 1235–1241.

Loy, R. E., Orynbayev, M., Xu, L., Andronache, Z., Apostol, S., Zvaritch, E., MacLennan, D. H., Meissner, G., Melzer, W., & Dirksen, R. T. (2011). Muscle weakness in Ryr1 I4895T/WT knock-in mice as a result of reduced ryanodine receptor Ca^{2+} ion permeation and release from the sarcoplasmic reticulum. *The Journal of General Physiology*, *137*(1), 43–57.

Lyfenko, A. D., & Dirksen, R. T. (2008). Differential dependence of store-operated and excitation-coupled Ca^{2+} entry in skeletal muscle on STIM1 and Orai1. *The Journal of Physiology*, *586*(20), 4815–4824.

Lynch, P. J., Tong, J., Lehane, M., Mallet, A., Giblin, L., Heffron, J. J., Vaughan, P., Zafra, G., MacLennan, D. H., & McCarthy, T. V. (1999). A mutation in the transmembrane/luminal domain of the ryanodine receptor is associated with abnormal Ca^{2+} release channel function and severe central core disease. *Proceedings of the National Academy of Sciences of the United States of America*, *96*(7), 4164–4169.

Maclennan, D. H., & Zvaritch, E. (2011). Mechanistic models for muscle diseases and disorders originating in the sarcoplasmic reticulum. *Biochimica Et Biophysica Acta*, *1813*(5), 948–964.

Martonosi, A. N. (1995). The structure and interactions of $Ca^{(2+)}$-ATPase. *Bioscience Reports*, *15*(5), 263–281.

McCarthy, T. V., Quane, K. A., & Lynch, P. J. (2000). Ryanodine receptor mutations in malignant hyperthermia and central core disease. *Human Mutation*, *15*(5), 410–417.

Melzer, W., Herrmann-Frank, A., & Lüttgau, H. C. (1995). The role of Ca^{2+} ions in excitation-contraction coupling of skeletal muscle fibres. *Biochimica Et Biophysica Acta*, *1241*(1), 59–116.

Merritt, A. (2013). Functional characterisation of genetic variants associated with malignant hyperthermia. Doctoral Dissertation, University of Leeds, West Yorkshire, England.

Mickelson, J. R., Litterer, L. A., Jacobson, B. A., & Louis, C. F. (1990). Stimulation and inhibition of [3H]ryanodine binding to sarcoplasmic reticulum from malignant hyperthermia susceptible pigs. *Archives of Biochemistry and Biophysics*, *278*(1), 251–257.

Monnier, N., Ferreiro, A., Marty, I., Labarre-Vila, A., Mezin, P., & Lunardi, J. (2003). A homozygous splicing mutation causing a depletion of skeletal muscle *RYR1* is associated with multi-minicore disease congenital myopathy with ophthalmoplegia. *Human Molecular Genetics*, *12*(10), 1171–1178.

Monnier, N., Kozak-Ribbens, G., Krivosic-Horber, R., Nivoche, Y., Qi, D., Kraev, N., Loke, J., Sharma, P., Tegazzin, V., Figarella-Branger, D., Roméro, N., Mezin, P., Bendahan, D., Payen, J.-F., Depret, T., Maclennan, D. H., & Lunardi, J. (2005). Correlations between genotype and pharmacological, histological, functional, and clinical phenotypes in malignant hyperthermia susceptibility. *Human Mutation*, *26*(5), 413–425.

Monnier, N., Krivosic-Horber, R., Payen, J.-F., Kozak-Ribbens, G., Nivoche, Y., Adnet, P., Reyford, H., & Lunardi, J. (2002). Presence of two different genetic traits in malignant hyperthermia families: implication for genetic analysis, diagnosis, and incidence of malignant hyperthermia susceptibility. *Anesthesiology*, *97*(5), 1067–1074.

Monnier, N., Marty, I., Faure, J., Castiglioni, C., Desnuelle, C., Sacconi, S., Estournet, B., Ferreiro, A., Romero, N., Laquerriere, A., Lazaro, L., Martin, J.-J., Morava, E., Rossi, A., Van der Kooi, A., de Visser, M., Verschuuren, C., & Lunardi, J. (2008). Null mutations causing depletion of the type 1 ryanodine receptor (*RYR1*) are commonly associated with recessive structural congenital myopathies with cores. *Human Mutation*, *29*(5), 670–678.

Monnier, N., Procaccio, V., Stieglitz, P., & Lunardi, J. (1997). Malignant-hyperthermia susceptibility is associated with a mutation of the alpha 1-subunit of the human dihydropyridine-sensitive L-type voltage-dependent calcium-channel receptor in skeletal muscle. *American Journal of Human Genetics*, *60*(6), 1316–1325.

Monnier, N., Romero, N. B., Lerale, J., Landrieu, P., Nivoche, Y., Fardeau, M., & Lunardi, J. (2001). Familial and sporadic forms of central core disease are associated with mutations in the C-terminal domain of the skeletal muscle ryanodine receptor. *Human Molecular Genetics*, *10*(22), 2581–2592.

Monnier, N., Romero, N. B., Lerale, J., Nivoche, Y., Qi, D., MacLennan, D. H., Fardeau, M., & Lunardi, J. (2000). An autosomal dominant congenital myopathy with cores and rods is associated with a neomutation in the *RYR1* gene encoding the skeletal muscle ryanodine receptor. *Human Molecular Genetics*, *9*(18), 2599–2608.

Müller, C. (2003). Criteria for gene mutations to be used in genetic testing of Malignant Hyperthermia susceptibility. European Malignant Hyperthermia Group.

Nakai, J., Dirksen, R. T., Nguyen, H. T., Pessah, I. N., Beam, K. G., & Allen, P. D. (1996). Enhanced dihydropyridine receptor channel activity in the presence of ryanodine receptor. *Nature*, *380*(6569), 72–75.

O'Brien, J. J., Feng, W., Allen, P. D., Chen, S. R. W., Pessah, I. N., & Beam, K. G. (2002). Ca2+ Activation of RyR1 is not necessary for the initiation of skeletal-type excitation-contraction coupling. *Biophysical Journal*, *82*(5), 2428–2435.

Ording, H. (1985). Incidence of malignant hyperthermia in Denmark. *Anesthesia and Analgesia*, *64*(7), 700–704.

Ording, H., Brancadoro, V., Cozzolino, S., Ellis, F. R., Glauber, V., Gonano, E. F., Halsall, P. J., Hartung, E., Heffron, J. J., Heytens, L., Kozak-Ribbens, G., Kress, H., Krivosic-Horber, R., Lehmann-Horn, F., Mortier, W., Nivoche, Y., Ranklev-Twetman, E., Sigurdsson, S., Snoeck, M., Stieglitz, P., Tegazzin, V., Urwyler, A., & Wappler, F. (1997). *In vitro* contracture test for diagnosis of malignant hyperthermia following the protocol of the European MH Group: results of testing patients surviving fulminant MH and unrelated low-risk subjects. The European Malignant Hyperthermia Group. *Acta Anaesthesiologica Scandinavica*, *41*(8), 955–966.

Orlova, E. V., Serysheva, I. I., van Heel, M., Hamilton, S. L., & Chiu, W. (1996). Two structural configurations of the skeletal muscle calcium release channel. *Nature Structural Biology*, *3*(6), 547–552.

Oyamada, H., Oguchi, K., Saitoh, N., Yamazawa, T., Hirose, K., Kawana, Y., Wakatsuki, K., Oguchi, K., Tagami, M., Hanaoka, K., Endo, M., & Iino, M. (2002). Novel mutations in C-terminal channel region of the ryanodine receptor in malignant hyperthermia patients. *Japanese Journal of Pharmacology*, *88*(2), 159–166.

Papworth, C., Bauer, J. C., Braman, J., & Wright, D. A. (1996). Site-directed mutagenesis in one day with >80% efficiency. *Strategies*, *9*(1), 3–4.

Prosser, B. L., Hernández-Ochoa, E. O., & Schneider, M. F. (2011). S100A1 and calmodulin regulation of ryanodine receptor in striated muscle. *Cell Calcium*, *50*(4), 323–331.

Protasi, F., Paolini, C., & Dainese, M. (2009). Calsequestrin-1: a new candidate gene for malignant hyperthermia and exertional/environmental heat stroke. *The Journal of Physiology*, *587*(13), 3095–3100.

Quane, K. A., Healy, J. M., Keating, K. E., Manning, B. M., Couch, F. J., Palmucci, L. M., Doriguzzi, C., Fagerlund, T. H., Berg, K., & Ording, H. (1993). Mutations in the ryanodine receptor gene in central core disease and malignant hyperthermia. *Nature Genetics*, *5*(1), 51–55.

Querfurth, H. W., Haughey, N. J., Greenway, S. C., Yacono, P. W., Golan, D. E., & Geiger, J. D. (1998). Expression of ryanodine receptors in human embryonic kidney (HEK293) cells. *The Biochemical Journal*, *334*(1), 79–86.

Quinlivan, R. M., Muller, C. R., Davis, M., Laing, N. G., Evans, G. A., Dwyer, J., Dove, J., Roberts, A. P., & Sewry, C. A. (2003). Central core disease: clinical, pathological, and genetic features. *Archives of Disease in Childhood*, *88*(12), 1051–1055.

Ranklev, E., Henriksson, K. G., Fletcher, R., Germundsson, K., Oldfors, A., & Kalimo, H. (1986). Clinical and muscle biopsy findings in malignant hyperthermia susceptibility. *Acta Neurologica Scandinavica*, *74*(6), 452–459.

Rios, E., & Brum, G. (1987). Involvement of dihydropyridine receptors in excitation-contraction coupling in skeletal muscle. *Nature*, *325*(6106), 717–720.

Robinson, R., Carpenter, D., Shaw, M.-A., Halsall, J., & Hopkins, P. (2006). Mutations in *RYR1* in malignant hyperthermia and central core disease. *Human Mutation*, *27*(10), 977–989.

Robinson, R., Hopkins, P., Carsana, A., Gilly, H., Halsall, J., Heytens, L., Islander, G., Jurkat-Rott, K., Müller, C., & Shaw, M.-A. (2003). Several interacting genes influence the malignant hyperthermia phenotype. *Human Genetics*, *112*(2), 217–218.

Robinson, R. L., Curran, J. L., Ellis, F. R., Halsall, P. J., Hall, W. J., Hopkins, P. M., Iles, D. E., West, S. P., & Shaw, M. A. (2000). Multiple interacting gene products may influence susceptibility to malignant hyperthermia. *Annals of Human Genetics*, *64*(Pt 4), 307–320.

Roesl, C., Sato, K., Schiemann, A., Pollock, N., & Stowell, K. M. (2014). Functional characterisation of the R2452W ryanodine receptor variant associated with malignant hyperthermia susceptibility. *Cell Calcium*, *56*(3), 195–201.

Rosenberg, H. (2013). Myopathic changes in malignant hyperthermia-susceptible patients. *Canadian Journal of Anesthesia/Journal canadien d'anesthésie*, *60*(10), 955–959.

Rosenberg, H., Davis, M., James, D., Pollock, N., & Stowell, K. (2007). Malignant hyperthermia. *Orphanet Journal of Rare Diseases*, *2*(21),.

Sambuughin, N., Holley, H., Muldoon, S., Brandom, B. W., de Bantel, A. M., Tobin, J. R., Nelson, T. E., & Goldfarb, L. G. (2005). Screening of the entire ryanodine receptor type 1 coding region for sequence variants associated with malignant

hyperthermia susceptibility in the north american population. *Anesthesiology*, *102*(3), 515–521.

Samsó, M., Wagenknecht, T., & Allen, P. (2005). Internal structure and visualization of transmembrane domains of the RyR1 calcium release channel by cryo-EM. *Nature structural & molecular biology*, *12*(6), 539–544.

Sanchez, E. J., Lewis, K. M., Danna, B. R., & Kang, C. (2012). High-capacity Ca^{2+} binding of human skeletal calsequestrin. *The Journal of Biological Chemistry*, *287*(14), 11592–11601.

Sato, K., Pollock, N., & Stowell, K. M. (2010). Functional studies of *RYR1* mutations in the skeletal muscle ryanodine receptor using human *RYR1* complementary DNA. *Anesthesiology*, *112*(6), 1350–1354.

Sato, K., Roesl, C., Pollock, N., & Stowell, K. M. (2013). Skeletal muscle ryanodine receptor mutations associated with malignant hyperthermia showed enhanced intensity and sensitivity to triggering drugs when expressed in human embryonic kidney cells. *Anesthesiology*, *119*(1), 111–118.

Schiemann, A. H., Dürholt, E. M., Pollock, N., & Stowell, K. M. (2013). Sequence capture and massively parallel sequencing to detect mutations associated with malignant hyperthermia. *British Journal of Anaesthesia*, *110*(1), 122–127.

Schiemann, A. H., Paul, N., Parker, R., Pollock, N., Bulger, T. F., & Stowell, K. M. (2014). Functional characterization of 2 known ryanodine receptor mutations causing malignant hyperthermia. *Anesthesia and Analgesia*, *118*(2), 375–380.

Sei, Y., Brandom, B. W., Bina, S., Hosoi, E., Gallagher, K. L., Wyre, H. W., Pudimat, P. A., Holman, S. J., Venzon, D. J., Daly, J. W., & Muldoon, S. (2002). Patients with malignant hyperthermia demonstrate an altered calcium control mechanism in B lymphocytes. *Anesthesiology*, *97*(5), 1052–1058.

Sewry, C. A., Müller, C., Davis, M., Dwyer, J. S. M., Dove, J., Evans, G., Schröder, R., Fürst, D., Helliwell, T., Laing, N., & Quinlivan, R. C. M. (2002). The spectrum of pathology in central core disease. *Neuromuscular disorders*, *12*(10), 930–938.

Shepherd, S., Ellis, F., Halsall, J., Hopkins, P., & Robinson, R. (2004). *RYR1* mutations in UK central core disease patients: more than just the C-terminal transmembrane region of the *RYR1* gene. *Journal of Medical Genetics*, *41*(3), e33.

Shy, G. M., & Magee, K. R. (1956). A new congenital non-progressive myopathy. *Brain: A Journal of Neurology*, *79*(4), 610–621.

Stewart, R., Zissimopoulos, S., & Lai, F. A. (2003). Oligomerization of the cardiac ryanodine receptor C-terminal tail. *The Biochemical Journal*, *376*(3), 795–799.

Stiber, J., Hawkins, A., Zhang, Z.-S., Wang, S., Burch, J., Graham, V., Ward, C. C., Seth, M., Finch, E., Malouf, N., Williams, R. S., Eu, J. P., & Rosenberg, P. (2008). STIM1

signalling controls store-operated calcium entry required for development and contractile function in skeletal muscle. *Nature Cell Biology*, *10*(6), 688–697.

Sztretye, M., Yi, J., Figueroa, L., Zhou, J., Royer, L., Allen, P., Brum, G., & Ríos, E. (2011). Measurement of RyR permeability reveals a role of calsequestrin in termination of SR Ca^{2+} release in skeletal muscle. *The Journal of General Physiology*, *138*(2), 231–247.

Takeshima, H., Lino, M., Takekura, H., Nishi, M., Kuno, J., Minowa, O., Takano, H., & Noda, T. (1994). Excitation-contraction uncoupling and muscular degeneration in mice lacking functional skeletal muscle ryanodine-receptor gene. *Nature*, *369*(6481), 556–559.

Tarroni, P., Rossi, D., Conti, A., & Sorrentino, V. (1997). Expression of the ryanodine receptor type 3 calcium release channel during development and differentiation of mammalian skeletal muscle cells. *The Journal of Biological Chemistry*, *272*(32), 19808–19813.

Tilgen, N., Zorzato, F., Halliger-Keller, B., Muntoni, F., Sewry, C., Palmucci, L. M., Schneider, C., Hauser, E., Lehmann-Horn, F., Müller, C. R., & Treves, S. (2001). Identification of four novel mutations in the C-terminal membrane spanning domain of the ryanodine receptor 1: association with central core disease and alteration of calcium homeostasis. *Human Molecular Genetics*, *10*(25), 2879–2887.

Tong, J., Du, G. G., Chen, S. R., & MacLennan, D. H. (1999a). HEK-293 cells possess a carbachol- and thapsigargin-sensitive intracellular Ca^{2+} store that is responsive to stop-flow medium changes and insensitive to caffeine and ryanodine. *Biochemical Journal*, *343*(1), 39–44.

Tong, J., McCarthy, T. V., & MacLennan, D. H. (1999b). Measurement of resting cytosolic Ca^{2+} concentrations and Ca^{2+} store size in HEK-293 cells transfected with malignant hyperthermia or central core disease mutant Ca^{2+} release channels. *Journal of Biological Chemistry*, *274*(2), 693–702.

Tong, J., Oyamada, H., Demaurex, N., Grinstein, S., McCarthy, T. V., & MacLennan, D. H. (1997). Caffeine and halothane sensitivity of intracellular Ca^{2+} release is altered by 15 calcium release channel (ryanodine receptor) mutations associated with malignant hyperthermia and/or central core disease. *The Journal of Biological Chemistry*, *272*(42), 26332–26339.

Treves, S., Jungbluth, H., Muntoni, F., & Zorzato, F. (2008). Congenital muscle disorders with cores: the ryanodine receptor calcium channel paradigm. *Current Opinion in Pharmacology*, *8*(3), 319–326.

Urnov, F. D., Rebar, E. J., Holmes, M. C., Zhang, H. S., & Gregory, P. D. (2010). Genome editing with engineered zinc finger nucleases. *Nature Reviews. Genetics*, *11*(9), 636–646.

Vukcevic, M., Spagnoli, G. C., Iezzi, G., Zorzato, F., & Treves, S. (2008). Ryanodine Receptor Activation by Cav1.2 Is Involved in Dendritic Cell Major Histocompatibility Complex Class II Surface Expression. *Journal of Biological Chemistry*, *283*(50), 34913–34922.

Wang, R., Zhong, X., Meng, X., Koop, A., Tian, X., Jones, P. P., Fruen, B. R., Wagenknecht, T., Liu, Z., & Chen, S. R. W. (2011). Localization of the dantrolene-binding sequence near the FK506-binding protein-binding site in the three-dimensional structure of the ryanodine receptor. *The Journal of Biological Chemistry*, *286*(14), 12202–12212.

Wappler, F., Fiege, M., Steinfath, M., Agarwal, K., Scholz, J., Singh, S., Matschke, J., & Schulte Am Esch, J. (2001). Evidence for susceptibility to malignant hyperthermia in patients with exercise-induced rhabdomyolysis. *Anesthesiology*, *94*(1), 95–100.

Wehner, M., Rueffert, H., Koenig, F., & Olthoff, D. (2004). Functional characterization of malignant hyperthermia-associated RyR1 mutations in exon 44, using the human myotube model. *Neuromuscular disorders: NMD*, *14*(7), 429–437.

Wei, L., Gallant, E. M., Dulhunty, A. F., & Beard, N. A. (2009). Junctin and triadin each activate skeletal ryanodine receptors but junctin alone mediates functional interactions with calsequestrin. *The International Journal of Biochemistry & Cell Biology*, *41*(11), 2214–2224.

Williams, A. J., West, D. J., & Sitsapesan, R. (2001). Light at the end of the $Ca^{(2+)}$-release channel tunnel: structures and mechanisms involved in ion translocation in ryanodine receptor channels. *Quarterly Reviews of Biophysics*, *34*(1), 61–104.

Wilmshurst, J. M., Lillis, S., Zhou, H., Pillay, K., Henderson, H., Kress, W., Müller, C. R., Ndondo, A., Cloke, V., Cullup, T., Bertini, E., Boennemann, C., Straub, V., Quinlivan, R., Dowling, J. J., Al-Sarraj, S., Treves, S., Abbs, S., Manzur, A. Y., Sewry, C. A., Muntoni, F., & Jungbluth, H. (2010). *RYR1* mutations are a common cause of congenital myopathies with central nuclei. *Annals of Neurology*, *68*(5), 717–726.

Wu, S., Ibarra, M. C. A., Malicdan, M. C. V., Murayama, K., Ichihara, Y., Kikuchi, H., Nonaka, I., Noguchi, S., Hayashi, Y. K., & Nishino, I. (2006). Central core disease is due to *RYR1* mutations in more than 90% of patients. *Brain: A Journal of Neurology*, *129*(6), 1470–1480.

Xu, L., Wang, Y., Yamaguchi, N., Pasek, D. A., & Meissner, G. (2008). Single channel properties of heterotetrameric mutant RyR1 ion channels linked to core myopathies. *The Journal of biological chemistry*, *283*(10), 6321–6329.

Yang, T., Riehl, J., Esteve, E., Matthaei, K. I., Goth, S., Allen, P. D., Pessah, I. N., & Lopez, J. R. (2006). Pharmacologic and functional characterization of malignant hyperthermia in the R163C RyR1 knock-in mouse. *Anesthesiology*, *105*(6), 1164–1175.

Yan, Z., Bai, X.-C., Yan, C., Wu, J., Li, Z., Xie, T., Peng, W., Yin, C.-C., Li, X., Scheres, S. H. W., Shi, Y., & Yan, N. (2015). Structure of the rabbit ryanodine receptor RyR1 at near-atomic resolution. *Nature*, *517*(7532), 50–55.

Yasuda, T., Delbono, O., Wang, Z.-M., Messi, M. L., Girard, T., Urwyler, A., Treves, S., & Zorzato, F. (2013). JP-45/JSRP1 variants affect skeletal muscle excitation-contraction coupling by decreasing the sensitivity of the dihydropyridine receptor. *Human Mutation*, *34*(1), 184–190.

Yuen, B., Boncompagni, S., Feng, W., Yang, T., Lopez, J. R., Matthaei, K. I., Goth, S. R., Protasi, F., Franzini-Armstrong, C., Allen, P. D., & Pessah, I. N. (2012). Mice expressing T4826I-*RYR1* are viable but exhibit sex- and genotype-dependent susceptibility to malignant hyperthermia and muscle damage. *FASEB journal: official publication of the Federation of American Societies for Experimental Biology*, *26*(3), 1311–1322.

Zhou, H., Jungbluth, H., Sewry, C. A., Feng, L., Bertini, E., Bushby, K., Straub, V., Roper, H., Rose, M. R., Brockington, M., Kinali, M., Manzur, A., Robb, S., Appleton, R., Messina, S., D'Amico, A., Quinlivan, R., Swash, M., Müller, C. R., Brown, S., Treves, S., & Muntoni, F. (2007). Molecular mechanisms and phenotypic variation in *RYR1*-related congenital myopathies. *Brain: A Journal of Neurology*, *130*(8), 2024–2036.

Zhou, H., Lillis, S., Loy, R. E., Ghassemi, F., Rose, M. R., Norwood, F., Mills, K., Al-Sarraj, S., Lane, R. J. M., Feng, L., Matthews, E., Sewry, C. A., Abbs, S., Buk, S., Hanna, M., Treves, S., Dirksen, R. T., Meissner, G., Muntoni, F., & Jungbluth, H. (2010). Multi-minicore disease and atypical periodic paralysis associated with novel mutations in the skeletal muscle ryanodine receptor (*RYR1*) gene. *Neuromuscular disorders: NMD*, *20*(3), 166–173.

Zhou, H., Rokach, O., Feng, L., Munteanu, I., Mamchaoui, K., Wilmshurst, J. M., Sewry, C., Manzur, A. Y., Pillay, K., Mouly, V., Duchen, M., Jungbluth, H., Treves, S., & Muntoni, F. (2013). RyR1 deficiency in congenital myopathies disrupts excitation-contraction coupling. *Human Mutation*, *34*(7), 986–996.

Zhou, H., Yamaguchi, N., Xu, L., Wang, Y., Sewry, C., Jungbluth, H., Zorzato, F., Bertini, E., Muntoni, F., Meissner, G., & Treves, S. (2006). Characterization of recessive *RYR1* mutations in core myopathies. *Human Molecular Genetics*, *15*(18), 2791–2803.

Zima, A. V., Bovo, E., Bers, D. M., & Blatter, L. A. (2010). Ca^{2+} spark-dependent and -independent sarcoplasmic reticulum Ca^{2+} leak in normal and failing rabbit ventricular myocytes. *The Journal of Physiology*, *588*(23), 4743–4757.

Zorzato, F., Fujii, J., Otsu, K., Phillips, M., Green, N. M., Lai, F. A., Meissner, G., & MacLennan, D. H. (1990). Molecular cloning of cDNA encoding human and rabbit forms of the Ca^{2+} release channel (ryanodine receptor) of skeletal muscle sarcoplasmic reticulum. *The Journal of Biological Chemistry*, *265*(4), 2244–2256.

Zorzato, F., Yamaguchi, N., Xu, L., Meissner, G., Müller, C. R., Pouliquin, P., Muntoni, F., Sewry, C., Girard, T., & Treves, S. (2003). Clinical and functional effects of a deletion in a COOH-terminal lumenal loop of the skeletal muscle ryanodine receptor. *Human Molecular Genetics*, *12*(4), 379–388.

Zvaritch, E., Depreux, F., Kraeva, N., Loy, R. E., Goonasekera, S. A., Boncompagni, S., Kraev, A., Gramolini, A. O., Dirksen, R. T., Franzini-Armstrong, C., Seidman, C. E., Seidman, J. G., & MacLennan, D. H. (2007). An Ryr1 I4895T mutation abolishes Ca^{2+} release channel function and delays development in homozygous offspring of a mutant mouse line. *Proceedings of the National Academy of Sciences*, *104*(47), 18537–18542.

APPENDICES

APPENDIX A: Plasmids used to clone *RYR1* cDNA

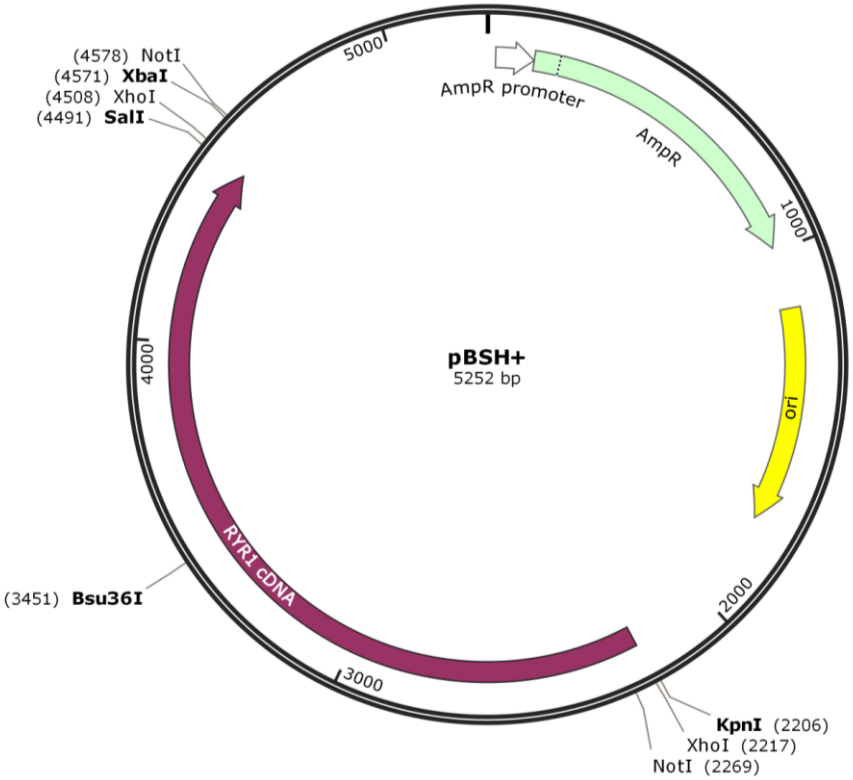

Map of the pBSH+ plasmid used in mutagenesis of *RYR1* variants

Restriction endonuclease recognition sites used in the present study for sub-cloning and identification purposes are labelled. Of these, unique recognition sites are in bold. The origin of replication (yellow), ampicillin resistance gene (green) and ~2.2 kb of the most 3' segment of human *RYR1* cDNA (purple) are labelled and their relative orientations are indicated by arrowheads. Created with SnapGene Viewer 2.6.2.

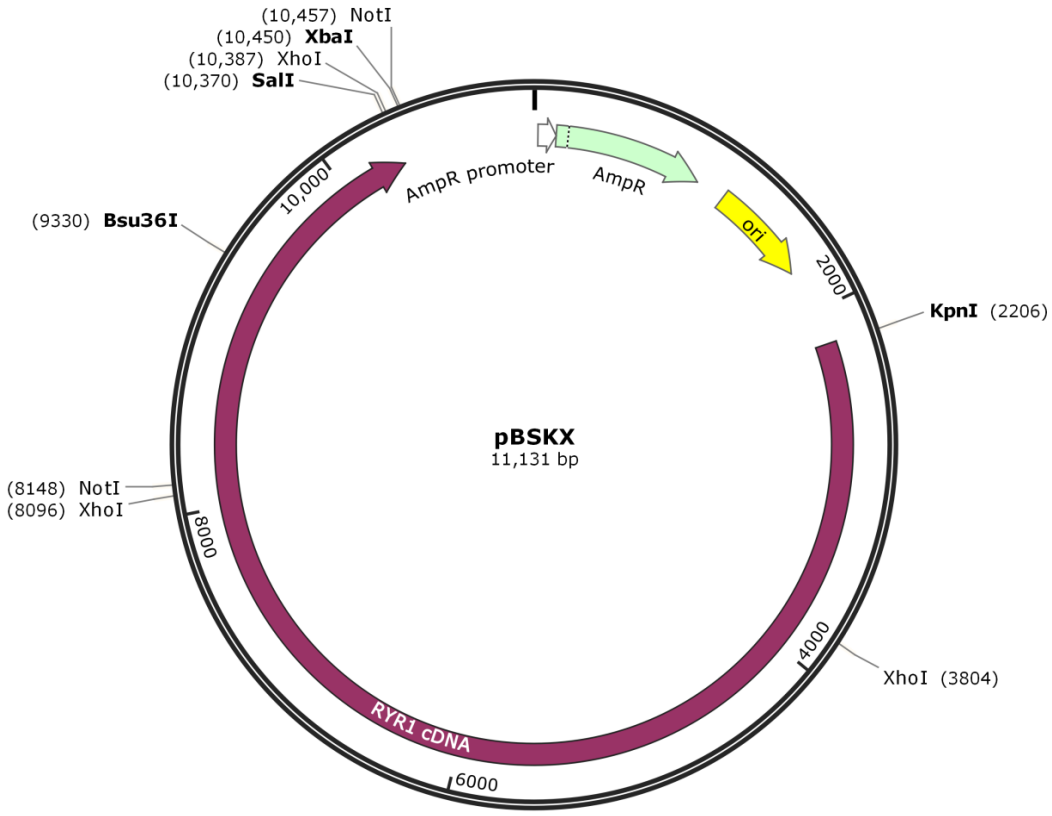

Map of the pBSKX plasmid used in sub-cloning *RYR1* variants

Restriction endonuclease recognition sites used in the current study for sub-cloning and identification purposes are labelled. Of these, unique recognition sites are in bold. The origin of replication (yellow), ampicillin resistance gene (green) and 3' half (~8.1 kb) of human *RYR1* cDNA (purple) are labelled and their relative orientations are indicated by arrowheads. Created with SnapGene Viewer 2.6.2.

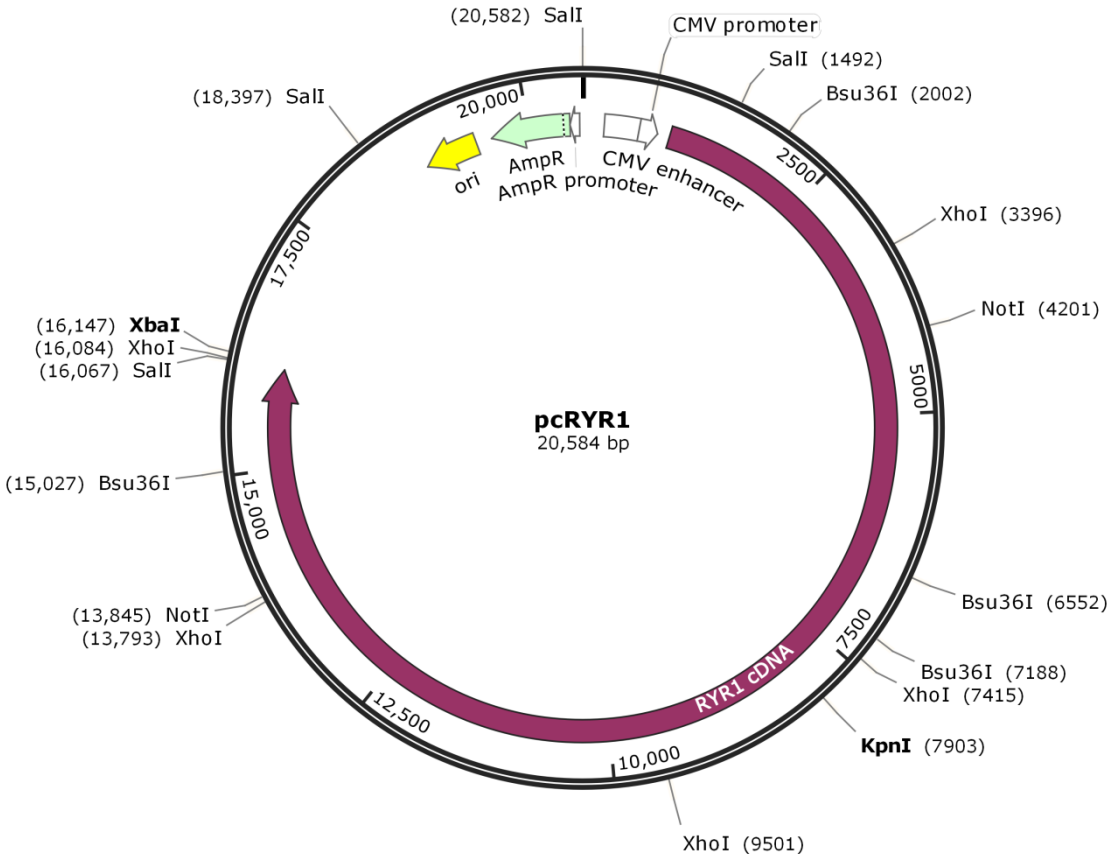

Map of the pcRYR1 plasmid used in functional studies

Restriction endonuclease recognition sites used in the present study for sub-cloning and identification purposes are labelled. Of these, unique recognition sites are in bold. The origin of replication (yellow), ampicillin resistance gene (green), cytomegalovirus promoter (white) and ~15 kb full-length human *RYR1* cDNA (purple) are labelled and their relative orientations are indicated by arrowheads. Created with SnapGene Viewer 2.6.2.

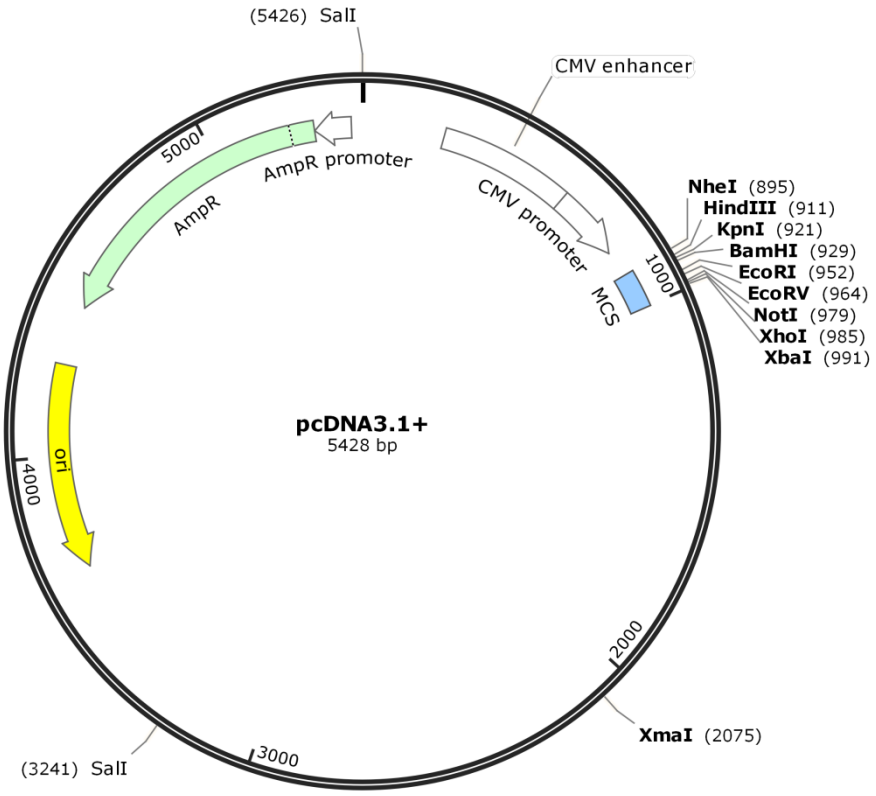

Map of the pcDNA3.1+ plasmid used in functional studies

Restriction endonuclease recognition sites used in the present study for sub-cloning and identification purposes as well as some additional useful recognition sites are labelled. Of these, unique recognition sites are in bold. The origin of repliction (yellow), ampicillin resistance gene (green), multiple cloning site (blue), cytomegalovirus promoter (white) and ~15 kb full-length human *RYR1* cDNA (purple) are labelled and their relative orientations are indicated by arrowheads. Created with SnapGene Viewer 2.6.2.

APPENDIX B: Sanger sequencing of SDM products

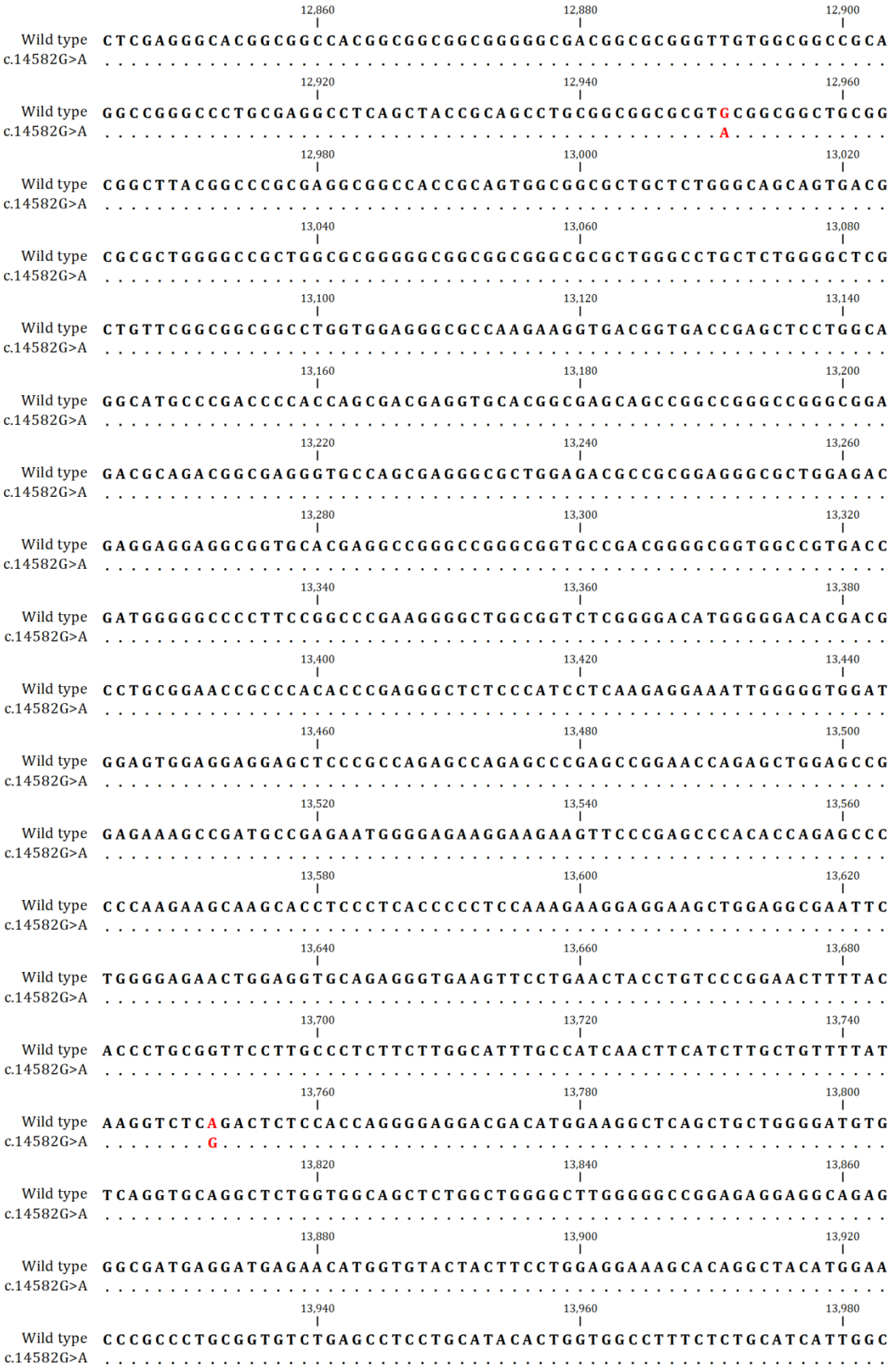

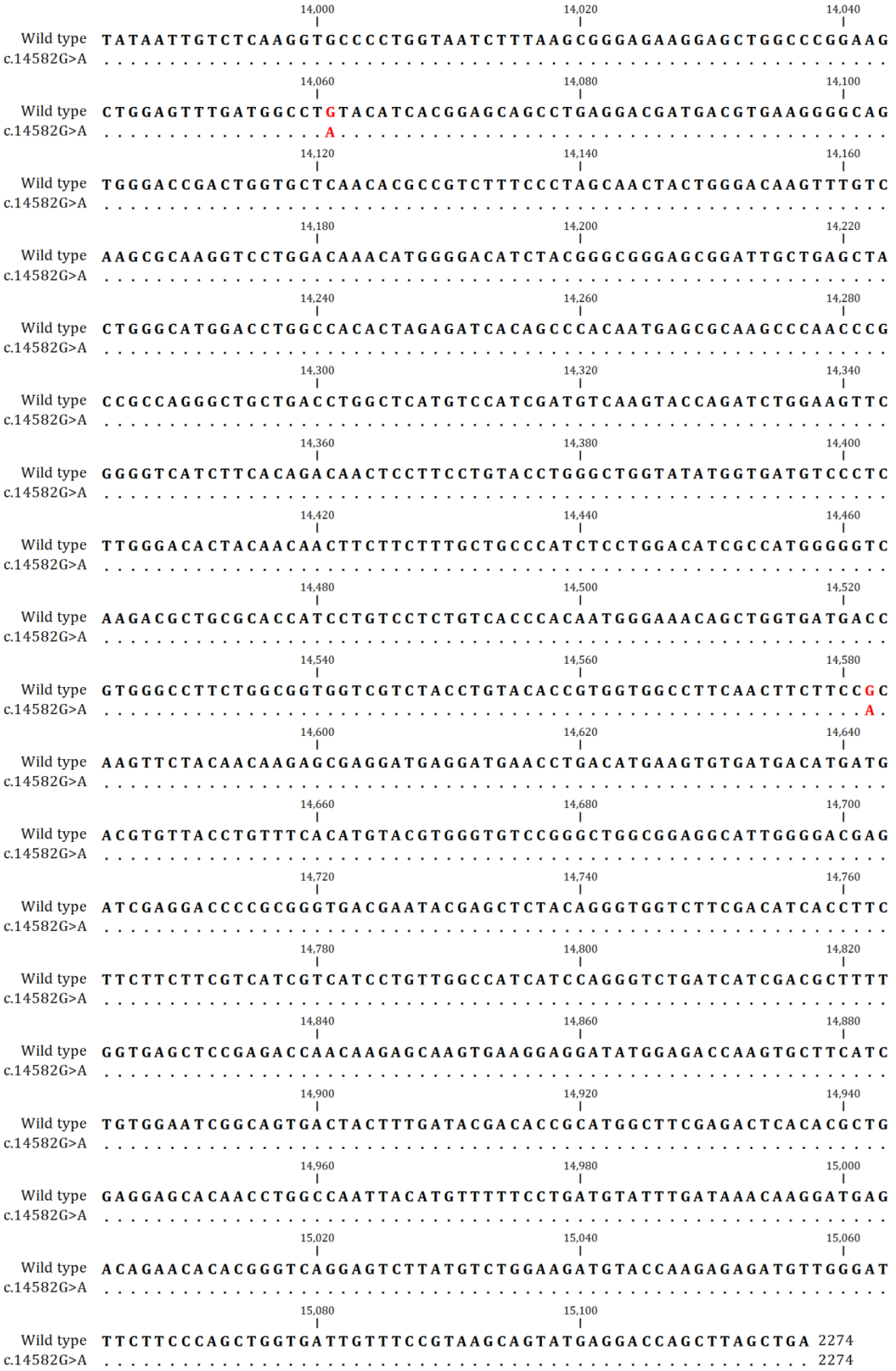
14,000
14,020
14,040
Wild type TATAATTGTCTCAAGGTGCCCCTGGTAATCTTTAAGCGGGAGAAGGAGCTGGCCCGGAAG
c.14582G>A . . . . . .
14,060
14,080
14,100
Wild type CTGGAGTTTGATGGCCTGTACATCACGGAGCAGCCTGAGGACGATGACGTGAAGGGGCAG
c.14582G>A . . . . . A . . . . . .
14,120
14,140
14,160
Wild type TGGGACCGACTGGTGCTCAACACGCCGTCTTTCCCTAGCAACTACTGGGACAAGTTTGTC
c.14582G>A . . . . . .
14,180
14,200
14,220
Wild type AAGCGCAAGGTCCTGGACAAACATGGGGACATCTACGGGCGGGAGCGGATTGCTGAGCTA
c.14582G>A . . . . . .
14,240
14,260
14,280
Wild type CTGGGCATGGACCTGGCCACACTAGAGATCACAGCCCACAATGAGCGCAAGCCCAACCCG
c.14582G>A . . . . . .
14,300
14,320
14,340
Wild type CCGCCAGGGCTGCTGACCTGGCTCATGTCCATCGATGTCAAGTACCAGATCTGGAAGTTC
c.14582G>A . . . . . .
14,360
14,380
14,400
Wild type GGGGTCATCTTCACAGACAACTCCTTCCTGTACCTGGGCTGGTATATGGTGATGTCCCTC
c.14582G>A . . . . . .
14,420
14,440
14,460
Wild type TTGGGACACTACAACAACTTCTTCTTTGCTGCCCATCTCCTGGACATCGCCATGGGGGTC
c.14582G>A . . . . . .
14,480
14,500
14,520
Wild type AAGACGCTGCGCACCATCCTGTCCTCTGTCACCCACAATGGGAAACAGCTGGTGATGACC
c.14582G>A . . . . . .
14,540
14,560
14,580
Wild type GTGGGCCTTCTGGCGGTGGTCGTCTACCTGTACACCGTGGTGGCCTTCAACTTCTTCCGC
c.14582G>A . . . . . A .
14,600
14,620
14,640
Wild type AAGTTCTACAACAAGAGCGAGGATGAGGATGAACCTGACATGAAGTGTGATGACATGATG
c.14582G>A . . . . . .
14,660
14,680
14,700
Wild type ACGTGTTACCTGTTTCACATGTACGTGGGTGTCCGGGCTGGCGGAGGCATTGGGGACGAG
c.14582G>A . . . . . .
14,720
14,740
14,760
Wild type ATCGAGGACCCCGCGGGTGACGAATACGAGCTCTACAGGGTGGTCTTCGACATCACCTTC
c.14582G>A . . . . . .
14,780
14,800
14,820
Wild type TTCTTCTTCGTCATCGTCATCCTGTTGGCCATCATCCAGGGTCTGATCATCGACGCTTTT
c.14582G>A . . . . . .
14,840
14,860
14,880
Wild type GGTGAGCTCCGAGACCAACAAGAGCAAGTGAAGGAGGATATGGAGACCAAGTGCTTCATC
c.14582G>A . . . . . .
14,900
14,920
14,940
Wild type TGTGGAATCGGCAGTGACTACTTTGATACGACACCGCATGGCTTCGAGACTCACACGCTG
c.14582G>A . . . . . .
14,960
14,980
15,000
Wild type GAGGAGCACAACCTGGCCAATTACATGTTTTTCCTGATGTATTTGATAAACAAGGATGAG
c.14582G>A . . . . . .
15,020
15,040
15,060
Wild type ACAGAACACACGGGTCAGGAGTCTTATGTCTGGAAGATGTACCAAGAGAGATGTTGGGAT
c.14582G>A . . . . . .
15,080
15,100
Wild type TTCTTCCCAGCTGGTGATTGTTTCCGTAAGCAGTATGAGGACCAGCTTAGCTGA 2274
c.14582G>A 2274

Alignment of wild type and variant *RYR1* cDNA from pBSH+ plasmids

The *RYR1* cDNA regions of pBSH+ plasmids after site-directed mutagenesis were sequenced to confirm the presence of each variant introduced and the absence of other amino acid changes. Individual sequences were joined together and then aligned using CLC Sequence Viewer 7.5 software. Shown is a representative alignment from Sanger sequencing of the *RYR1* cDNA of the pBSH+ plasmid containing the c.14582G>A variant (GenBank accession NM_000540.2). Nucleotides are numbered according to their position in the full-length human cDNA sequence (GenBank accession NM_000540.2). Consensus nucleotides in the variant sequence are indicated by a dot while nucleotide changes are indicated in red. In this sequence, two additional nucleotides were substituted by the DNA polymerase enzyme during PCR: c.12951G>A and c.13752A>G; both were silent changes.

Primers used for Sanger sequencing plasmids

PRIMER	PRIMER SEQUENCE
Primer A	5’ – AGCGGATAACAATTTCACACAGG – 3’
Primer B	5’ – GACGGGGCGGTGGCCGTGAC – 3’
Primer C	5’ – GAACCCGCCCTGCGGTGTCTG – 3’
Primer D	5’ – GCACCATCCTGTCCTCTGTCA – 3’

APPENDIX C: Confirmation of pcRYR1 variants

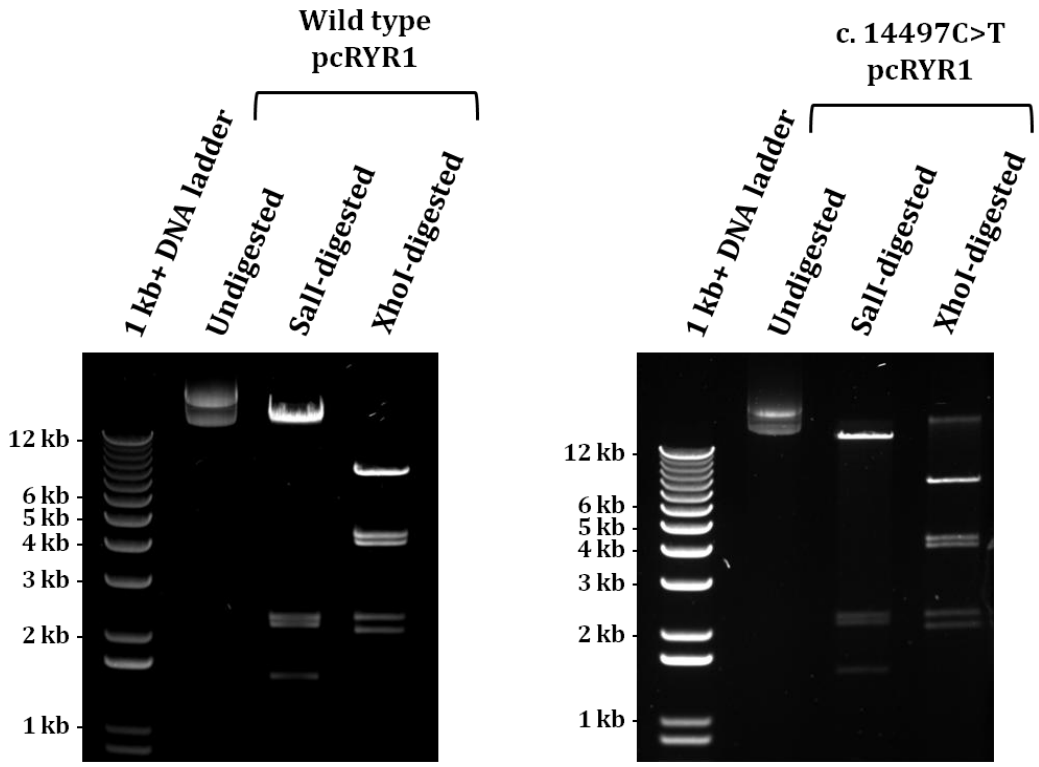

Confirmation of wild type and p.H4833Y pcRYR1 plasmids

The pcRYR1 plasmids containing wild type and c.14497C>T (p.H4833Y: GenBank accessions NM_000540.2 and NP_000531.2) *RYR1* cDNA were digested by restriction endonucleases SalI and XhoI. These digests were analysed by gel electrophoresis in a 0.7% agarose gel at 90 V alongside a 1kb+ DNA ladder and visualised using UV (A_{260}) light. The 1.5 kb band in lane 3 of each image may be difficult to perceive.

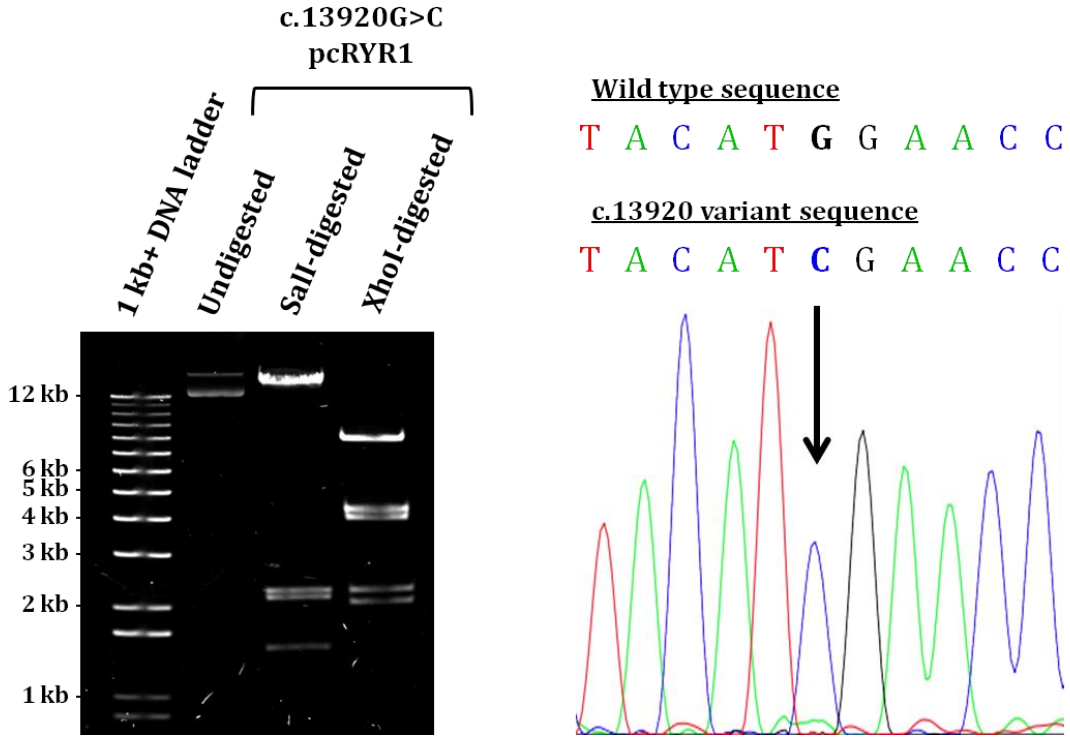

Confirmation of p.M4640I variant in the pcRYR1 plasmid

The pcRYR1 plasmid containing c.13920G>C (p.M4640I: GenBank accessions NM_000540.2 and NP_000531.2) *RYR1* cDNA was digested by restriction endonucleases SalI and XhoI. These digests were analysed by gel electrophoresis in a 0.7% agarose gel at 90 V alongside a 1kb+ DNA ladder and visualised using UV (A_{260}) light. The 1.5 kb band in lane 3 may be difficult to perceive in this image. Shown is a representative chromatogram from Sanger sequencing the region containing the c.13920G>C variant.

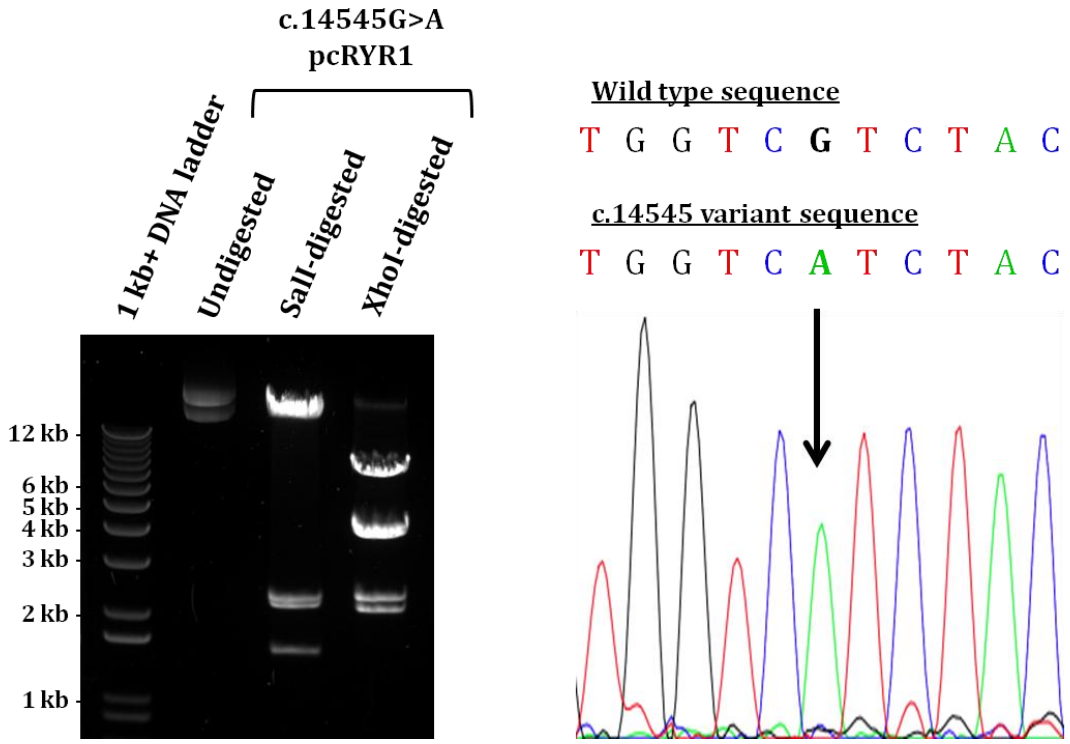

Confirmation of p.V4849I variant in the pcRYR1 plasmid

The pcRYR1 plasmid containing c.14545G>A (p.V4849I: GenBank accessions NM_000540.2 and NP_000531.2) *RYR1* cDNA was digested by restriction endonucleases SalI and XhoI. These digests were analysed by gel electrophoresis in a 0.7% agarose gel at 90 V alongside a 1kb+ DNA ladder and visualised using UV (A260) light. Shown is a representative chromatogram from Sanger sequencing the region containing the c.14545G>A variant.

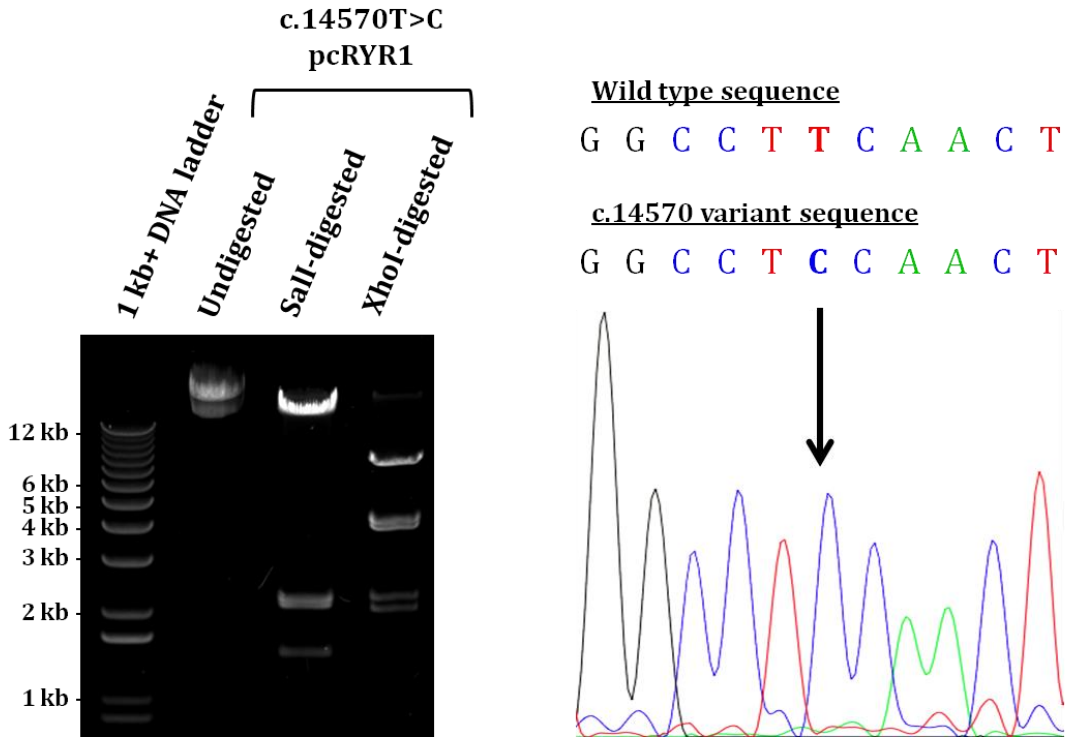

Confirmation of p.F4857S variant in the pcRYR1 plasmid

The pcRYR1 plasmid containing c.14570T>C (p.F4857S: GenBank accessions NM_000540.2 and NP_000531.2) *RYR1* cDNA was digested by restriction endonucleases SalI and XhoI. These digests were analysed by gel electrophoresis in a 0.7% agarose gel at 90 V alongside a 1kb+ DNA ladder and visualised using UV (A_{260}) light. The 1.5 kb band in lane 3 may be difficult to perceive in this image. Shown is a representative chromatogram from Sanger sequencing the region containing the c.14570T>C variant.

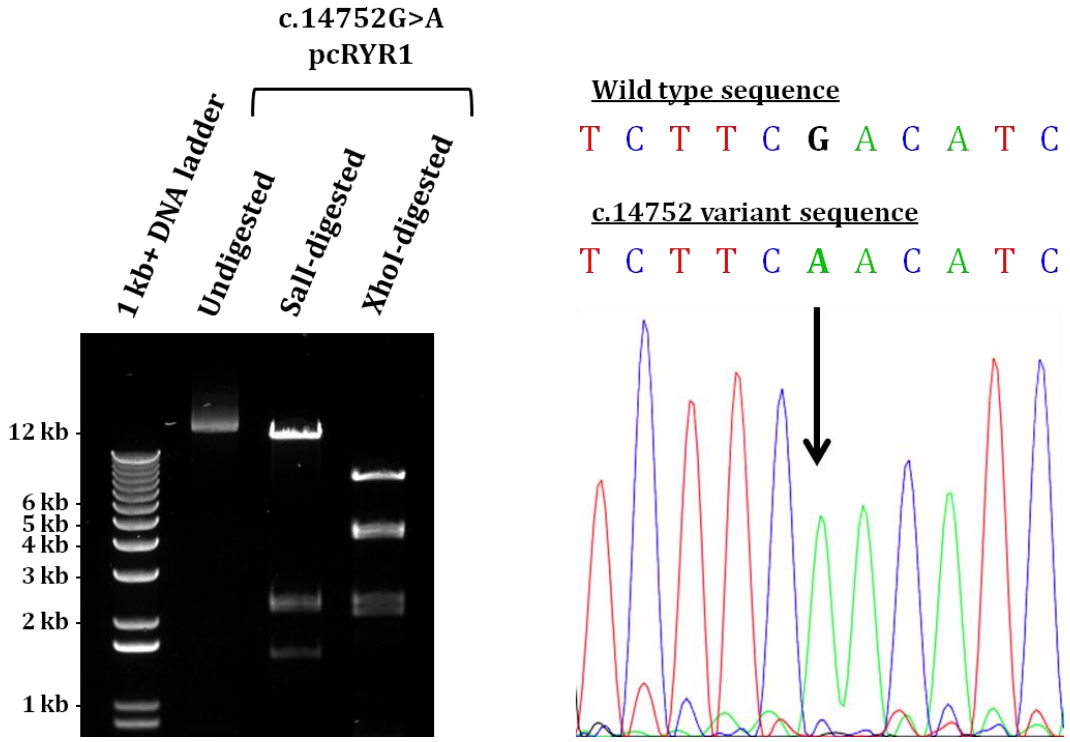

Confirmation of p.D4918N variant in the pcRYR1 plasmid

The pcRYR1 plasmid containing c.14572G>A (p.D4918N: GenBank accessions NM_000540.2 and NP_000531.2) *RYR1* cDNA was digested by restriction endonucleases SalI and XhoI. These digests were analysed by gel electrophoresis in a 0.7% agarose gel at 90 V alongside a 1kb+ DNA ladder and visualised using UV (A_{260}) light. The 1.5 kb band in lane 3 may be difficult to perceive in this image. Shown is a representative chromatogram from Sanger sequencing the region containing the c.14572G>A variant.

APPENDIX D: Raw calcium release assay data

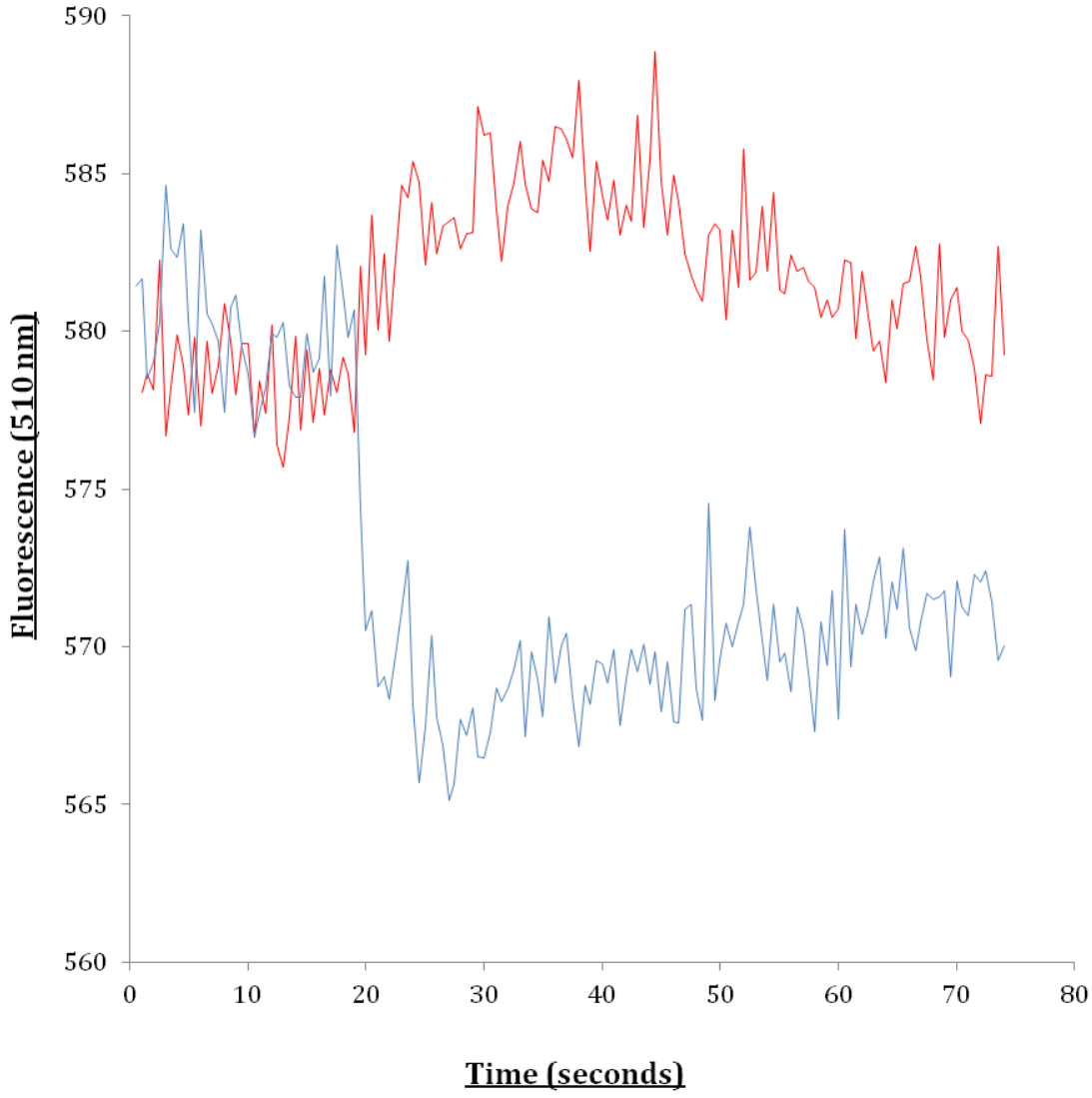

Raw data from a representative HEK-293T calcium release assay

Shown is the change in the 340 nm (red) and 380 nm (blue) excitation fluorescence upon addition of 1000 µM 4-C*m*C in the p.H4833Y-transfected (GenBank accession NP_000531.2) HEK-293T cells measured using the PerkinElmer LS50 spectrofluorometer. A fluorescence baseline was established before addition of 1000 µM 4-C*m*C at ~20 seconds, at which point the fluorescence ratio increased rapidly before beginning to decrease at ~35 seconds.

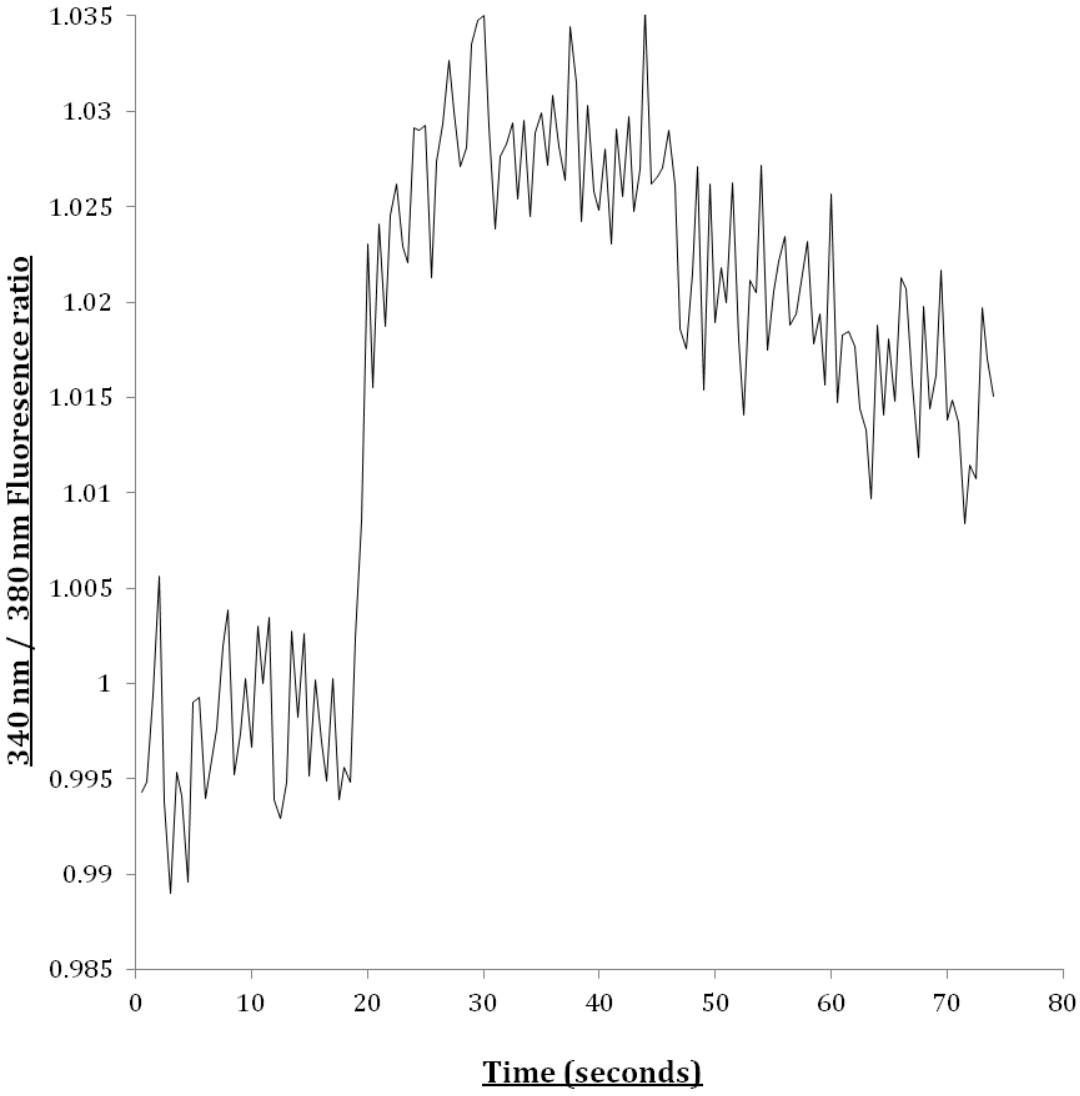

Calcium release measured in HEK-293T calcium release assays

Shown is the change in the 340 nm / 380 nm excitation ratio fluorescence upon addition of 1000 µM 4-C*m*C in the p.H4833Y-transfected (GenBank accession NP_000531.2) HEK-293T cells measured using the PerkinElmer LS50 spectrofluorometer. A fluorescence baseline was established before addition of 1000 µM 4-C*m*C at ~20 seconds, at which point the fluorescence ratio increased rapidly before beginning to decrease at ~35 seconds.

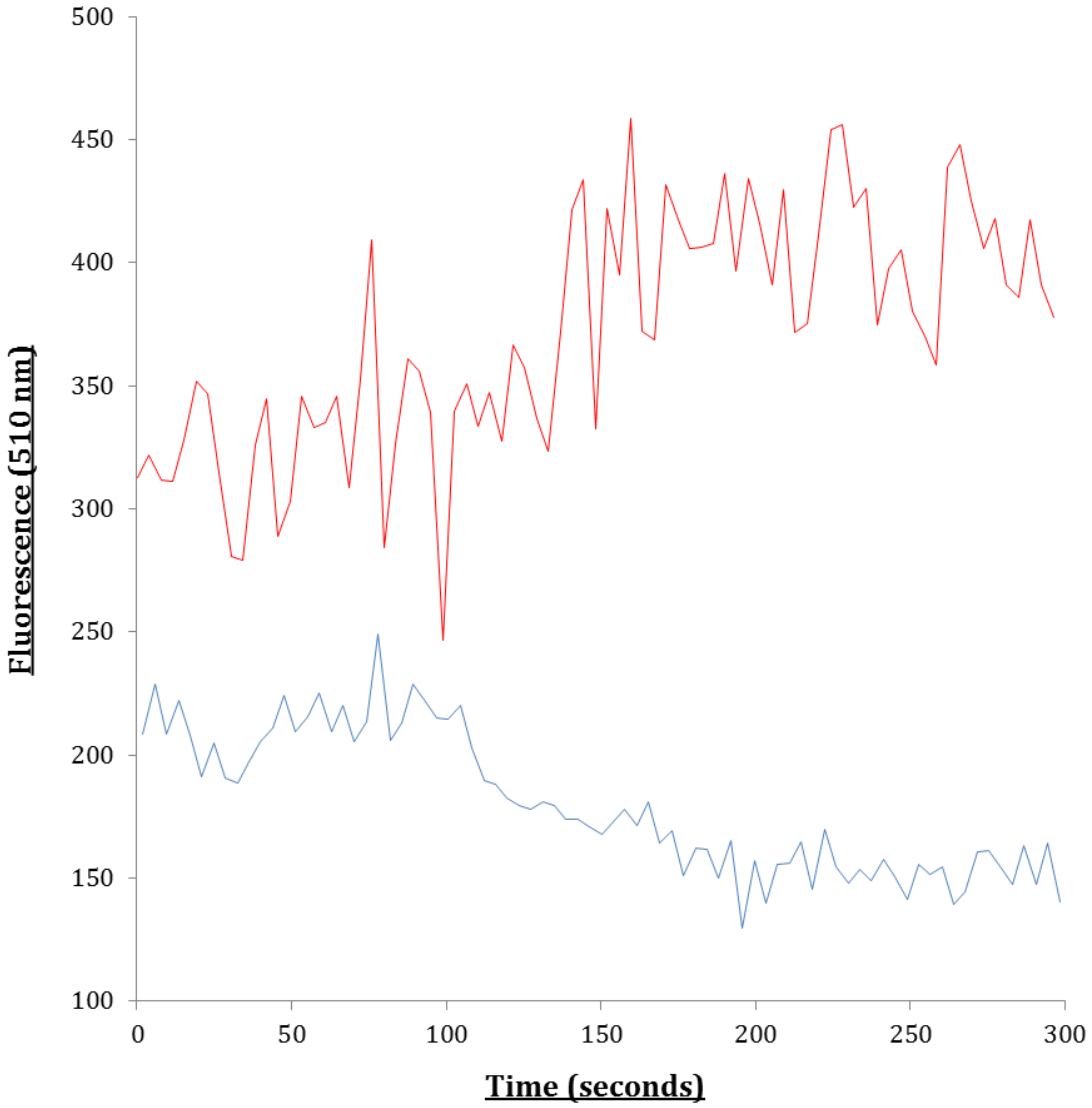

Raw data from a representative B-lymphocyte calcium release assay

Shown is the change in the 340 nm (red) and 380 nm (blue) excitation fluorescence upon addition of 1000 µM 4-C*m*C in a representative calcium release assay of the individual III:4 cell line measured using the PerkinElmer LS50 spectrofluorometer. A fluorescence baseline was established before addition of 1000 µM 4-C*m*C at ~100 seconds, at which point the fluorescence ratio increased rapidly before levelling off at ~200 seconds.

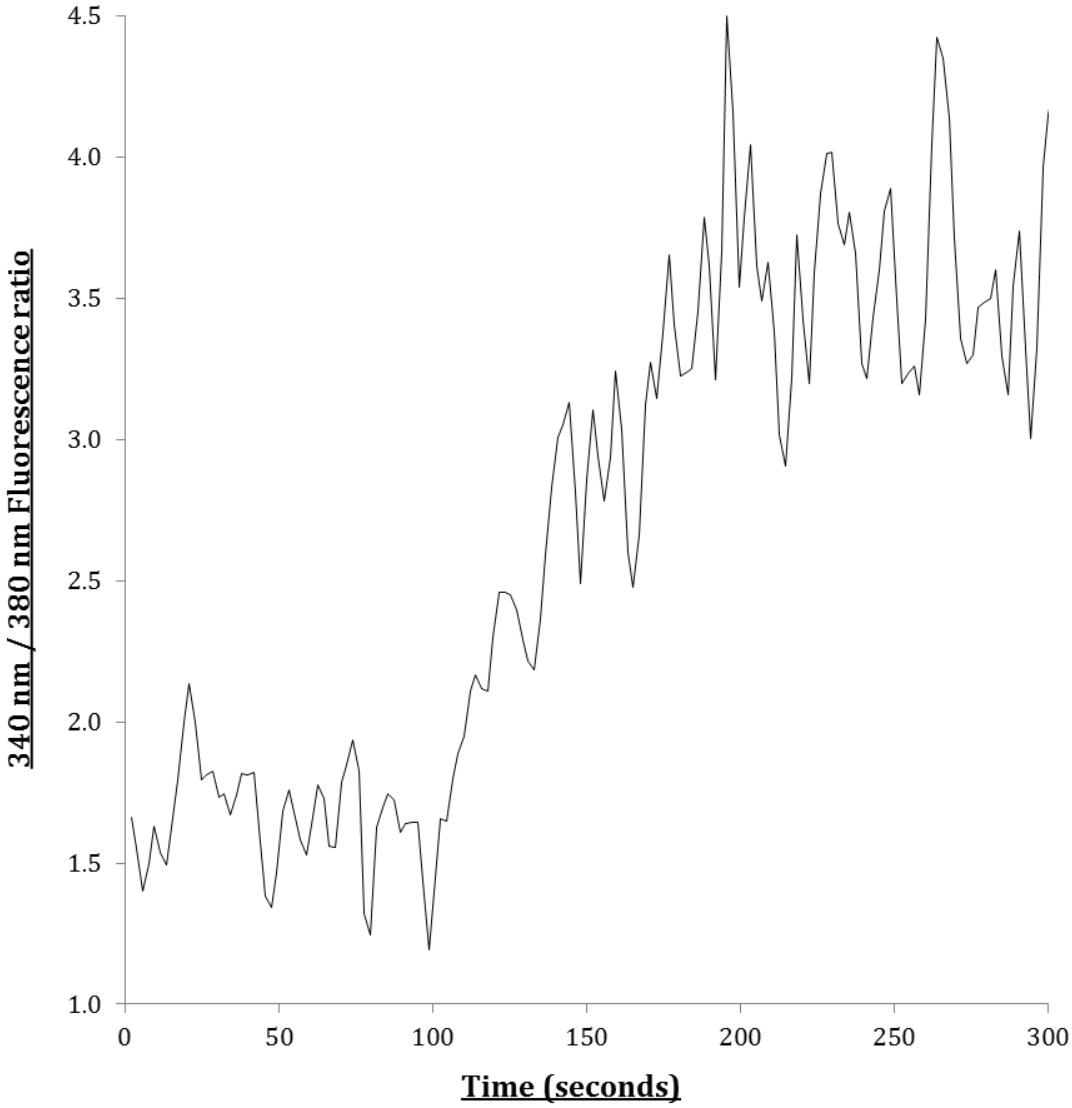

Calcium release measured in B-lymphocyte calcium release assays

Shown is the change in the 340 nm / 380 nm excitation ratio fluorescence upon addition of 1000 µM 4-C*m*C in a representative calcium release assay of the individual III:4 cell line measured using the PerkinElmer LS50 spectrofluorometer. A fluorescence baseline was established before addition of 4-C*m*C at ~100 seconds, at which point the fluorescence ratio increased rapidly before levelling off at ~200 seconds.

$$\frac{\left(R_{\chi f} - R_{\chi i} \right)}{\left(R_{\max f} - R_{\max i} \right)} \times 100\%$$

Sample calculation for percentage of total calcium release

A representative calculation for the percentage of calcium release in calcium release assays with HEK-293T cells or B-lymphocytes. ‘R’ symbolises the 340 nm / 380 nm excitation ratio of fluorescence measured at 510 nm; ‘χ’ symbolises the different concentrations of 4-C*m*C used in each assay; ‘max’ symbolises 100% calcium release defined as the change in fluorescence after addition of 1000 µM 4-C*m*C; ‘f’ symbolises the final fluorescence ratio after addition of 4-C*m*C; and ‘i’ symbolises the initial fluorescence ratio before addition of 4-C*m*C.

APPENDIX E: Difference curves from HRM assays

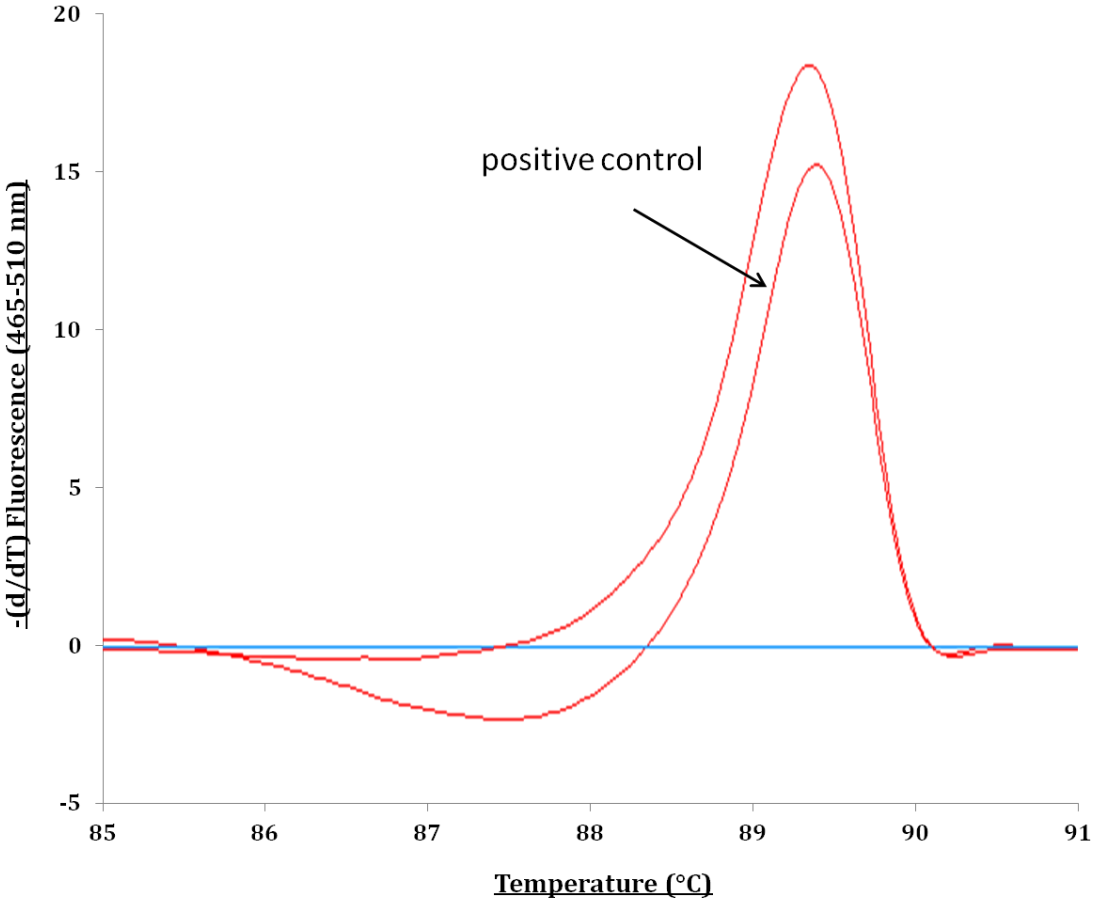

Identification of the p.R2355W variant in B-lymphocytes

Shown are the difference curves from the HRM assays carried out to confirm the presence of the g.38499670C>T variant (Genomic accession number ENSG00000196218.9) in the gDNA extracted from the positive control, R2355W (GenBank accession NP_000531.2), individual's B-lymphocytes. The difference curves were plotted as the relative difference in the fluorescence signal at 465 – 510 nm from the negative control (shown as a line at zero fluorescence) versus temperature (degrees Celsius) using the LightCycler 480 Gene Scanning software (Roche). Positive and negative controls are shown as red and blue melting curves, respectively.

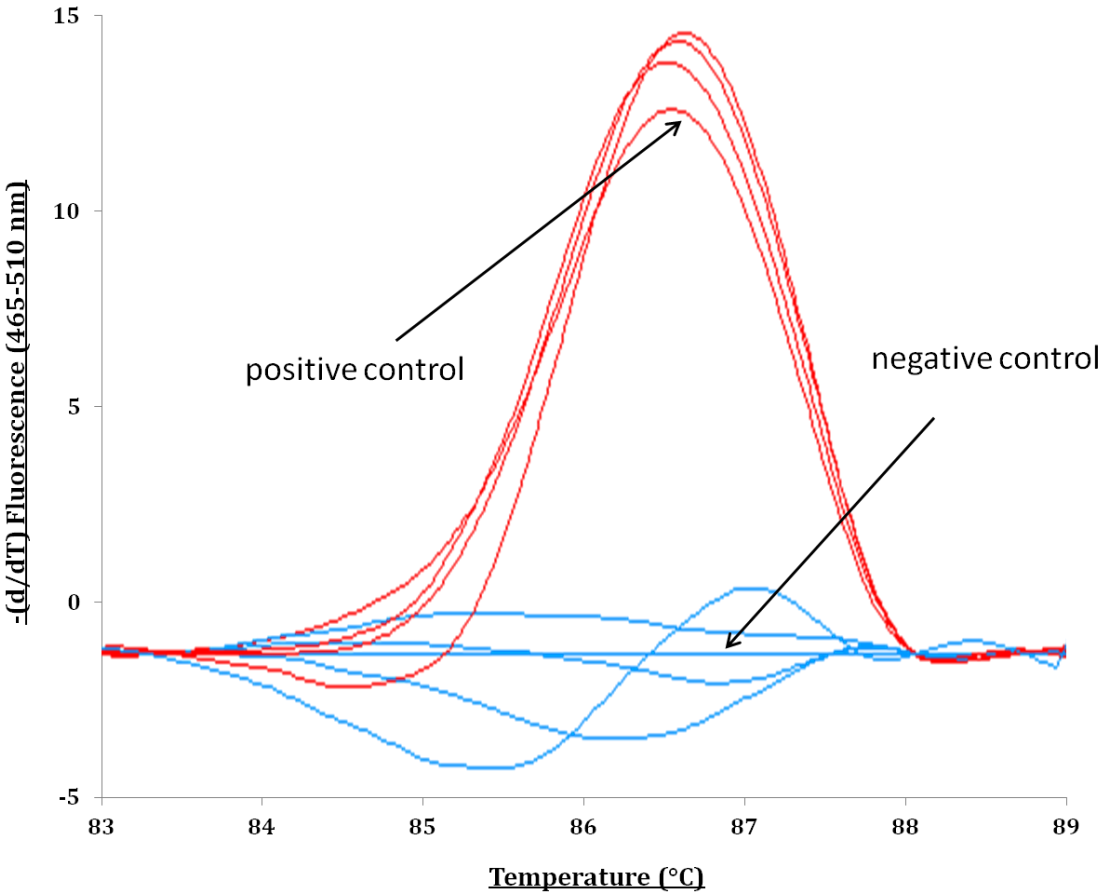

Identification of the p.D4918N variant in B-lymphocytes

Shown are the difference curves from the HRM assays carried out to confirm the presence or absence of the g.38585048G>A variant (Genomic accession number ENSG00000196218.9) in the gDNA extracted from the B-lymphocytes of a family in which the p.D4918N variant (GenBank accession NP_000531.2) was found to segregate with CCD. HRM analysis was also carried out on the gDNA from MHS and MHN controls for calcium release assays and the positive and negative gDNA controls for the genotype encoding the p.D4918N mutation. The difference curves were plotted as the relative difference in the fluorescence signal at 465 – 510 nm from the negative control (shown as a line at 0) versus temperature (degrees Celsius) using the LightCycler 480 Gene Scanning software (Roche). Positive and negative controls are shown as red and blue melting curves, respectively.